School of Civil and Mechanical Engineering

System Identification of Civil Structures under Operational Conditions Considering Uncertainties

Yu Xin

This thesis is presented for the Degree of
Doctor of Philosophy
of
Curtin University

August 2020

Declaration

To the best of my knowledge and belief this thesis contains no material previously published by any other person except where due acknowledgement has been made.

This thesis contains no material which has been accepted for the award of any other degree or diploma in any university.

ABSTRACT

Vibration based system identification has attracted significant amount of attention in civil engineering community, and the identified structural vibration characteristics can be further used for structural damage detection, condition assessment and long term structural health monitoring. Modal identification of existing civil engineering structures is critical to capture the changes in structural modal parameters, including natural frequencies, mode shapes and damping ratios, from the measured dynamic responses under ambient vibrations. However, when civil structures are under the extreme operational conditions, e.g. earthquakes, typhoons, and other extreme loadings, the measured structural responses are usually non-stationary and nonlinear. Under these circumstances, the traditional modal identification techniques would be less accurate and reliable to analyse these non-stationary vibration signals. To overcome this problem, the advanced time-frequency analysis approaches should be employed to track the time-varying modal parameters from the measured non-stationary vibration responses. The identified instantaneous modal parameters can be further used for structural damage detection by combining with some novel damage indices. In addition, the identified instantaneous modal parameters can also be used as input of Bayesian based nonlinear model updating, and the calibrated nonlinear model can be used for condition assessment of civil engineering structures subjected to extreme operational conditions.

The investigations carried out in this thesis focus on the development and application of vibration based linear and nonlinear system identification techniques for damage detection, nonlinear model updating and condition assessment of civil engineering structures under operational conditions, both ambient and extreme loading conditions. The contents of this thesis include:

(1) To perform operational modal identification of civil structures under ambient vibrations, an improved Empirical Wavelet Transform (EWT) approach is proposed in this study. Two steps are involved in the improved EWT approach. In the first step, the standardised autoregressive power spectrum of the measured response is calculated to define the boundaries of frequency components for the subsequent EWT analysis. The second step is to decompose the measured response into a number of Intrinsic Mode Functions (IMFs) by using EWT. When the IMFs are obtained, structural modal information, such as natural frequencies, mode shapes and damping ratios, can be identified by using Hilbert transform and Random Decrement Technique (RDT).

(2) When civil engineering structures are excited by the extreme operational conditions, e.g. earthquakes, typhoons, and other extreme loadings, the measured structural dynamic responses are usually non-stationary and nonlinear. To identify instantaneous modal

parameters of civil structures subjected to extreme operational conditions, an enhanced EWT approach based on Synchroextracting Transform (SET) is developed in this thesis. According to the proposed procedure, SET is conducted to analyse the frequency components of a non-stationary vibration signal, and then the filtering boundaries for EWT analysis are defined. The individual components of the non-stationary vibration signal are obtained by performing EWT analysis. Once the mono-modes are obtained, the instantaneous frequencies of each component are identified by using Hilbert Transform.

(3) To analyse non-stationary vibration signals with coupled frequency modulated components in terms of their frequency spectra, analytical mode decomposition (AMD) with an adaptive time-varying cutoff frequency identification algorithm is developed in this study. In the proposed approach, time-frequency representation of a non-stationary signal is performed by using multisynchrosqueezing transform (MSST), and time-varying cutoff frequencies of the AMD based low-pass filter are automatically identified based on the developed algorithm. Once the time varying cut-off frequencies are determined, AMD based filter can be used to adaptively decompose the non-stationary signal into individual components. Each mono-component represents an amplitude modulated and frequency modulated signal with a limited frequency bandwidth, and the instantaneous modal parameters of each mono-component, including instantaneous natural frequencies, mode shapes and damping ratios are identified in this study.

(4) Nonlinearities in the dynamic behaviors of civil structures degrade the performance of damage detection by using the traditional time- and frequency- domain methods based on the linear theory. To overcome this challenging, in this thesis, a novel damage detection approach for initially nonlinear structures is developed based on Variational Mode Decomposition (VMD). In the proposed damage detection procedure, the measured dynamic responses from nonlinear structures under earthquake excitations are adaptively decomposed into individual components by VMD analysis. Then, instantaneous modal parameters of each decomposed mono-component, including instantaneous frequencies and mode shapes, are identified by performing Hilbert transform. Based on the identified instantaneous modal parameters, two novel damage indices are defined to detect the location and severity of structural damage, respectively.

(5) Bayesian based nonlinear model updating approach using the instantaneous amplitudes of the decomposed dynamic responses is developed in this thesis. Uncertainty quantification of the model updating results due to the measurement noise is conducted. The residual of the instantaneous amplitudes of the decomposed structural dynamic responses between the test structure and the analytical nonlinear model is used to construct the maximum likelihood function. Since nonlinear model parameters and simulated error variances of the

instantaneous parameters are all unknown, the extended maximum likelihood estimation method is used to update these parameters. The uncertainty in the updated nonlinear model parameters can be evaluated by using the Cram-Rao lower bound theorem with the exact Fisher Information matrix. The numerical and experimental results demonstrate that the proposed approach is reliable and accurate for nonlinear model updating, with the capacity of considering the uncertain noise effect in the measurements.

In summary, the research work presented and the results obtained in this thesis contribute to the development of robust and reliable vibration based system identification and nonlinear model updating techniques for monitoring the conditions of civil engineering structures.

ACKNOWLEDGEMENTS

First and foremost, I would like to express my sincerest and deepest gratitude and respect to my supervisor Prof. Hong Hao and co-supervisor Associate Prof. Jun Li, who have been giving me invaluable guidance and constant encouragement throughout these years. Your wisdom and generous helps have made my PhD study a valuable journey to gain knowledge and broaden my research mind, which are invaluable for my future career and life.

Many thanks to members of the Centre for Infrastructure Monitoring and Protection (CIMP) at Curtin University for their friendship and kind help during my PhD study in Australia.

Here, I also would like to acknowledge the financial supports from the China Scholarship Council Postgraduate Scholarship Grant 201606690031, and postgraduate top-up scholarship at Curtin University to support me to carry out my PhD study at Curtin University.

Last but not least, I wish to express my sincere gratitude to my parents and elder sister for their unconditional love, inspiration and support. I also deeply appreciate my wife for her constant love and encouragement.

LIST OF PUBLISHED WORK AND/OR WORK PREPARED FOR PUBLICATION

This thesis contains published work and/or work prepared for publication, which have been co-authored. The bibliographical details of the work and where they appear in the thesis are outlined below.

Chapter 2

Xin, Y., Hao, H. & Li, J. (2019). Operational modal identification of structures based on improved empirical wavelet transform. *Structural Control & Health Monitoring*, *e2323*. https://doi.org/10.1002/stc.2232

Chapter 3

Xin, Y., Hao, H. & Li, J. (2019). Time-varying system identification by enhanced Empirical Wavelet Transform based on Synchroextracting Transform. *Engineering Structures*, *109313*. https://doi.org/10.1016/j.engstruct.2019.109313.

Chapter 4

Xin, Y., Li, J. & Hao, H. Enhanced Vibration Decomposition Method based on Multisynchrosqueezing Transform and Analytical Mode Decomposition. *Structural Control & Health Monitoring.* (Under Re-review)

Chapter 5

Xin, Y., Li, J. & Hao, H. Damage Detection in Initially Nonlinear Structures based on Variational Mode Decomposition. *International Journal of Structural Stability and Dynamics*. https://doi.org/10.1142/S0219455420420092.

Chapter 6

Xin, Y., Hao, H., Li, J., Wang Z., Wan H. & Ren W. (2019). Bayesian based nonlinear model updating using instantaneous characteristics of structural dynamic responses. *Engineering Structures*, 183:459-474. https://doi.org/10.1016/j.engstruct.2019.01.043.

STATEMENT OF CONTRIBUTION OF OTHERS

The works presented in this thesis were primarily designed, numerically executed, interpreted and written by the candidate and also the first author of the publications (Yu Xin). Significant input to the works was also provided by co-authors. Contributions of the co-authors are described below. The signed contribution form is attached in the appendix.

Chapters 2 -5

In these studies, Hong Hao and Jun Li defined the overall scope and objectives of the works and suggested research methodologies. All the numerical simulations and experimental applications were developed and carried out by Yu Xin. The manuscripts were written by Yu Xin with revisions and editions from Jun Li and Hong Hao, both of whom also provided additional intellectual input in the discussions of the results.

Chapter 6

In this research, all the numerical simulations and experimental applications were carried out by Yu Xin. Hua-Ping Wan provided some help on the MALAB program of Bayesian approaches. Zuo-Cai Wang and Wei-Xin Ren modified the manuscript and provided some constructive suggestions. The manuscript was written by Yu Xin, which was thoroughly revised by Jun Li and Hong Hao.

LIST OF RELEVANT ADDITIONAL PUBLICATIONS

The additional publications relevant to the thesis with the bibliographical details are listed below.

[1] Z. Peng, J. Li, H. Hao, **Y. Xin**, High Resolution Time Frequency Representation for Instantaneous Frequency Identification by Adaptive Duffing Oscillator, *Structural Control and Health Monitoring*. https://doi.org/10.1002/stc.2635. (**Online**)

[2] G. Fan, J. Li, H. Hao, **Y. Xin**, Dynamic Response Reconstruction under Extreme Loading Conditions using Segment based Generative Adversarial Network, *Engineering Structures*. (**Under Re-review**);

[3] **Y. Xin**, H. Hao, J. Li, Using Novel Time-frequency Analysis Method For Time-varying System Identification, *16th East Asia-Pacific Conference on Structural Engineering & Construction (EASEC16),* Brisbane, Australia.

[4] **Y. Xin**, J. Li, H. Hao, Nonlinear Model Updating Based on Dynamic Response Decomposition, *Newsletter of Australian Network of Structural Health Monitoring,* Issue 20, June 2019.

[5] J. Li, **Y. Xin**, H. Hao, An improved empirical wavelet transform approach for modal identification of structures, *The 7th World Conference on Structural Control and Monitoring*, Qingdao, China.

[6] H. Hao, J. Li, **Y. Xin**, KM Bi, G. Fan, Living Laboratory Project at Curtin University for Building Structural Condition Monitoring, *Australian Earthquake Engineering Society Conference (AEES 2018)*, Perth, Nov 2018**.**

TABLE OF CONTENTS

LIST OF FIGURES

LIST OF TABLES

CHAPTER 1 INTRODUCTION

1.1 Background

Structural health monitoring (SHM) has been an emerging research field since two decades ago. The overall goal of a SHM system is to timely detect the possible damage and stiffness degradation of the existing structures at the earliest stage so that preventative measures can be taken to avoid the unexpected structural failures [1-3]. SHM techniques can be classified as local and global methods, depending on the techniques used for condition monitoring [4]. The local methods are developed to detect local damage in a small region of the structure. Often referred to as nondestructive evaluation, these techniques include acoustics emission, hardness testing, thermal field mapping, etc., [5-6]. However, these methods require that the vicinity of the damage is known a priori and that the portion of a structure being inspected must be accessible. Due to these limitations, the local methods are often limited to the damage detection on or near the surface of the structure. On the other hand, the global methods can be applied to evaluate the condition of complex civil structures by the examination of changes in vibration characteristics [7] and/or dynamic responses.

To track the changes in structural vibration characteristics, vibration based methods for system identification have been widely studied in SHM community [8]. The basic idea is that the modal parameters of a structure, including natural frequencies, mode shapes and damping ratios, have internal relationships with structural physical properties, such as mass, damping and stiffness. Therefore, changes in physical properties will cause changes in the modal properties. The main advantage of vibration based methods is that measurements at a limited number of locations can be used to assess the condition of the whole structure.

The primary goal of the vibration based system identification is to extract modal parameters of a structure (i.e. natural frequencies, mode shapes and damping ratios) from structural responses, which can then be used to identify structural physical parameters or evaluate structural conditions. System identification involves various methods in frequency domain

such as frequency response methods [9-11], in time domain such as least-squares estimation and stochastic subspace methods [12-14], and in time-frequency domain such as wavelet transform and Hilbert transform based methods [15-17]. The identified structural parameters can serve as input to perform structural model updating, damage detection, condition assessment and long-term health monitoring. However, some challenges still exist when using the vibration based methods for structural system identification. For the complex civil structures under ambient vibrations, structural dynamic responses usually consist of several closely-spaced components, how to decompose and identify these modal parameters from structural responses is still a challenge in operational modal identification. In addition, it should be noticed that most of the structural parameter identification methods in time domain or in frequency domain have been focusing on the identification of time-invariant linear systems. When the structures are under the extreme operational conditions, e.g. earthquakes, typhoons and other extreme loadings, measured responses are typically non-stationary and the modal parameters in frequency-domain may change over time. Under this circumstance, the time-frequency analysis is essential to decompose and analyse these non-stationary responses instead of using the traditional time-domain and frequency domain methods [18]. Although the time-frequency analysis methods have been successfully applied for time-varying or nonlinear system identification, some problems still exist in some engineering applications: 1) the high-resolution time-frequency representation is required to address the non-stationary vibration signals with closely-spaced modes; 2) how to use the identified instantaneous characteristics from the decomposed dynamic responses for nonlinear structural damage detection and model updating is another challenge [19].

1.2 Research Objectives

To address the above challenges, the main aim of this thesis is to develop various vibration based system identification methods for modal identification with closely-spaced modes, time-varying dynamic characteristics identification and damage detection of civil structures under operating conditions. The specific objectives of this research are listed as follows:

1. To develop an improved Empirical Wavelet Transform (EWT) approach for structural modal parameter identification based on the Standardised Auto-Regressive (SAR) power spectrum under ambient vibrations;
2. To apply the Sychroextracting Transform (SET) based time-frequency representation approach to enhance EWT method for non-stationary signal analysis and time-varying system identification;
3. To apply an enhanced vibration decomposition approach for non-stationary signal analysis and damage detection of civil structures under earthquake excitations;
4. To define the novel damage indices for nonlinear structural damage detection based on the identified instantaneous modal parameters of civil structures subjected to the extreme loadings;
5. To propose a Bayesian based nonlinear model updating approach by using the identified instantaneous characteristics of the decomposed dynamic response of structures subjected to the extreme operating conditions.

1.3 Research Outline

This thesis comprises seven chapters. The contents of these chapters following this introductory chapter are described below:

Chapter 2 develops an improved EWT approach for structural operational modal identification based on the SAR power spectrum. Two steps are involved in the improved EWT approach. In the first step, the SAR power spectrum of the measured response is calculated to define the boundaries of frequency components for the subsequent EWT analysis. The second step is to decompose the measured response into a number of Intrinsic Mode Functions (IMFs) by using EWT. When the IMFs are obtained, structural modal information such as natural frequencies, mode shapes and damping ratios can be identified by using Hilbert transform and Random Decrement Technique (RDT).

Chapter 3 presents an enhanced EWT method with SET for non-stationary signal analysis and time-varying system identification. In this method, SET is first conducted to analyse the frequency components of a non-stationary vibration signal measured from a time-varying system instead of using classical Fourier Spectrum. Then the filtering boundaries for EWT analysis can be defined. The non-stationary vibration signal can be decomposed into a finite number of IMFs with the improved EWT. When the IMFs are obtained, the instantaneous frequencies of each mode can be effectively identified by using Hilbert Transform.

Chapter 4 proposes an enhanced vibration decomposition approach based on Analytical Mode Decomposition (AMD) and Multisynchrosqueezing Transform (MSST). Although AMD based low-pass filter has been applied for signal decomposition with time varying cut-off frequencies, these cut-off frequencies are usually manually selected from the wavelet scalogram of the target signal. The process therefore significantly reduces the computational efficiency by using AMD based low-pass filter for non-stationary signal analysis. To overcome this problem, MSST with a time varying cut-off frequency detection algorithm is used to automatically define the time-varying bisecting frequencies for the AMD analysis. Once the time varying cut-off frequencies are identified, AMD can be used to adaptively decompose the non-stationary signal into individual components.

In Chapter 5, a novel nonlinear damage detection approach is proposed based on the Variational Mode Decomposition (VMD). Based on the proposed procedure, the measured dynamic responses from nonlinear structures under earthquake excitations are adaptively decomposed into a finite number of mono-components by using VMD. Hilbert transform is then employed to identify the instantaneous modal parameters of the decomposed mono-modes, including instantaneous frequencies and mode shapes. Based on the identified modal parameters from the decomposed structural dynamic responses, two damage indices are defined to identify the location and severity of structural damage, respectively.

Chapter 6 proposes a Bayesian based nonlinear model updating approach by using the instantaneous amplitudes of the decomposed dynamic responses. Uncertainty quantification of the updated results due to the measurement noise is conducted. The residual of the instantaneous amplitudes of the decomposed structural dynamic responses between the test structure and the analytical nonlinear model is used to construct the maximum likelihood

function. Since nonlinear model parameters and simulated error variances of the instantaneous parameters are all unknown, the extended maximum likelihood estimation method is used to update these parameters. The uncertainty in the updated nonlinear model parameters can be evaluated by using the Cram-Rao lower bound theorem with the exact Fisher Information matrix.

The conclusions and recommendations for the future research are presented in Chapter 7.

It should be noted that this thesis is compiled by combining the technical papers prepared by the candidate during his PhD study. Therefore, Chapters 2 to 6 can be read independently. On the other hand, to make each technical paper complete, the numerical simulations and experimental applications are introduced in almost every chapter (i.e. in each independent chapter). These parts thus might be slightly repetitive with each other.

References

[1] Doebling S.W, Farrar C.R., Prime M.B. (1998). A summary review of vibration-based damage identification methods. *Shock and Vibration Digest*, 30(2): 91-105.

[2] Ren W.X, Zong Z.H. (2004). Output-only modal parameter identification of civil engineering structures. *Structural Engineering and Mechanics*, 17(3-4): 429-44.

[3] Yan Y, Cheng L, Wu Z, Yam L. (2007). Development in vibration-based structural damage detection technique. *Mechanical Systems and Signal Processing*, 21(5): 2198-211.

[4] Wang Z.C. (2011). Hilbert transform applications in signal analysis and non-parametric identification of linear and nonlinear systems. Doctoral Dissertations. 2012.

[5] Sohn H., Farrar C.R., Hemez F.M., Czarnecki J.J., Shunk D.D., Stinemates D.W., Nadler B.R. (2004). A review of Structural Health Monitoring Literature: 1996-2001. *Report Number LA-13976-MS*, Los Alamos National Laboratory, Los Alamos, NM.

[6] Pandey A., Biswas M. (1991). Damage detection from changes in curvature mode shapes. *Journal of Sound and Vibration*, 145(2): 321-32.

[7] Bao C.X., Hao H., Li Z.X., Zhu X.Q. (2009). Time-varying system identification using a newly improved HHT algorithm. *Computers and Structures*, 87(23-24): 1611-1623.

[8] Xin Y., Hao H., Li J. (2019). Operational modal identification of structures based on improved empirical wavelet transform. *Structural Control & Health Monitoring*, e2323.

[9] Ren W.X., Zhao T., Harik I.E. (2003). Experimental and analytical modal analysis of a steel arch bridge. *Journal of Structural Engineering ASCE*, 130(7): 1022-1031.

[10] Cunha A., Caetano E., Delgado R. (2001). Dynamic tests on large cable-stayed bridge. *Journal of Bridge Engineering ASCE*, 6(1): 46-53.

[11] Zhou X.Q., Huang W. (2013). Vibration-based Structural Damage Detection under Varying Temperature Conditions. *International Journal of Structural Stability and Dynamics*, 13 (5):1250082.

[12] Van Overschee P., De Moor B. (1996). Subspace identification for linear systems: theory, implementation and application. Dordrecht, Netherlands: Kluwer Academic Publisher, 254pp.

[13] James III G.H., Carne T.G., Lauffer J.P. (1993). The natural excitation technique (NExT) for modal parameter extraction from operating wind turbines. SAND 92-1666 UC-261, Sandia National Laboratories, Albuquerque, NM.

[14] Caicedo J.M., Dyke S.J., Johnson E.A. (2004). Natural excitation technique and eigensystem realization algorithm for phase I of the IASC-ASCE benchmark problem: Simulated data. *Journal of Engineering Mechanics ASCE*,130: 49-60.

[15] Lardies J., Gouttebroze S. (2002). Identification of modal parameters using the wavelet transform. *Mechanical Science*, 44: 2263-2283.

[16] Staszewski-Correa T., Kareem A. (2007). Performance of wavelet transform and

empirical mode decomposition in extracting signals embedded in noise. *Journal of Engineering Mechanics ASCE*, 133(7): 849-52.

[17] Feldman, M. (2008). Theoretical Analysis and Comparison of the Hilbert Transform Decomposition Methods. *Mechanical Systems and Signal Processing*, 22: 509-519.

[18] Wang C., Ren W.X., Wang Z.C., Zhu H.P. (2013). Instantaneous frequency identification of time-varying structures by continuous wavelet transform. *Engineering Structures*, 50: 17-25.

[19] Noël J.P., Kerschen G. (2017). Nonlinear system identification in structural dynamics: 10 more years of progress. *Mechanical Systems and Signal Processing*, 83: 2-35.

CHAPTER 2 OPERATIONAL MODAL IDENTIFICATION OF STRUCTURES BASED ON IMPROVED EMPIRICAL WAVELET TRANSFORM

ABSTRACT[1]

This chapter proposes an improved Empirical Wavelet Transform (EWT) approach for structural operational modal identification based on measured dynamic responses of structures under ambient vibrations. Two steps are involved in the improved EWT approach. In the first step, the Standardised Auto-Regressive (SAR) power spectrum of the measured response is calculated to define the boundaries of frequency components for the subsequent EWT analysis. The second step is to decompose the measured response into a number of Intrinsic Mode Functions (IMFs) by using EWT. When the IMFs are obtained, structural modal information such as natural frequencies, mode shapes and damping ratios can be identified by using Hilbert transform and Random Decrement Technique. In numerical studies, a simulated signal is used to investigate the effectiveness of the proposed approach. Operational modal identification based on the proposed approach and procedure is conducted to identify the modal parameters of a simulated spatial frame structure under the ambient excitations.The proposed approach is further used for operational modal identification of a seven-storey shear type steel frame structure in the laboratory and a real footbridge under ambient vibrations to verify the accuracy and performance. The modal identification results from both numerical simulations and experimental validations demonstrate that the proposed approach can effectively and accurately decompose the vibration responses and identify the structural modal parameters under operational conditions.

2.1 Introduction

Modal identification technique is essential to identify accurately the structural vibration

[1]This chapter was published in Structural Control & Health Monitoring with the full bibliographic citation as follows: Xin, Y., Hao, H. & Li, J. (2019). Operational modal identification of structures based on improved empirical wavelet transform. *Structural Control & Health Monitoring*, e2323. https://doi.org/10.1002/stc.2232

characteristics from measured dynamic responses for health monitoring of engineering structures. The identified vibration characteristics can be used for structural damage detection, condition assessment and long-term monitoring. In the past several decades, modal identification has attracted significant attention and numerous methods have been developed, e.g. by using the rational fraction polynomials method to extract frequency response functions based on both the input excitation and output vibration response measurements [1-3].In terms of engineering applications, it is very difficult to measure the dynamic external excitations applied on the structures. Operational modal identification technique based on output responses only becomes a desirable alternative in civil engineering applications [4-9]. Existing methods including peak-picking from power spectral density spectrum [10], stochastic subspace identification (SSI) approach [11, 12] and natural excitation technique (NExT) [13, 14], have been developed and widely used for modal identification of civil structures. Nonetheless, the challenges associated with these methods still exist, which are to identify the modal information of structures with closely-spaced modes, and to accommodate the significant noise effect in the vibration responses measured from the structures under the ambient vibrations.

In the recent years, time-frequency analysis methods, i.e. Continuous Wavelet Transform (CWT) and Hilbert-Huang Transform (HHT), have received increasing attentions for modal identification and damage detection of civil structures [15-20]. Staszewski [21] proposed three different procedures to identify the damping ratios of a multi-degree-of-freedom (MDOF) system based on the CWT. Ruzzene [22] developed using wavelet transform to identify the structural modal parameters, i.e. natural frequencies and damping ratios. Kijewski-Correa and Kareem [23] used CWT and Empirical Mode Decomposition (EMD) to separate two closely-spaced cosine waves, and the results demonstrated that the frequency resolution capacities of these two techniques can be problematic.

HHT is an alternative time-frequency analysis method based on EMD [24], which is to decompose adaptively a signal into a discrete number of Intrinsic Mode Functions (IMFs).These IMFs represent natural oscillatory modes embedded in the signal and behave as basic functions which are derived from the signal itself. EMD has been widely applied for

modal identification and structural damage identification [25-28]. To improve the performance of using EMD for response decomposition against the noise effect in measured responses, Ensemble Empirical Mode Decomposition (EEMD) has been proposed [29]. However, the problem of mode mixing still exists. To overcome this shortcoming, a novel adaptive filter method named Empirical Wavelet Transform (EWT) was proposed [30], which can be used to extract the different modes of a vibration response signal by designing an appropriate wavelet filter bank in the Fourier spectrum. EWT has been applied to detect the defects of rolling bearings with good results [31-33]. Analysis of the noisy and non-stationary signals based on Fourier spectrum would be less effective. It will be difficult for EWT to detect the proper boundaries in the Fourier spectrum for extracting the modes, since false modes may be observed leading to an improper segmentation in the frequency domain [34].

This chapter proposes an improved EWT approach to perform the signal decomposition and conduct the structural operational modal identification from the measured responses of structures under ambient excitations. Two steps are involved in the improved EWT approach. In the first step, a standardised auto-regression (SAR) power spectrum [36-38] issued to define the appropriate boundaries for EWT analysis, instead of using the ordinary Fourier spectrum suffering from the mode mixing effect. The second step is to decompose the measured response into a number of IMFs by using EWT. The obtained IMFs can be further used to identify the structural modal parameters, i.e. natural frequencies, mode shapes and damping ratios, by using Hilbert Transform and Random Decrement Technique (RDT). Numerical and experimental studies will be conducted in this chapter to demonstrate the effectiveness and accuracy of using the proposed approach for operational modal identification.

The remainder of this chapter is organized as follows. Section 2 briefly explains the background of the original EWT method, and the SAR power spectrum is introduced. In Section 3, the proposed improved EWT approach for structural operational modal identification is described. In Section 4, a synthetic signal is first employed to verify the feasibility and effectiveness of the proposed approach. Numerical studies on a

three-dimensional 4-storey frame structure under the ambient excitation are conducted to validate the accuracy and performance of using the proposed approach for operational modal identification. Experimental validations on a 7-storey shear type steel frame model and a real footbridge under ambient vibrations are conducted in Section 5 to further verify the capability of the proposed approach. Finally, the conclusions are summarized in Section 6.

2.2 Theoretical Background and Development

2.1.1 The traditional EWT

A time domain signal $x(t)$ is assumed to consist of *N* IMFs, that is, $x_i(t)$ (*i=1, 2, ..., N*). The Fourier spectrum of the signal can be divided into *N* segments, and each segment includes an individual IMF of the signal.ω_n is denoted as the boundary of Fourier Spectrum required for EWT analysis, and each segment is filtered by an interval$[\omega_{n-1}, \omega_n]$ (where $\omega_0 = 0$and$\omega_n = \pi$). A transient phase with a width of $2\tau_n$ is defined for eachω_n, and each τ_n is defined as

$$\tau_n = \gamma \times \omega_n \tag{2.1}$$

$$0 < \ \gamma < min_n \frac{\omega_{n+1}-\omega_n}{\omega_{n+1}+\omega_n} \tag{2.2}$$

The empirical scaling function and the empirical wavelets [30] are then defined as follows

$$\widehat{\emptyset}_n(\omega) = \begin{cases} 1 & if \ \ |\omega| \leq (1-\gamma)\omega_n \\ \cos\left[\frac{\pi}{2}\beta\left(\left(\frac{1}{2\gamma\omega_n}(|\omega| - (1-\gamma)\omega_n)\right)\right)\right] & if \ \ (1-\gamma)\omega_n \leq |\omega| \leq (1+\gamma)\omega_n \\ 0 & \text{oherwise} \end{cases} \tag{2.3}$$

$$\widehat{\Psi}_n(\omega) = \begin{cases} 1 & if \ \ \omega_n + \tau_n \leq |\omega| \leq \omega_{n+1} - \tau_{n+1} \\ \cos\left[\frac{\pi}{2}\beta\left(\frac{1}{2\tau_{n+1}}(|\omega| - \omega_{n+1} - \tau_{n+1})\right)\right] & if \ \ \omega_{n+1} - \tau_{n+1} \leq |\omega| \leq \omega_{n+1} + \tau_{n+1} \\ \sin\left[\frac{\pi}{2}\beta\left(\frac{1}{2\tau_n}(|\omega| - \omega_n + \tau_n)\right)\right] & if \ \ \omega_n - \tau_n \leq |\omega| \leq \omega_n + \tau_n \\ 0 & \text{oherwise} \end{cases} \tag{2.4}$$

in which, $\beta(x)$ is an arbitrary function which is defined on [0,1] and satisfies:

$$\begin{cases} \beta(x) = 0 & if \;\; x \leq 0 \\ \beta(x) + \beta(1-x) = 1 & \forall x \in [0,1] \\ 1 & if \;\; x \geq 1 \end{cases} \tag{2.5}$$

Many functions satisfy the characteristics of Equation (2.5), and the most used function $\beta(x)$ in literature [30-34] is:

$$\beta(x) = x^4(35 - 84x + 70x^2 - 20x^3) \qquad \forall x \in [0,1] \tag{2.6}$$

By adopting Fourier spectrum segment information into Equations (2.3) and (2.4), the empirical wavelet filter bank is constructed. After the scaling function and empirical wavelets are derived, the detail coefficients are given by the inner products

$$W_x(n,t) = \int x(\tau)\Psi_n(\tau - t)d\tau = F^{-1}\left(\hat{X}(\omega)\overline{\widehat{\Psi}_n(\omega)}\right) \tag{2.7}$$

The approximation coefficients are given as

$$W_x(0,t) = \int x(\tau)\emptyset_n(\tau - t)d\tau = F^{-1}\left(\hat{X}(\omega)\overline{\widehat{\emptyset}_n(\omega)}\right) \tag{2.8}$$

Then the empirical modes decomposed from the signal are given as

$$f_0(t) = W_x(0,t) * \emptyset_1(t) \tag{2.9}$$

$$f_k(t) = W_x(k,t) * \Psi_k(t) \tag{2.10}$$

and the reconstruction signal can be obtained as

$$\hat{x}(t) = W_x(0,t) * \emptyset_1(t) + \sum_{n=1}^{N} W_x(n,t) * \Psi_n(t) = F^{-1}\Big(W_x(0,\omega)\widehat{\emptyset}_1(\omega) + \sum_{n=1}^{N} \widehat{W}_x(n,\omega) * \widehat{\Psi}_n(\omega)\Big) \tag{2.11}$$

2.2.2 The improved EWT approach

As mentioned in the literature [34], it is a big challenge to employ Fourier spectrum for determining the boundaries associated with EWT analysis when a signal is contaminated with significant noise and/or non-stationary components. Under these circumstances, a spectral analysis method, namely, SAR power spectrum, is employed to improve the effectiveness and accuracy in defining the boundaries for using EWT to perform the signal

decomposition.

2.2.3 SAR power spectrum

When a signal is contaminated with the significant noise effect, the SAR power spectrum can be used to better define the boundaries of EWT than using the ordinary Fourier spectrum. Since the SAR power spectrum is smoothed with a lower level variance compared with Fourier spectrum, it is more suitable to use this to define the boundaries in EWT analysis instead of Fourier spectrum for signals with low signal-to-noise ratios.

Assuming that a linear system $S(Z)$ is excited by Gaussian white noise $w(n)$ with zero mean and variance σ^2, its auto-regressive (AR) model can be written as [35]

$$x(n) = -\sum_{k=1}^{q} a_k x(n-k) + w(n) \tag{2.12}$$

in which, $x(n)$ represents the output of the linear system, q denotes the order of the AR model, and a_k are called predicted coefficients of the AR model. The auto-correlation function of the AR model can be expressed in matrix form as:

$$\begin{bmatrix} r_x(0) & r_x(1) & r_x(2) & \cdots & r_x(q) \\ r_x(1) & r_x(0) & r_x(1) & \cdots & r_x(q-1) \\ r_x(2) & r_x(1) & r_x(0) & \cdots & r_x(q-2) \\ \vdots & \vdots & \vdots & \vdots & \vdots \\ r_x(q) & r_x(q-1) & r_x(q-2) & \cdots & r_x(0) \end{bmatrix} \begin{bmatrix} 1 \\ a_1 \\ a_2 \\ \vdots \\ a_q \end{bmatrix} = \begin{bmatrix} \sigma^2 \\ 0 \\ 0 \\ \vdots \\ 0 \end{bmatrix} \tag{2.13}$$

where $r_x(\ \ )$ is the auto-correlation function. These linear equations described in Equation (2.13) are called Yule-Walker equation, and the coefficients a_k and σ^2can be obtained by using the Levinson-Durbin recursion algorithm [35].

Once the linear system is determined, the standardised power spectrum $P_{SAR}(e^{j\omega})$ of AR model can be estimated by using the obtained linear parameters of $S(Z)$

$$P_{AR}(e^{j\omega}) = \frac{\sigma^2}{\left|1+\sum_{k=1}^{q} a_k e^{-j\omega k}\right|^2} \tag{2.14}$$

$$P_{SAR}(e^{j\omega}) = P_{AR}(e^{j\omega})/max(P_{AR}(e^{j\omega})) \tag{2.15}$$

where *max*( ) denotes the maximum value of $P_{AR}(e^{j\omega})$.

The order q is a major parameter in AR model, and it determines the identification accuracy

of the AR model. Several methods used to determine the value of q have been developed, including Singular Value Decomposition (SVD), Akaika Information Criterion (AIC) and Final Prediction Error Criterion (FPE) [39]. In this chapter, FPE is used to estimate the optimal parameter q of AR model, which can be defined as:

$$FPE(p) = det\left(\frac{1}{N}\sum_{i=1}^{N}\varepsilon(t,q)\left(\varepsilon(t,q)\right)^{T}\right)\left(\frac{1+d/N}{1-d/N}\right) \tag{2.16}$$

in which N is the number of data samples in the processed signal, $\varepsilon(t)$is the prediction error corresponding to the order q, d is the number of parameters of AR model which equals to q+1, and *det*( ) expresses the determinant [40]. Once p is determined, the SAR power spectrum is calculated by using the Burg algorithm [36].

Based on the spectral analysis method mentioned above, the procedure of the improved EWT approach is shown in Figure1. In the first step, the SAR power spectrum of the measured response is calculated to determine the boundaries. A smoothed SAR power spectrum can be applied for the signals with significant noise effect. When the boundaries are defined, EWT analysis is performed to decompose the vibration response into a number of IMFs based on the defined filtering boundaries. The modal information, i.e. natural frequencies, mode shapes and damping ratios, is then identified consequently, which will be presented in details in the next section.

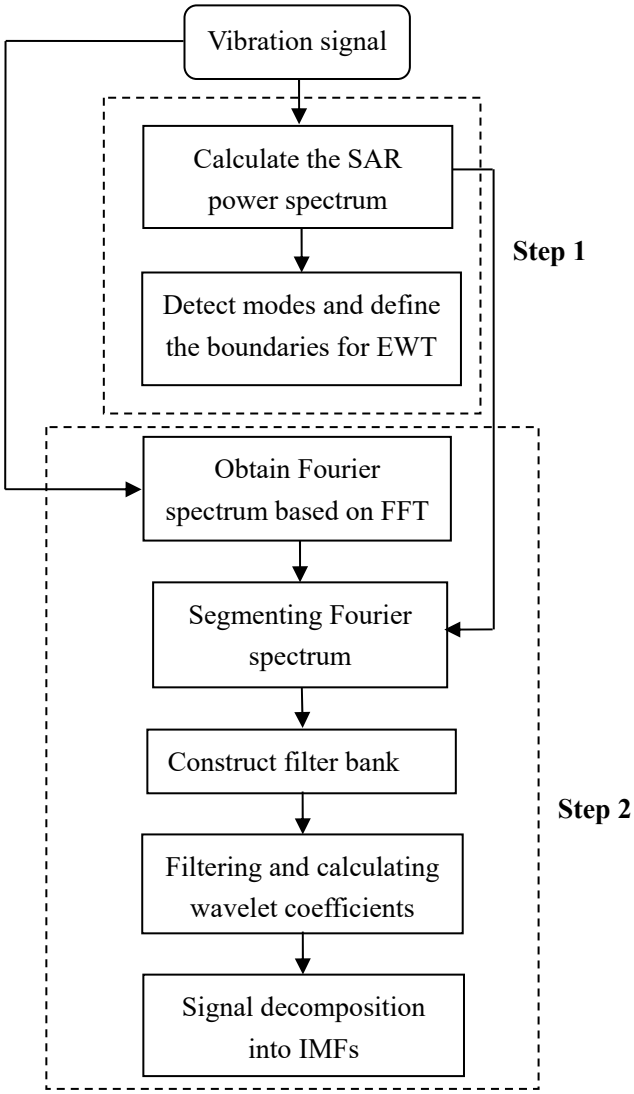

Figure 2-1 Flowchart of the proposed improved EWT approach

2.3.4 Operational modal identification based on the improved EWT approach

For a structural system with n Degrees-of-Freedom (DOFs), the equation of motion can be described as

$$\mathbf{M}\ddot{u}(t) + \mathbf{C}\dot{u}(t) + \mathbf{K}u(t) = -\mathbf{M}L\ddot{x}_s(t) \tag{2.17}$$

where $\mathbf{M}$,$\mathbf{C}$ and $\mathbf{K}$ are the mass, damping and stiffness matrices, respectively; $\ddot{u}(t)$,$\dot{u}(t)$ and $u(t)$ are the acceleration, velocity and displacement response vectors of the system, respectively; L is the mapping vector of applied excitation at the associated DOFs of the structure, and $\ddot{x}_s(t)$ is the applied ambient acceleration excitation. The improved EWT

approach described in Section 2 is used to decompose structural vibration responses into individual IMFs. Then Hilbert Transform and RDT [41, 42] will be employed to identify structural modal parameters based on the decomposed IMFs, to obtain natural frequencies, mode shapes and damping ratios. The identification process is described in Figure 2-1.

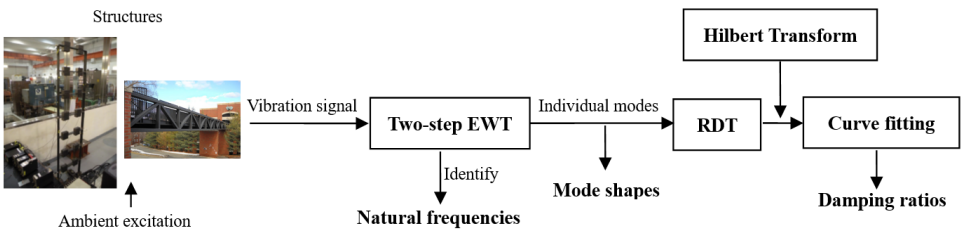

Figure 2-2 Using the improved EWT approach for operational modal identification

With the decomposed IMFs from the improved EWT approach, RDT is applied to estimate the free vibration response of each mode, which can be expressed as

$$u_r^f(t) = \frac{1}{N}\sum_{i=1}^{N} u_r(t_i + \tau) \qquad (0 \le \tau \le t_{seg}) \tag{2.18}$$

in which $u_r^f(t)$ represents the estimated free vibration response of the rth mono-component, $u_r(t_i + \tau)$ is the rth IMF of the measured response,t_i isthe start time for each segment, and t_{seg} is the duration of a segment, which is the same for all the segments.

Each estimated free vibration response $u_r^f(t)$ has a narrow frequency band corresponding to the extracted IMF $u_r(t)$.The analytical signal of $u_r^f(t)$can be written as

$$A_r(t)e^{j\theta_r(t)} = u_r^f(t) + jH\left[u_r^f(t)\right] \tag{2.19}$$

in which$A_r(t)$ and $\theta_r(t)$ are the instantaneous amplitude and phase angle of the rth free vibration response $u_r^f(t)$, respectively; H[ ] represents the Hilbert Transform. The phase and amplitude can be expressed as [43, 44]

$$\theta_r = \tan^{-1}\left\{\frac{u_r^f(t)}{H\left[u_r^f(t)\right]}\right\}, A_r(t) = \sqrt{\{A_r(t)\}^2 + \left\{H\left[u_r^f(t)\right]\right\}^2} \tag{2.20}$$

Afterwards a nonlinear curve-fitting technique is used to identify the exponentially decaying curve for calculating the damping ratio of each individual mode. The estimated curve can be written as

$$G_{fitted}(t) = \hat{A}_r e^{-dt} \tag{2.21}$$

where $\hat{A}_r$ represents the fitted amplitude of the rth free vibration response, d defines the decay rate of the exponential function, which can be estimated based on the nonlinear curve-fitting analysis. According to the obtained damped free vibration response [45], the damping ratio can be approximately identified as

$$\hat{A}_r e^{-dt} \approx A_r(t) e^{-\xi_r \theta_{ri}(t)} \quad \Rightarrow \quad \xi_r = \frac{b}{\theta_r} \tag{2.22}$$

In addition, considering the rth modal contributions $\varphi_{kr} q_r(t)$and $\varphi_{lr} q_r(t)$from the kth and l^{th} DOFs respectively, the mode shape can be identified as

$$\left|\frac{\varphi_{kr}}{\varphi_{lr}}\right| = \frac{A_{kr}(t)}{A_{lr}(t)} \tag{2.23}$$

2.3 Numerical Studies

2.3.1 Analysis of a simulated signal

A simulated signal with a time-varying amplitude, as defined in Equation (2.24), which consists of three frequency components of 16Hz, 20Hz and 28Hz, is used in this section to investigate the effectiveness of using the SAR power spectrum to define the boundaries for EWT analysis. The time-varying amplitude of this signal is simulated by using the exponential function. Gaussian white noise is added to the multi-component signal to simulate the effect of noise, and the noisy signal $y_{noise}(t)$ is described in Equation (2.25).

$$y_1(t) = \mathrm{e}^{-0.5\mathrm{t}}\cos(32\,\pi\, t) + 0.5\mathrm{e}^{-\mathrm{t}}\cos(40\,\pi\, t) + 0.5\mathrm{e}^{-1.2\mathrm{t}}\cos(56\,\pi\, t) \tag{2.24}$$

$$y_{noise}(t) = awgn(y_1(t), \mathrm{SNR}, '\mathrm{measured}') \tag{2.25}$$

in which, *awgn* is an in-built function in MATLAB, SNR denotes the signal-to-noise ratio, and the option 'measured' indicates the SNR used in this function is the measured SNR. In this study, the value of the SNR is set as -5.98dB, which denotes a significant noise effect. The sampling duration is defined as 5s with a sampling rate of 240Hz, and the simulated signal is shown in Figure 2-3.

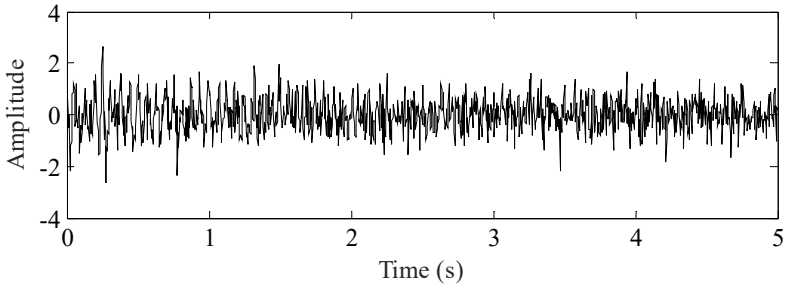

Figure 2-3 The simulated signal

It is mentioned that in Section 2 that SAR power spectrum performs well for the case under ambient excitations. Fourier spectrum and SAR power spectrum of the second simulated signal are calculated and shown in Figures 2-4 (a) and (b), respectively. It can be seen that the three frequency components are not clearly identified and then the boundaries cannot be clearly defined by using the Fourier spectrum due to the influence of significant noise effect. SAR power spectrum clearly shows these three frequency components so as to effectively detect the boundaries in EWT analysis, although the second and third modes are weakly excited. The comparison of defined boundaries by using the Fourier spectrum and the SAR power spectrum are shown in Figures 2-5 (a) and (b), respectively. It is obvious that using the SAR power spectrum can more effectively serve the purpose of defining the boundaries to separate three frequency components than the Fourier spectrum.

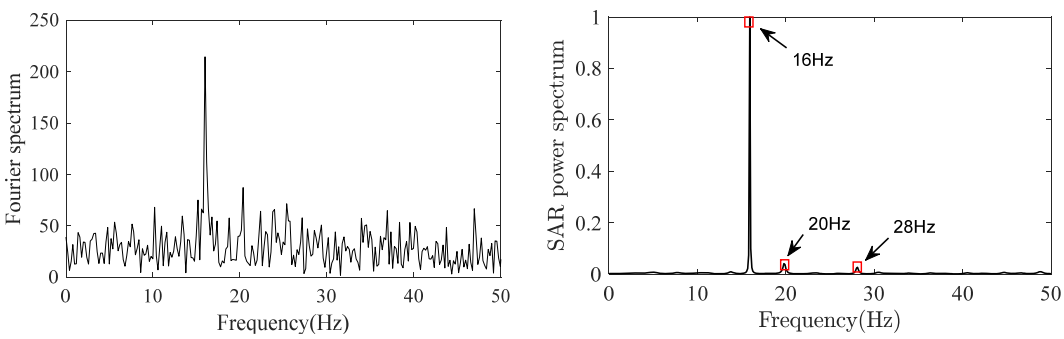

(a) (b)

Figure 2-4 Spectral analysis of the simulated signal: (a) Fourier spectrum, (b) SAR power spectrum

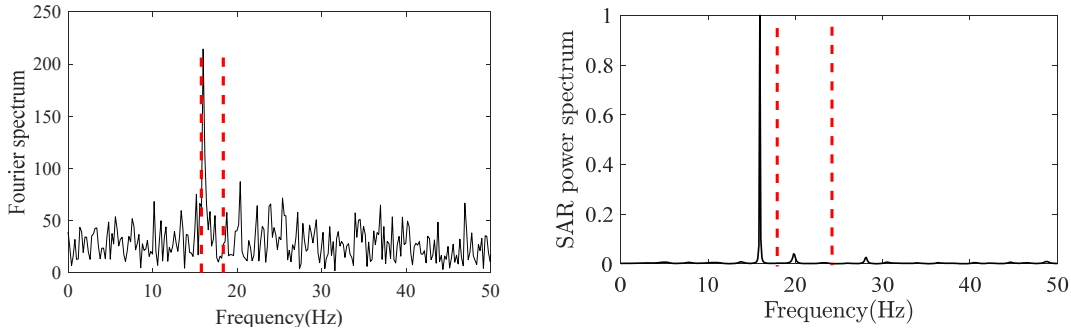

(a) (b)

Figure 2-5 Comparison of the defined boundaries by using: (a) Fourier spectrum; (b) SAR power spectrum

2.3.2 Numerical study on a four-storey spatial frame structure

Numerical studies on a spatial 4-storey two-bay concrete frame structure, as shown in Figure6,areconducted to verify the effectiveness and accuracy of using the proposed approach for structural operational modal identification. The frame structure is modelled with the finite element analysis package "Opensees" [46]. The elastic beam elements are used to model the structure. The heights of the first storey and the rest floors are 4.5m and 3m, respectively. The lengths of beams in the *x*-direction and *y*-direction are 6m and 5m, respectively. The elastic modulus of the concrete material is set as 3.25×10^{10}N/m^2. The cross section of the first floor column is 0.6m×0.6m, and the cross section of the other floor columns is 0.4m×0.4m. The cross sections of beams in the *x*-direction and *y*-direction are defined as 0.4m×0.6m and 0.3m×0.4m, respectively. The damping ratio is assumed as 1% for each mode of the frame structure. The bottom of the frame structure is fixed to the ground. A Gaussian white noise with a maximum amplitude of 5 m/s^2 is simulated as the applied ambient excitations to the frame structure along both the *x*-, *y*- and *z*-axes. The acceleration signals along the *x*- and *y*- axes of all the beam-column joints of the structure are recorded with 24 accelerometers. The accelerometer locations are defined as S1, S2, … , S24, as shown in Figure6. The sampling duration is defined as 30s with a sampling frequency of 240 Hz.

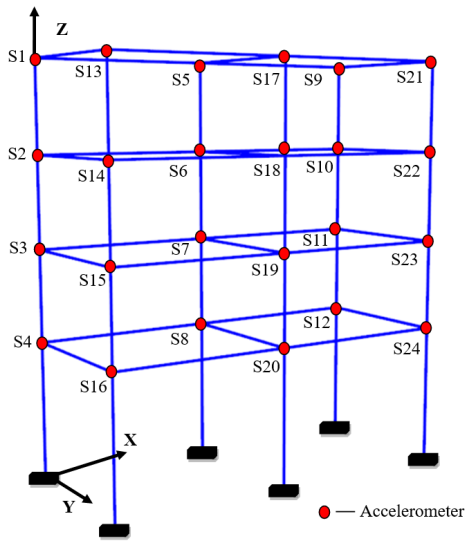

Figure 2-6 The spatial frame structure in the numerical study

The measured responses are analysed with the proposed approach and procedure as described in Figure 2 to identify the modal information, such as natural frequencies, mode shapes and damping ratios of the frame structure. To further investigate the robustness of the proposed approach, Gaussian white noise is added to the structural vibration responses, and the noise level is 30%. The modal identification results obtained from the proposed approach are compared with those obtained from the existing widely used Stochastic Subspace Identification (SSI) method [12, 13]. The dynamic responses of S2 in the *y*-direction and S6 in the *x*-direction are shown in Figures7 (a) and (b), respectively. The SAR power spectra of the vibration responses from S1-S8sensorsin the *y*-direction are shown in Figure8 (a), and it is clearly observed that five natural frequencies corresponding to the vibration modes in the *y*-direction can be effectively identified. The SAR power spectra of the vibration responses from S1-S8 sensors in the *x*-direction are shown in Figure8 (b). It can be seen from Figure8(b) that five natural frequencies corresponding to the modes in the *x*-direction are detected including two close mode components at 16.46Hz and 16.99Hz, respectively. Figure9 shows the ten IMFs extracted from structural vibration responses of S2 response in the *y*-direction and S6 response in the *x*-direction by using the improved EWT approach. It shall be noted that Mode1, Mode 3, Mode 6, Mode 7 and Mode 10 correspond to the vibration modes in the *y*-direction, and Mode 2, Mode 4, Mode

5, Mode 8 and Mode 9 correspond to the vibration modes in the *x*-direction. The estimated free vibration responses of the corresponding IMFs obtained by using RDT are shown in Figure10. The envelop curves of the vibration responses are then obtained with the nonlinear curve fitting technique.

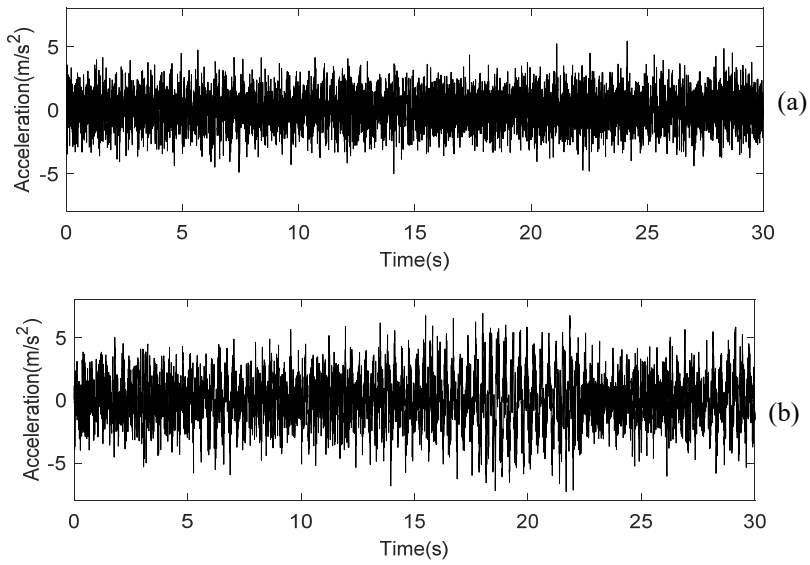

Figure 2-7 The simulated acceleration responses: (a) S2 in *y*-direction; (b) S6 in *x*-direction

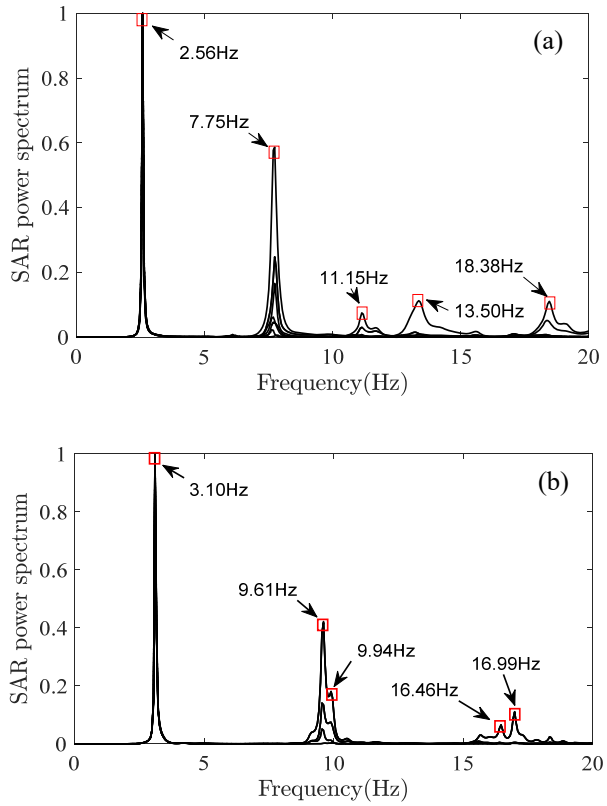

Figure 2-8 SAR power spectrum analysis results: (a) using S1-S8 responses in the *y*-direction; (b) using S1-S8 responses in the *x*-direction

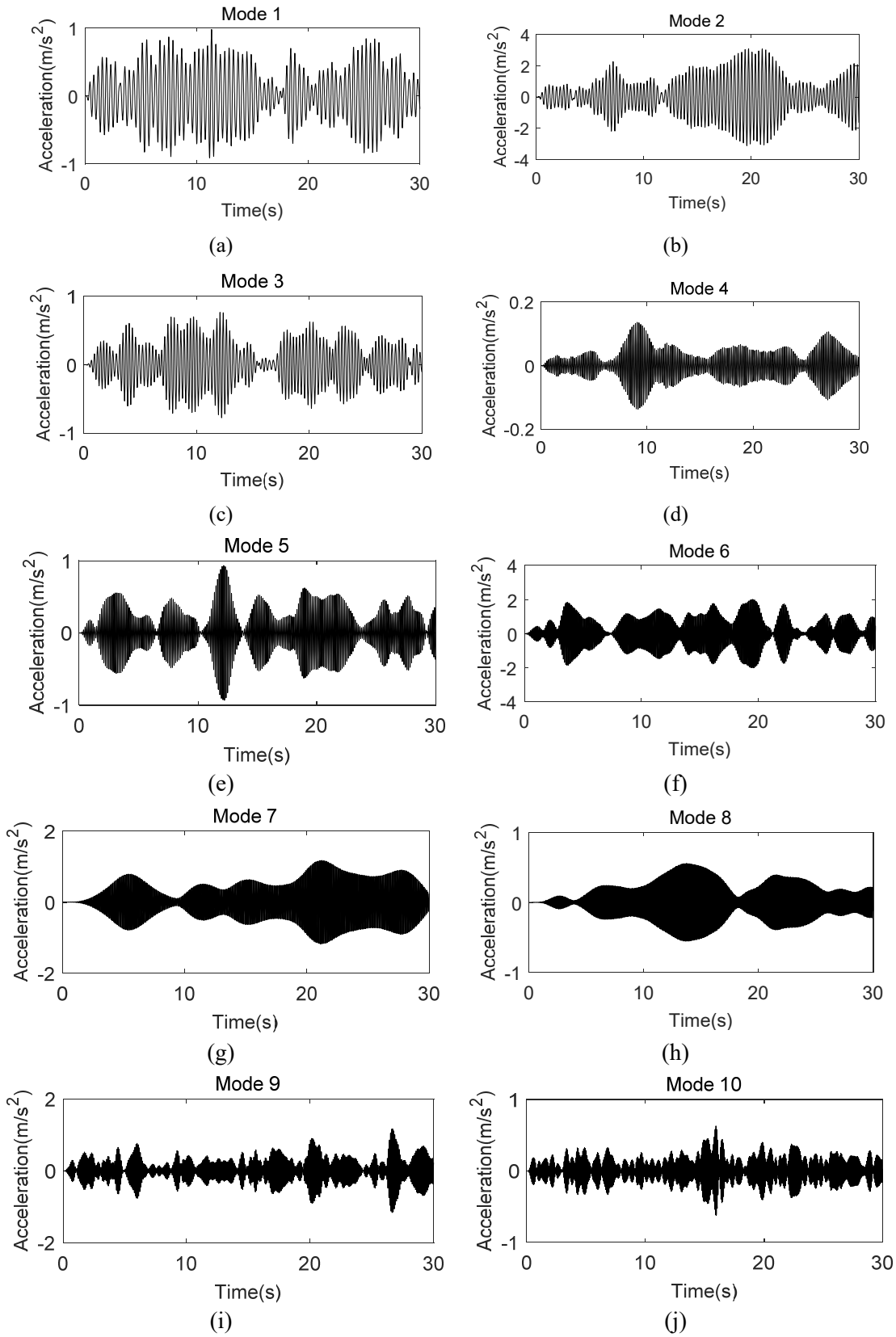

Figure 2-9 The first ten extracted IMFs using the improved EWT approach: (a) Mode 1; (b) Mode 2; (c) Mode 3; (d) Mode 4; (e) Mode 5; (f) Mode 6; (g) Mode 7; (h) Mode 8; (i) Mode 9; (j) Mode 10

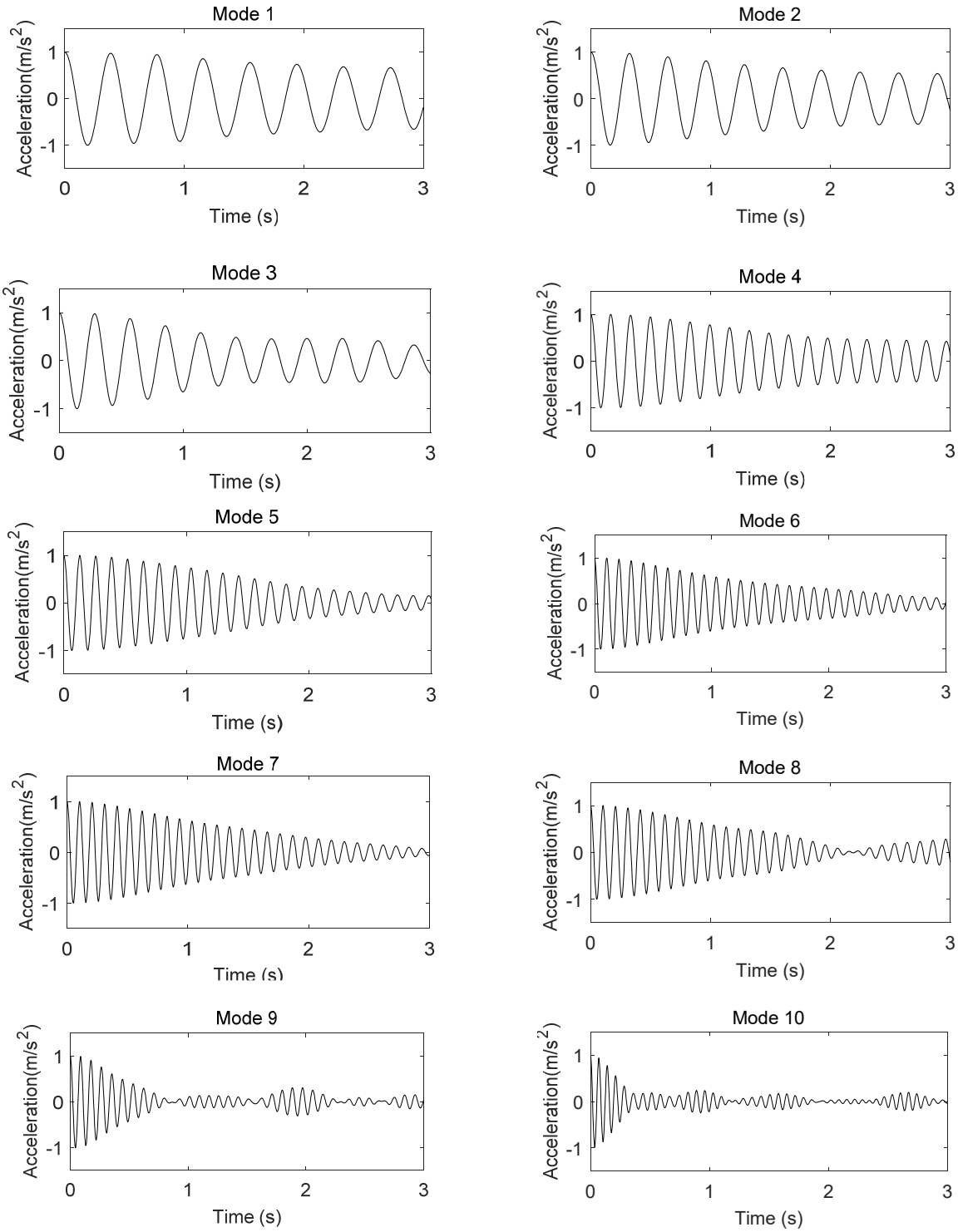

Figure 2-10 The estimated free vibration responses using the improved EWT approach

Table 1 lists the identified ten frequencies and damping ratios by using the proposed approach and the traditional SSI method. It is noted that the analytical results are obtained from the modal Analysis based on the finite element model. Due to the page limit, the first three mode shapes in the *y*-direction and the first two mode shapes in the *x*-direction are

shown in Figure11. To further verify the accuracy of the identified mode shapes, Modal Assurance Criterion (MAC) [9] is calculated to evaluate the correlation between the analytical and identified mode shapes. MAC values of those five mode shapes are shown in Figure11. As observed from Table 1, the proposed approach can accurately identify the structural modal parameters, i.e. natural frequencies and damping ratios. It should be noted that although 30% noise is added to the measured responses, the closely spaced frequencies can also be effectively identified. In addition, by comparing with the modal identification results obtained from the traditional SSI method, it can be concluded that the proposed approach is generally more accurate to perform the operational modal identification, particularly for those closely spaced modes. The results demonstrate that the significant noise has a little effect on the identification results of the proposed approach.

It is noted that a better spectrum analysis method, namely SAR power spectrum, is used to identify the modes of the measured vibration response and define the boundaries for EWT analysis. By segmenting the spectrum using SAR, individual vibration modes are obtained and the extracted IMFs represent those individual vibration modes. These can also be evidenced by examining the modal identification results listed in Table 1 and mode shapes as shown in Figure 11. The identified results demonstrate that the proposed approach can effectively and reliably identify the vibration modes of the structure, even for those closely-spaced modes.

Table 2-1 Modal identification results in the numerical study

Mode(direction)	Natural Frequency (Hz) (Relative error, %)			Damping Ratio (%) (Relative error, %)		
	Analytical	SSI	The proposed approach	Analytical	SSI	The proposed approach
1(y)	2.56	2.57(0.4)	2.56(0.0)	1.0	0.93(7)	0.96(4)
2(x)	3.10	3.10(0.0)	3.10(0.0)	1.0	0.95(5)	1.04(4)
3(y)	7.72	7.75(0.4)	7.73(0.1)	1.0	0.91(9)	1.03(3)
4(x)	9.58	9.61(0.3)	9.60(0.2)	1.0	1.21(21)	1.09(9)
5(rotational)	9.98	10.05(0.7)	9.94(0.4)	1.0	1.14(14)	0.95(5)
6(rotational)	11.15	11.13(0.2)	11.15(0.0)	1.0	0.89(11)	1.01(1)
7(y)	13.39	13.21(1.3)	13.50(0.8)	1.0	1.08(8)	1.03(3)
8(rotational)	16.43	16.51(0.5)	16.46(0.2)	1.0	0.94(4)	0.90(10)
9(y)	16.77	-	16.99(1.3)	1.0	-	0.90(10)
10(rotational)	18.18	18.35(0.9)	18.38(1.1)	1.0	0.87(13)	0.94(6)

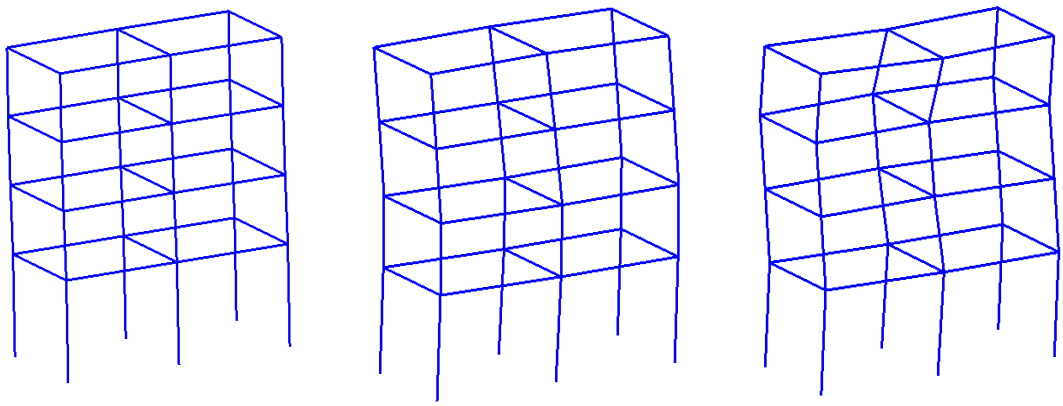

1st mode shape in the *y*-direction (f_1=2.56Hz, ξ_1=0.96%, MAC=0.94)

2nd mode shape in the *y*-direction (f_2=7.73Hz, ξ_2=1.03%, MAC=0.91)

3rd mode shape in the *y*-direction (f_3=13.50Hz, ξ_3=1.03%, MAC=0.88)

(a)

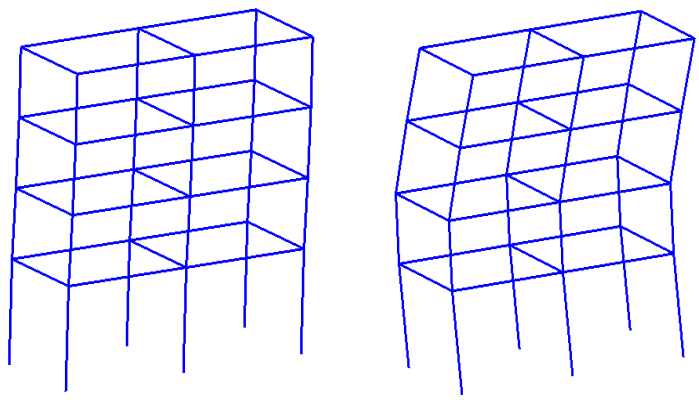

1st mode shape in the *x*-direction (f_1=3.10Hz, ξ_1=1.04%,MAC=0.92)

2nd mode shape in the *x*-direction (f_2=9.60Hz, ξ_2=1.09%, MAC=0.89)

(b)

Figure 2-11 Identified mode shapes: (a) The first three mode shapes in the *y*-direction; (b) The first two mode shapes in the *x*-direction.

2.4 Experimental Validations

2.4.1 Verification on a laboratory shear type steel frame structure

A fabricated seven-storey steel frame structure under ambient excitation as shown in Figure12 is used to verify the effectiveness and accuracy of using the proposed approach for operational modal identification. The total height of the frame column is 2.1m with each

story of 0.3m. The length of steel beam is 0.5m. To simulate the weight of each story, two pairs of steel mass blocks are bolted to the top and bottom of the beam so that the added steel blocks do not change the centroid of the beam section. The detailed geometrical dimensions and materials properties can be referred to [47].The theoretical first seven natural frequencies are 2.54Hz, 7.66Hz, 12.86Hz, 18.03Hz, 22.96Hz, 26.99Hz and 29.91Hz. It is noted that the higher modes from the fifth to seventh frequencies are closely spaced, and these higher modes are usually weakly exited under the ambient excitations. Experimental studies will be conducted to investigate whether the proposed approach can be effectively used for operational modal identification, and the performance will be compared with the existing method, i.e. SSI.

Figure 2-12 A laboratory 7-storey steel frame structure

Figure13 shows the sensor layout in the conducted ambient test. 10accelerometerswere installed on the steel frame to measure the horizontal acceleration responses under ambient excitations. They are numbered as S1, S2, …, S10. National Instruments (NI) compact DAQ data acquisition system was employed to record the structural dynamic responses. The sampling frequency is set as 2000Hz, and the ambient test data of 500s were recorded. The

recorded acceleration response from S4 is shown in Figure14. Since the experimental ambient test of the steel frame was conducted in the nighttime in the laboratory, the measurement noise is relatively low. Fourier spectrum of S4 response is shown in Figure15. It can be observed that the first seven natural frequencies of the frame structure can be identified by using the Fourier spectrum analysis. However, several false identification results are observed at, i.e. 11.64 Hz, 15.95 Hz and 21.16 Hz. SAR power spectrum analysis is then applied to analyse the acceleration responses recorded from sensorsS1 to S7 and the proposed approach is used for operational modal identification.Figure16 shows the SAR power spectra of the measured acceleration responses from S1-S7.It can be observed that seven natural frequencies are clearly and correctly identified in the SAR power spectrum, and no false identifications present in Figure 16. The comparison of frequency identification results between the proposed approach and the results available in literature [47] is listed in Table 2.The procedure described in Figure 2 is followed to further decompose the measured responses from S1-S7 to identify the mode shapes and damping ratios. The identified damping ratio of these seven vibration modes are presented in Table 2. The first seven bending mode shapes are shown in Figure17 by using the acceleration signals recorded from 7 accelerometers on the left side of the steel frame. The identification results demonstrate that the proposed approach provides accurate and reliable modal identification results of a 7-story steel frame structure under ambient excitation.

Table 2-2 Modal identification results of the laboratory frame structure

Mode	Natural Frequency (Hz)			Damping Ratio (%)	
	Ref. [47]	SSI	The proposed approach	SSI	The proposed approach
1	2.54	2.55	2.54	0.36	0.35
2	7.66	7.64	7.62	0.10	0.10
3	12.86	12.83	12.89	0.08	0.06
4	18.03	18.01	17.97	0.09	0.09
5	22.96	22.81	22.85	0.10	0.12
6	26.99	26.85	26.95	0.08	0.05
7	29.91	29.67	29.69	0.03	0.04

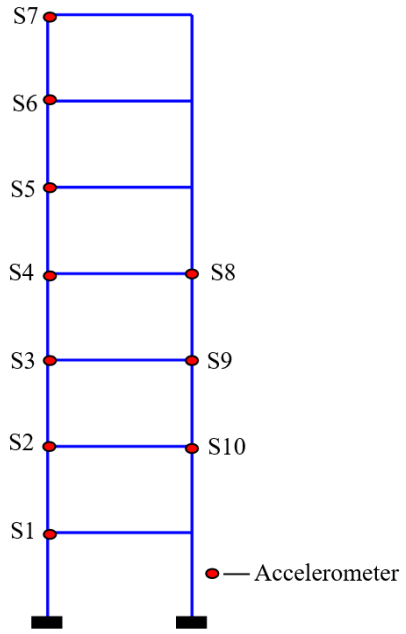

Figure 2-13 Sensor layout of the ambient test

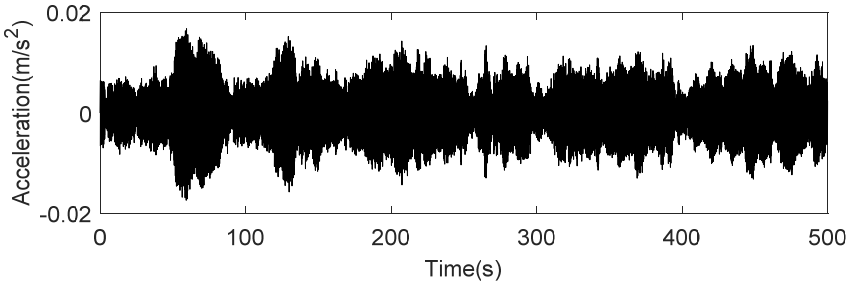

Figure 2-14 The recorded acceleration signal from S4

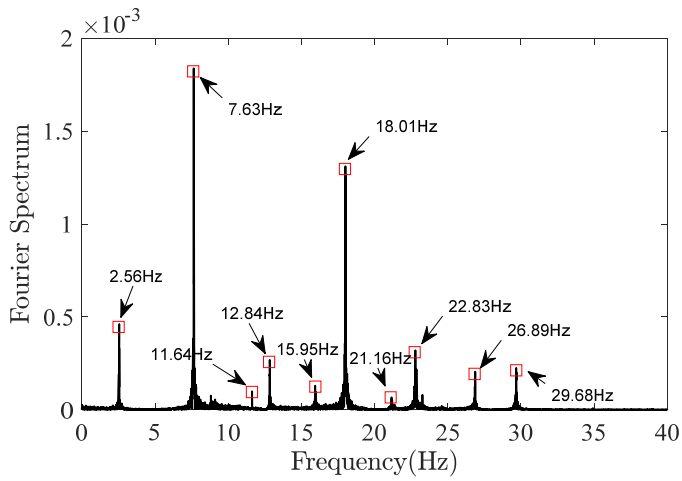

Figure 2-15 Fourier spectrum of the measured acceleration response from S4

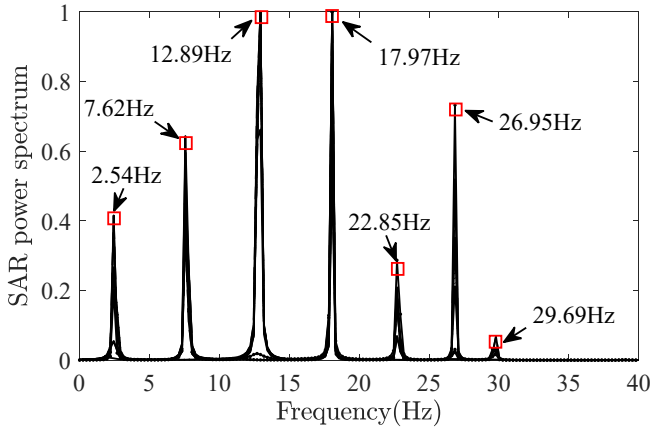

Figure 2-16 SAR power spectra of the measured acceleration responses from S1-S7

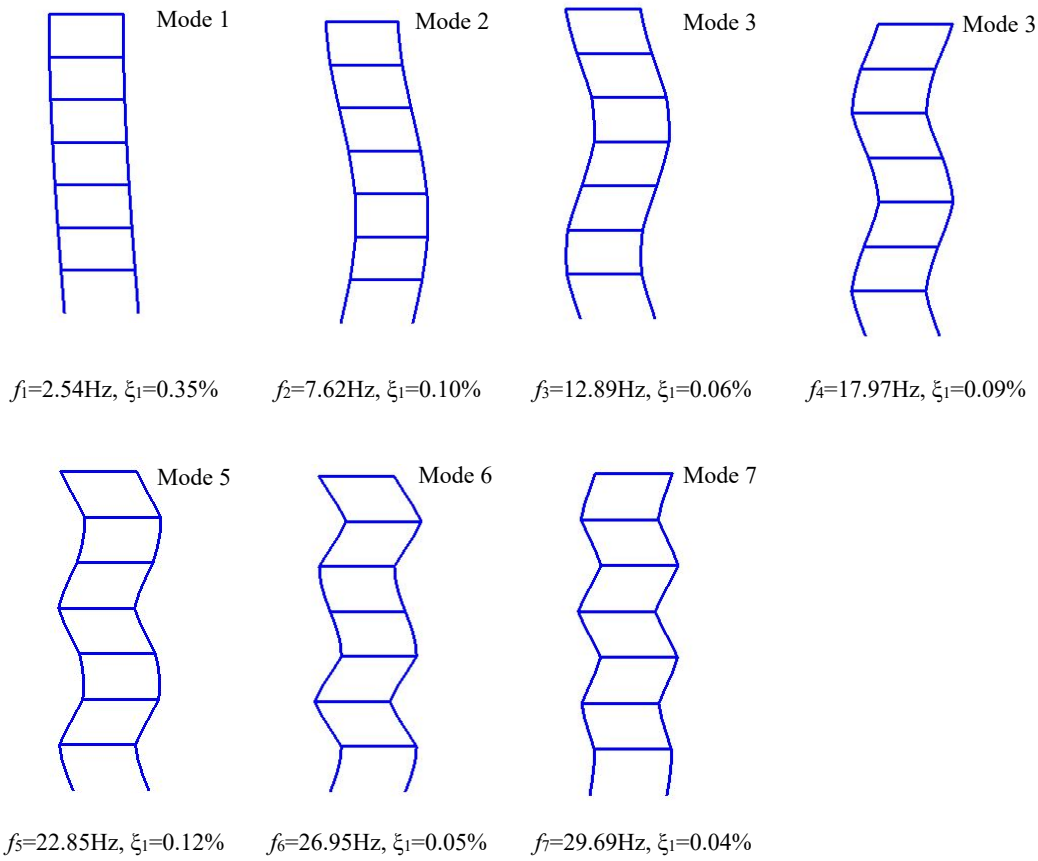

Figure 2-17 Identified mode shapes of the frame structure by using the proposed approach

2.4.2 Verification on a real footbridge under ambient vibration

In this section, a continuously monitored footbridge under ambient vibration is used to validate the effectiveness and performance of using the proposed approach for modal identification. This footbridge is located on the Medford campus of Tufts University, as

shown in Figure18 (a). The full length of the footbridge is 44m with two 22m spans, and the width is 3.9m. It is a composite bridge with a reinforced concrete deck supported on a steel frame structure. The more detailed material properties and geometrical parameters can be referred to [48-51]. The footbridge has been continuously monitored from January 2010 to May 2010 with 8 accelerometers installed on the footbridge, as shown in Figure18 (b). These accelerometers are numbered as S1, S2, …, S8. 17 weeks of measured data are available to public. A 300s data sample with a sampling frequency of 2048Hz was recorded once each hour during the operation of monitoring system. In addition, the measured data are down-sampled from 2048Hz to 128Hz to improve the computational efficiency.

(a)

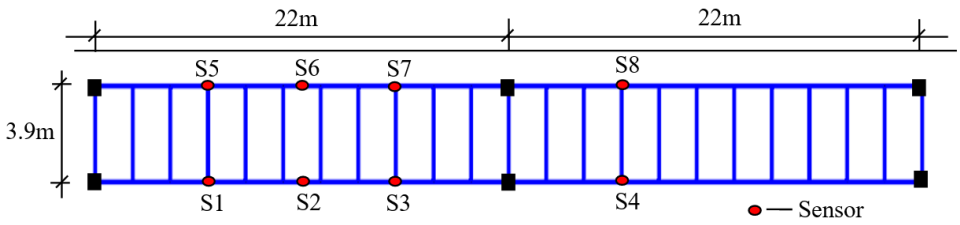

(b)

Figure 2-18 A real Footbridge and its sensor placement: (a) Overview of Dowling Hall Footbridge, (b) Sensor layout

In this study, the recorded acceleration data at10:00pm on 26April 2010 under environmental ambient vibration are selected for structural modal identification. Vibration signal measured byS1and the SAR power spectra of sensor responses S1-S4 are shown in Figures19 (a) and (b), respectively. It can be seen that six natural frequencies are effectively identified and

listed in Table 3. The identification results are compared with those available in a previous study [48]. The detected frequency components as shown in the SAR power spectra will be used to define the boundaries for EWT analysis. The decomposed six modes using the proposed improved EWT approach are shown in Figure20, and the estimated free vibration responses of the six modes are shown in Figure21.The damping ratios can be obtained from the envelop curves of free vibration responses by using the nonlinear curve fitting technique. The identified damping ratios are also listed in Table 3, and compared with the results in literature [48]. It can be observed that the identified modal parameters are close to those reported in the existing study. Minor differences are observed in several frequencies. This is because the environmental conditions when the acceleration responses were recorded in this study and in the previous study [48] were not exactly the same, which affected the vibration frequencies. Generally, the proposed approach can accurately identify the modal parameters of the footbridge under ambient vibration. The closely spaced modes, i.e. 13.10 Hz and 13.58 Hz as shown in Figure 19(b) can be well identified. However, when using traditional methods, i.e. SSI, very careful attention is required to select the appropriate order to obtain the reasonable identification results on frequencies and damping ratios.

Table 2-3 Modal identification results of a real footbridge

Mode	Natural Frequency (Hz)		Damping Ratio (%)	
	Ref. [48]	The proposed approach	Ref. [48]	The proposed approach
1	4.63	4.65	1.0	1.0
2	6.07	5.93	0.6	0.6
3	7.07	7.08	0.7	0.7
4	8.90	8.88	0.3	0.4
5	13.13	13.10	0.8	0.8
6	13.56	13.58	1.1	1.1

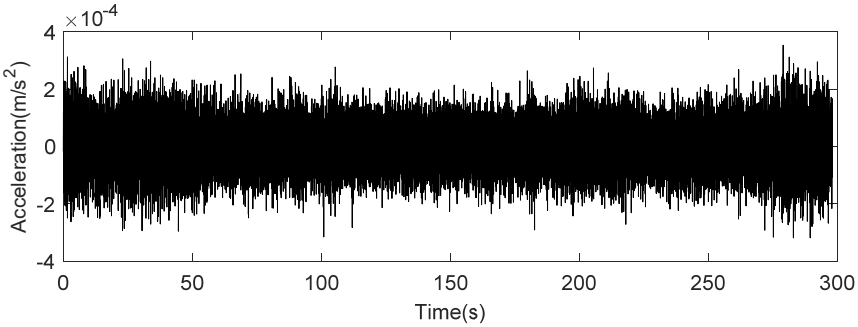

(a)

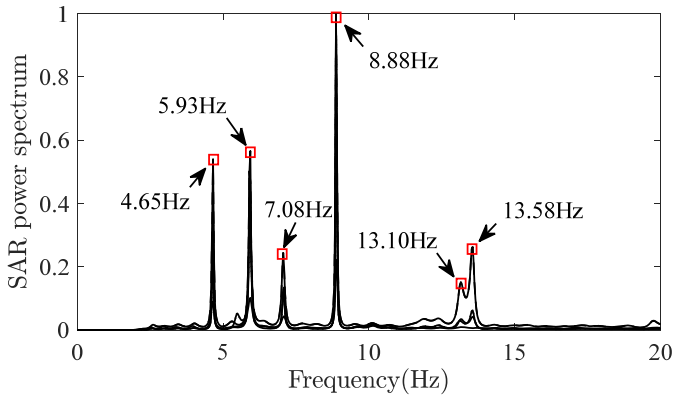

(b)

Figure 2-19 Measured response and spectrum analysis: (a) The measured acceleration from S1; (b) SAR power spectrum of S1-S4 responses

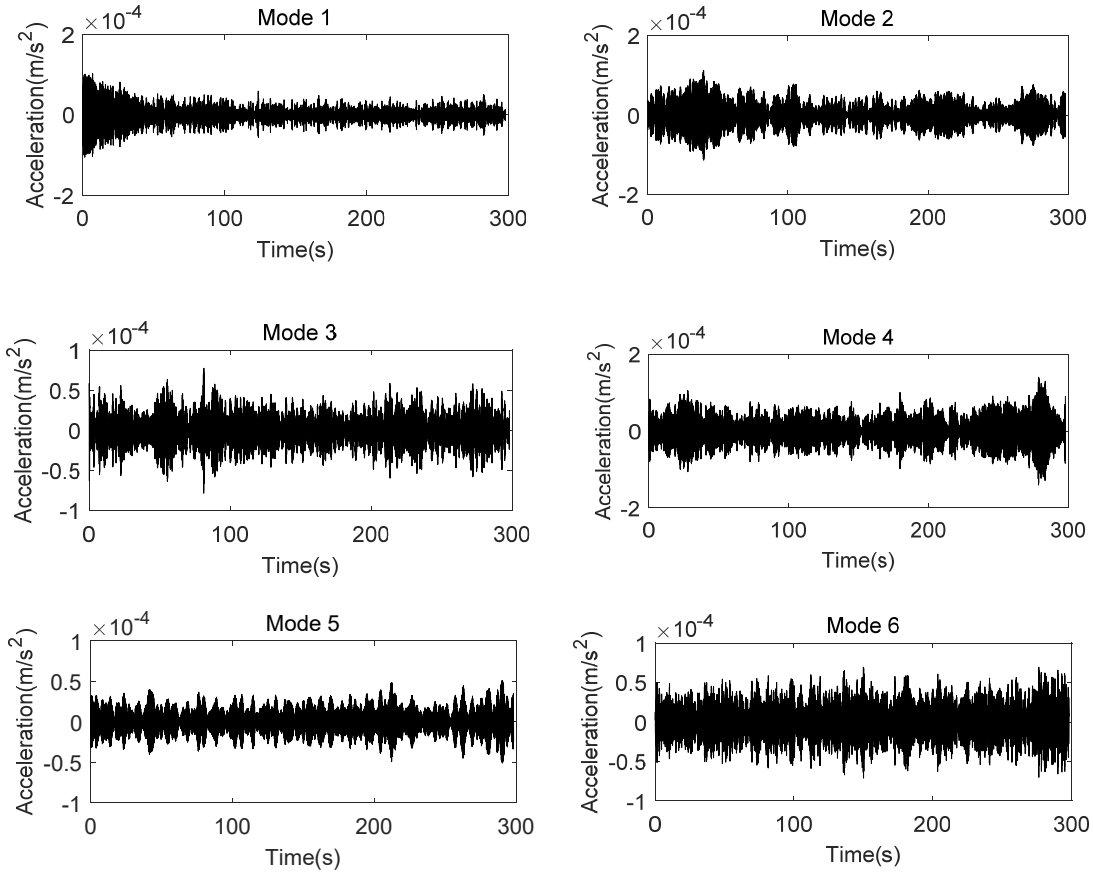

Figure 2-20 The decomposed IMFs of the acceleration response from S1

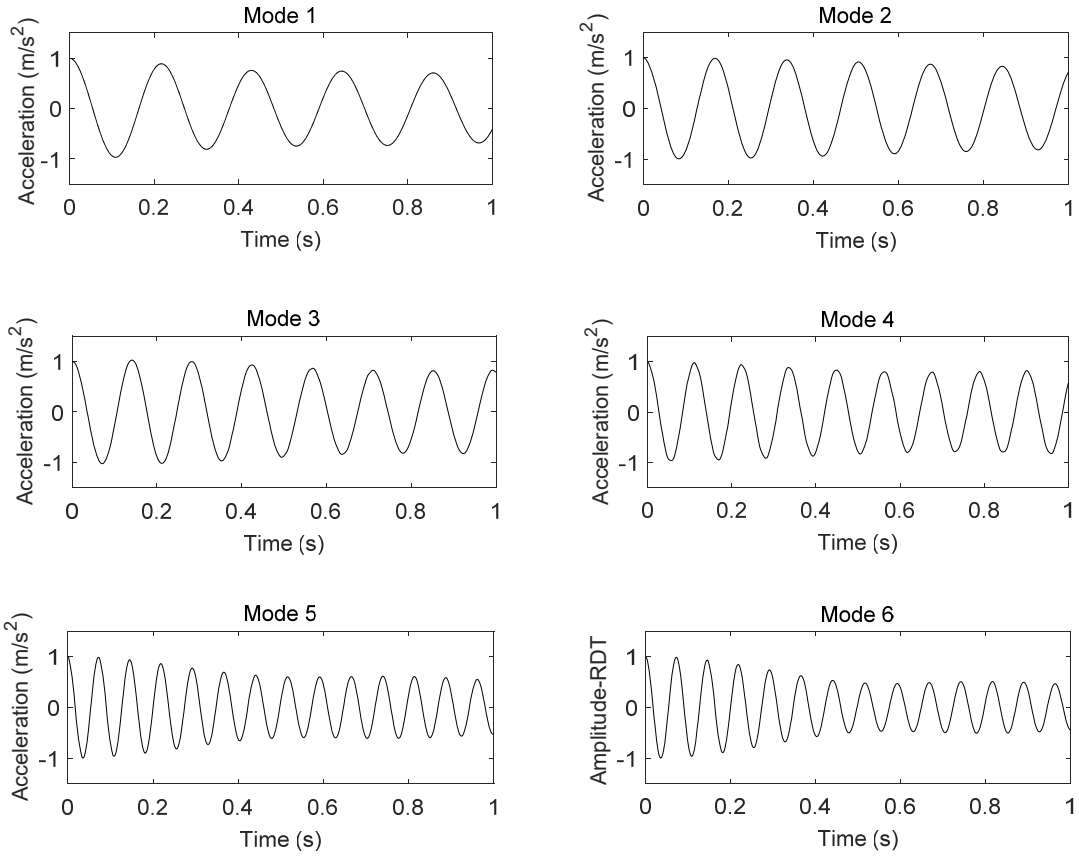

Figure 2-21 Estimated free vibration responses of individual modes of the acceleration response from S1

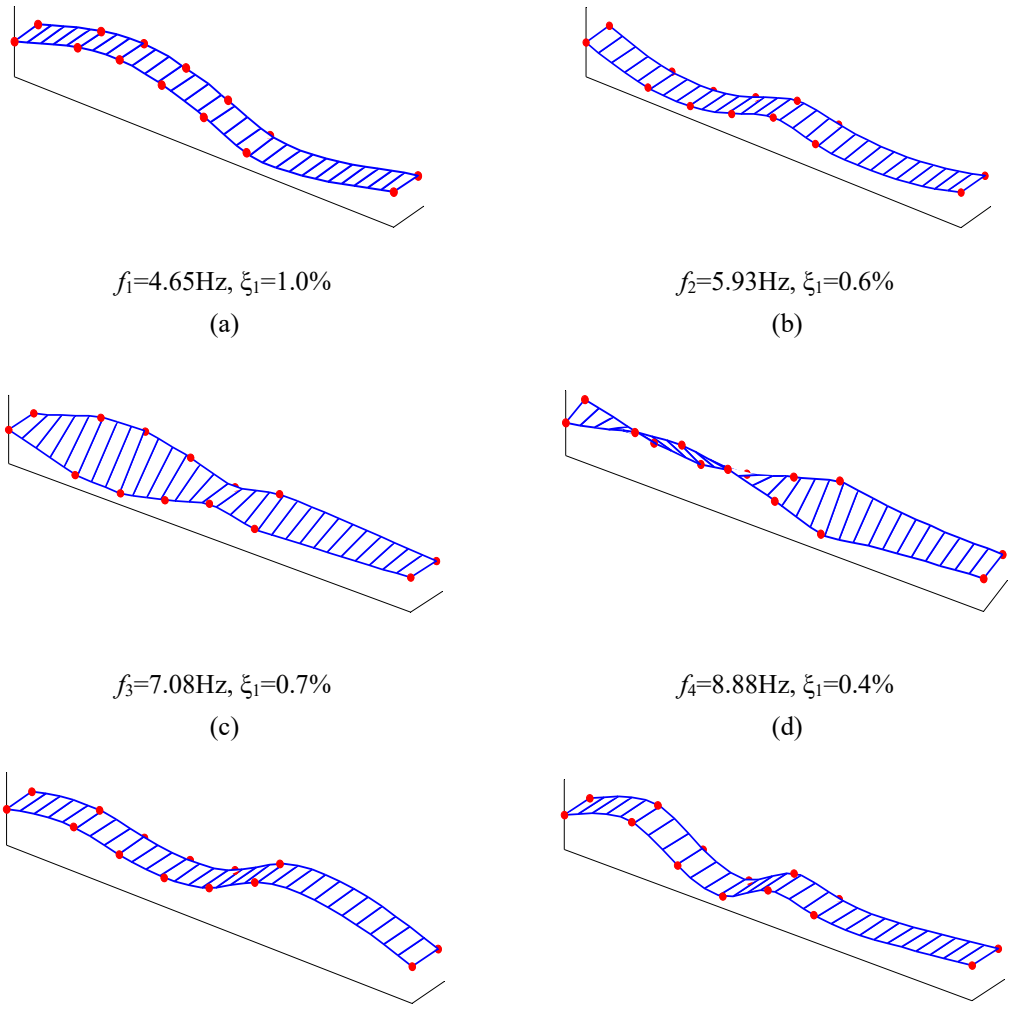

Figure 2-22. Identified six mode shapes of a real footbridge: (a) Mode 1; (b) Mode 2; (c) Mode 3; (d) Mode 4; (e) Mode 5; (f) Mode 6

2.5 Conclusions

This chapter proposes an improved EWT approach along with Hilbert Transform and RDT to perform the operational modal identification of civil engineering structures. Firstly, a spectral analysis approach, namely, the SAR power spectrum is employed to better define the boundaries of frequency components associated with EWT analysis. Then the second step is to employ EWT to decompose the measured vibration response into individual IMFs. Hilbert Transform and RDT are then performed to identify the structural modal parameters, i.e. frequencies, mode shapes and damping ratios, based on the extracted IMFs. The feasibility

and effectiveness of using SAR power spectrum for defining the filtering boundaries for EWT analysis is investigated with a simulated signal contaminated with a significant Gaussian white noise. The result shows that the SAR power spectrum is more reliable and effective to analyse the response with a significant noise than the Fourier spectrum. Numerical studies on a 4-storeyspatial frame structure under the ambient excitation are then conducted to validate the effectiveness and accuracy of using the proposed approach for operational modal identification. Experimental studies on a 7-story steel frame and a real footbridge under ambient excitation are further conducted to verify the accuracy and performance of the proposed approach. Based on numerical and experimental results, the following conclusions can be drawn:

(1) SAR power spectrum can effectively determine the boundaries of frequency components associated with EWT analysis, even for signals with significant noise effect;

(2) Closely-spaced modes can be effectively identified and decomposed by using the improved EWT approach; and

(3) Operational modal identification based on the proposed approach is accurate and reliable to identify modal parameters of structures under ambient vibration, i.e. natural frequencies, mode shapes and damping ratios.

In this chapter, the proposed approach is successfully applied for operational modal identification of linear structures. The further development and application of using this approach for time-varying or nonlinear system identification will be further studied.

References

[1] D. Ewins, Modal Testing: Theory and Practice and Application. Research Studies Press Ltd, 2nd edition, England, 2003.

[2] Brock J.E. (1983). Optimal Matrices Describing Linear Systems. *AIAA Journal*, 6(7): 1292-1296.

[3] Doebling S.W., Farrar C.R., Prime M.B. (1998). A summary review of vibration-based damage identification methods. *Shock and Vibration Digest*, 30(2): 91-105.

[4] Li J., Hao H. (2016). A review of recent research advances on structural health monitoring in Western Australia, *Structural Monitoring and Maintenance*, 3(1): 33-49.

[5] Li H., Li S.L., Ou J.P., Li H.W. (2009). Modal identification of bridges under varying environmental conditions: Temperature and wind effects. *Structural Control& Health Monitoring*, 17:495-512.

[6] Ren W.X, Zong Z.H. (2004). Output-only modal parameter identification of civil engineering structures. *Structural Engineering and Mechanics*, 17(3-4): 429-44.

[7] Brownjohn J.M.W., Magalhaes F., Caetano E., Cunha A. (2010). Ambient vibration re-testing and operational modal analysis of the Humber Bridge. *Engineering Structures*, 32(8): 2003-2018.

[8] Hu J., Lam H.F., Yang J.H. (2017). Operational modal identification and finite element model updating of a coupled building following Bayesian approach. *Structural Control& Health Monitoring*, 25(2):e2089.

[9] Cunha A., Caetano E., Delgado R. (2001). Dynamic tests on large cable-stayed bridge. *Journal of Bridge Engineering ASCE*, 6(1): 46-53.

[10] Bendat J.S., Piersol A.G. (1993). 2ndedition, New York: John Willey and Sons, pp.458.

[11] Dohler M., Lam X.B., Mevel L. (2013). Uncertainty quantification for modal parameters from stochastic subspace identification on multi-setup measurements. *Mechanical system and signal processing*, 36:562-581.

[12] Van Overschee P., De Moor B. (1996). Subspace identification for linear systems: theory, implementation and application. Dordrecht, Netherlands: Kluwer Academic Publisher, 254pp.

[13] James III G.H., Carne T.G., Lauffer J.P. (1993). The natural excitation technique (NExT) for modal parameter extraction from operating wind turbines. SAND 92-1666 UC-261, Sandia National Laboratories, Albuquerque, NM.

[14] Caicedo J.M., Dyke S.J., Johnson E.A. (2004). Natural excitation technique and eigensystem realization algorithm for phase I of the IASC-ASCE benchmark problem: Simulated data. *Journal of Engineering Mechanics ASCE,* 130: 49-60.

[15] Nagarajaiah S., Basu B. (2009). Output only modal identification and structural damage detection using time frequency & wavelet techniques, *Earthquake Engineering and Engineering Vibration*, 8(4): 583-605.

[16] Li J., Hao H., Zhu H.P. (2014). Dynamic assessment of shear connectors in composite bridges with ambient vibration measurements. *Advances in Structural Engineering*, 17(5): 617-638.

[17] Ni P.H., Li J., Hao H., Xia Y., Wang X.Y., Lee J.M., Jung K.H. (2018). Time-varying system identification using variational mode decomposition. *Structural Control & Health Monitoring*, 25, e2175.

[18] Dziedziech K., Staszewski W.J., Ghosh A., Basu B., Uhl T. (2017). Characterisation of instantaneous dynamic parameters in vibration analysis of tuned liquid column dampers. *Nonlinear Dynamics*, 90(1):717-731.

[19] Staszewski W.J. (1997). Identification of damping in mdof systems using time-scale decomposition. *Journal of Sound and Vibration*, 203(2):283-305.

[20] Ruzzene M., Fasana A., Garibaldi L., Piombo B. (1997). Natural frequencies and dampings identification using Wavelet Transform: application to real data. *Mechanical Systems and Signal Processing*, 11(2): 207-218

[21] Staszewski-Correa T., Kareem A. (2006). Efficacy of Hilbert and wavelet transforms for time-frequency analysis. *Journal of Engineering Mechanics ASCE*, 132(10): 1037-49.

[22] Huang N.E., Shen Z., Long S.R., Wu M.C., Shih H.H., Zheng Q., Yen N.C., Tung C., Liu H.H. (1998). The empirical mode decomposition and the Hilbert spectrum for nonlinear and non-stationary time-series analysis, Proceedings of the Royal Society of London A: Mathematical, Physical and Engineering Sciences: The Royal Society, p. 903-995.

[23] Nagarajaiah S. (2009). Adaptive passive, semiactive, smart tuned mass dampers: identification and control using empirical mode decomposition, Hilbert transform, and short-term Fourier transform. *Structural Control & Health Monitoring*, 16(7–8):800-841.

[24] Mahato S., Teja M.V., Chakraborty A. (2015). Adaptive HHT (AHHT) based modal parameter estimation from limited measurements of an RC framed building under multi-component earthquake excitations. *Structural Control & Health Monitoring*, 22(7):984-1001.

[25] Yang J.N., Lei Y., Pan S., Huang N. (2003). System identification of linear structures based on Hilbert-Huang spectral analysis, Part I: normal modes. *Earthquake Engineering and Structural Dynamics*, 32(9):1443-67.

[26] Bao C.X., Hao H., Li Z.X., Zhu X.Q. (2009). Time-varying system identification using a newly improved HHT algorithm. *Computer and Structures*, 87: 1611-23.

[27] Wu Z., Huang N.E. (2009). Ensemble Empirical Mode Decomposition: A Noise-Assisted Data Analysis Method. *Advances in Adaptive Data Analysis*, 1: 1-41.

[28] Gilles J. (2013). Empirical Wavelet Transform. *IEEE Transactions on Signal Processing*, 61(16): 3999-4010.

[29] Pan J., Chen J.L., Zi Y.Y., Li Y.M., He Z.J. (2016). Mono-component feature extraction for mechanical fault diagnosis using modified empirical wavelet transform via data-driven adaptive Fourier spectrum segment. *Mechanical Systems and Signal Processing*, 72-73: 160-183.

[30] Kedadouche M., Thomas M., Tahan A. (2016). A comparative study between Empirical Wavelet Transforms and Empirical Mode Decomposition Methods: Application to bearing defect diagnosis. *Mechanical Systems and Signal Processing*, 81: 88-107.

[31] Hu Y., Tu X.T., Li F.C., Li H.G., Meng G. (2017). An adaptive and tacholess order analysis method based on enhanced empirical wavelet transform for fault detection of bearing with varying speeds. *Journal of Sound and Vibration*, 409: 241-255.

[32] Amezquita-Sanchez J.P., Adeli H. (2015). A new music-empirical wavelet transform

methodology for time-frequency analysis of noisy nonlinear and non-stationary signals. *Digital Signal Processing*, 45: 55-68.

[33] Ljung L. (1999). System Identification: Theory for the User. 2nd Edition, Upper Saddle River, NJ: Prentice Hall.

[34] Marple L. (1980). A New Autoregressive Spectrum Analysis Algorithm. *IEEE Transactions on Acoustics Speech and Signal Processing*, 28(4): 441-454.

[35] Kay S.M. (1988). Modern Spectral Estimation: Theory and Application. Englewood Cliffs, NJ: Prentice-Hall.

[36] Stoica P. (1988). A high-order Yule-Walker method for estimation of the AR parameters of an ARMA model. *Systems and Control Letters*, 11: 99-105.

[37] Matlab Optimization Toolbox, User's Guide, R2017a.

[38] Vandiver J.K., Dunwoody A.B., Campbell R.B., Cook M.F. (1982). A mathematical basis for the random decrement vibration signature analysis technique. *ASME Journal of Mechanical Design*, 104(3): 307-13.

[39] Kua C.J., Cermakb J.E., Chouc L.S. (2007). Random decrement based method for modal parameter identification of a dynamic system using acceleration responses. *Journal of Wind Engineering and Industrial Aerodynamics*, 95(6): 389-401.

[40] Wang Z.C., Chen G.D. (2012). Recursive Hilbert-Huang Transform Method for Time-Varying Property Identification of Linear Shear-Type Buildings under Base Excitations. *Journal of Engineering Mechanics ASCE*, 138(6): 631-639.

[41] Wang Z.C., Chen G.D. (2013). Analytical mode decomposition of time series with decaying amplitudes and overlapping instantaneous frequencies. *Smart Materials and Structures*, 138(6): 631-639.

[42] Amezquita-Sanchez J.P., Park H.S., Adeli H. (2017). A novel methodology for modal parameters identification of large smart structures using MUSIC, empirical wavelet transform, and Hilbert transform. *Engineering Structures*, 147: 148-59.

[43] Mazzoni S., Scott M.H., Mckenna F., Fenves G.L., et al. (2006). Open system for earthquake engineering simulation-user manual. Pacific Earthquake Engineering Research Center, University of California, Berkeley, California.

[44] Li J., Law S.S., Ding Y. (2012). Substructure damage identification based on response reconstruction in frequency domain and model updating. *Engineering Structures*, 41: 270-284.

[45] Behmanesh I., Moaveni B. (2016). Accounting for environmental variability, modeling errors, and parameters estimation uncertainties in structural identification. *Journal of Sound and Vibration*, 374: 92-110.

[46] Moaveni B., Behmanesh I. (2012). Effects of changing ambient temperature on finite element model updating of the Dowling Hall Footbridge. *Engineering Structures*, 42: 58-68.

[47] Behmanesh I., Moaveni B. (2015). Probabilistic identification of simulated damage on the Dowling Hall footbridge through Bayesian finite element model updating. *Structural Control & Health Monitoring*, 22(3): 463-483.

[48] Moser P., Moaveni B. (2013). Design and deployment of a continuous monitoring system for the Dowling Hall Footbridge. Experimental Techniques, 37:15-26.

CHAPTER 3 TIME-VARYING SYSTEM IDENTIFICATION BY ENHANCED EMPIRICAL WAVELET TRANSFORM BASED ON SYNCHROEXTRACTING TRANSFORM

ABSTRACT[2]

This chapter proposes an improved Empirical Wavelet Transform (EWT) approach based on Synchroextracting Transform (SET) for time-varying system identification. SET is first conducted to analyse the frequency components of a non-stationary vibration signal measured from a time-varying system instead of using classical Fourier Spectrum. Then the filtering boundaries for EWT analysis can be defined. The non-stationary vibration signal can be decomposed into a finite number of intrinsic mode functions (IMFs) with the improved EWT. When the IMFs are obtained, the instantaneous frequencies of each mode can be effectively identified by using Hilbert Transform. In numerical simulations, a simulated signal with a high level noise is analysed to verify the feasibility of using SET to define the filtering boundaries. The proposed approach is used to identify the instantaneous frequencies of a time-varying two-storey shear type building under earthquake and Gaussian white noise excitations, respectively. Experimental investigations on a time-varying bridge-vehicle system are conducted to verify the effectiveness of the proposed method. The results in numerical simulations and experimental validations demonstrate that the proposed approach can identify and track the instantaneous frequencies of a time-varying system with good accuracy.

3.1 Introduction

Vibration characteristics of engineering structures often change over time due to the environmental condition changes, mass and stiffness changes due to the material loss or

[2]This chaper was published in *Engineering Structures* with the full bibliographic citation as follows: Xin, Y., Hao, H. & Li, J. (2019). Time-varying system identification by enhanced Empirical Wavelet Transform based on Synchroextracting Transform. *Engineering Structures*, 109313. https://doi.org/10.1016/j.engstruct.2019.109313.

strength degradation, and the effects of extreme loads, etc. These time-varying system effects can be widely observed in the field of civil and mechanical engineering. For example, the friction mechanisms used in industry can introduce the changes in the stiffness and damping of a structure under normal operations. Civil engineering structures, such as long-span bridges and high-rise buildings, may also exhibit time varying vibration characteristics under earthquake, tornados and hurricanes, because of the nonlinearities in the structures, and the changes in the stiffness and boundary conditions [1]. Therefore, identifying the vibration characteristics of time-variant structures is vital for researchers and engineers to understand and assess the operational conditions of structures.

Over the past decades, system identification of time-variant structures based on the measured dynamic responses (i.e. acceleration, displacement responses) has obtained a significant amount of attention. Various techniques have been developed and reported in the literatures [2-3]. Generally, these methods could be classified into two categories: (1) time-varying system identification based on adaptive algorithms [4-6]; (2) Time-varying system identification by using time-frequency analysis techniques [7-9]. For example, Wang et al. [3] used a slide-window least-squares (LS) parameter estimation method to track the real-time frequency of the high-voltage switch structures under the cyclic loading excitations in the laboratory. Yang et al. [6] developed an online adaptive tracking technique based on LS parameter estimation to identify the system parameters of a time- variant structure. In addition, in the literature [10], an improved LS strategy is developed to identify the hysteretic parameters of a nonlinear system under arbitrary external excitations.

In recent years, time-frequency analysis techniques have been widely conducted for system identification of time-variant structures, i.e. by using Hilbert Transform (HT) [11-12] and Wavelet Transform (WT) [13-15]. Shi et al. [16] applied Empirical Mode Decomposition (EMD) with HT to identify the modal parameters of a time-varying multi-degree-of-freedom (MDOF) system. Bao et al. [2] developed an improved Hilbert-Huang Transform (HHT) method for time-varying system identification by using the autocorrelation functions of structural dynamic responses as the input to HHT, and therefore reduced the noise effect and improved the accuracy of identification. Wang et al. [17] proposed a recursive HT system

identification approach, which have been successfully used to track the real-time structural characteristics of linear shear-type buildings under the forced vibration. WT, as an alternative time-frequency analysis technique, has been widely used for the system identification of linear and non-linear structures, and non-stationary signal analysis. Hou et al. [18] proposed a continuous wavelet transform (CWT) based technique for instantaneous modal identification of a time-varying structure subjected to an earthquake excitation. Wang et al. [7] used the extracted wavelet ridges to identify the instantaneous frequency (IF) of a time-varying structure under the stochastic excitations.

More recently, a new time-frequency analysis technique, named Synchrosqueezing Transform (SST), has been developed by Daubechies et al. [19], and has been applied for IF identification [20-21]. The main advantage of SST is that it squeezes the time-frequency coefficients into the IF trajectory, which can be approximated to an ideal tine-frequency analysis representation. However, SST has a lower time-frequency resolution when it is used to reconstruct the interested components of a non-stationary signal. Based on the theory of SST, a novel time-frequency analysis method, namely Synchroextracting Transform (SET), have been developed by Yu et al. [22], which can generate a more energy-concentrated analysis result than using SST.

In this study, an improved Empirical Wavelet Transform (EWT) approach [23] based on SET is developed for IF identification of time-varying structures. In the past studies [24-25], several modified EWT methods have been successfully applied for linear system identification and mechanical fault diagnosis. However, to the authors' best knowledge, there has been no study yet on using or improving EWT for IF identification of time-varying structures. With the vibration responses measured from a time-varying structure, time-frequency analysis based on SET is first performed to determine the filtering boundaries of EWT instead of using the ordinary Fourier Spectrum. Then EWT is applied to extract the individual modes from the vibration response signals. Each mode is an amplitude-modulation and frequency-modulation signal with a narrow-band property with a varying IF. The IF of each time-variant component can be identified by using HT. A synthetic signal which consists of two time-varying frequency components is first used to verify the

feasibility and accuracy of the proposed approach. Then the proposed method is employed to identify the IF of a two-storey shear-type building under the forced vibration. Experimental studies on a real bridge under the heavy traffic loads are conducted to further validate the effectiveness of the proposed method.

The remainder of this chapter is organized as follows. Section 2 briefly explains the principle of EWT and SET, and provides a fundamental process of time-varying system identification based on the proposed approach. In Section 3, numerical studies on a synthetic signal and a two-storey time-varying structure are conducted to investigate the accuracy and effectiveness of the proposed approach. In Section 4, Experimental verifications on a highway bridge under the traffic loads are performed to identify the instantaneous frequencies. Section 5 provides the discussions and conclusions on the obtained results.

3.2 Theoretical Background and Development

3.2.1 The traditional Empirical Wavelet Transform (EWT)

Assuming $x(t)$ is a time domain signal which consists of N Intrinsic Mode Functions (IMFs), that is $x(t) = \sum_{i=1}^{N} x_i(t)$. The Fourier spectrum of the signal can be divided into N segments, and each segment includes an individual IMF of the signal. ω_n is denoted as the boundary of Fourier Spectrum required for EWT analysis, and each segment is filtered by an interval $[\omega_n, \omega_{n+1}]$ (where $\omega_0 = 0$ and $\omega_n = \pi$). A transient phase with a width of $2\tau_n$ is defined for each ω_n, and τ_n is written as

$$\tau_n = \gamma \times \omega_n \tag{3.1}$$

$$0 < \gamma < min_n \frac{\omega_{n+1} - \omega_n}{\omega_{n+1} + \omega_n} \tag{3.2}$$

The empirical scaling function and the empirical wavelets can be then defined as follows [23]

$$\widehat{\emptyset}_n(\omega) = \begin{cases} 1 & if \ \ |\omega| \leq (1-\gamma)\omega_n \\ \cos\left[\frac{\pi}{2}\beta\left(\left(\frac{1}{2\gamma\omega_n}(|\omega| - (1-\gamma)\omega_n)\right)\right)\right] & if \ \ (1-\gamma)\omega_n \leq |\omega| \leq (1+\gamma)\omega_n \\ 0 & \text{oherwise} \end{cases} \tag{3.3}$$

$$\widehat{\Psi}_n(\omega) = \begin{cases} 1 & if \ \ \omega_n + \tau_n \leq |\omega| \leq \omega_{n+1} - \tau_{n+1} \\ \cos\left[\frac{\pi}{2}\beta\left(\frac{1}{2\tau_{n+1}}(|\omega| - \omega_{n+1} - \tau_{n+1})\right)\right] & if \ \ \omega_{n+1} - \tau_{n+1} \leq |\omega| \leq \omega_{n+1} + \tau_{n+1} \\ \sin\left[\frac{\pi}{2}\beta\left(\frac{1}{2\tau_n}(|\omega| - \omega_n + \tau_n)\right)\right] & if \ \ \omega_n - \tau_n \leq |\omega| \leq \omega_n + \tau_n \\ 0 & \text{oherwise} \end{cases} \tag{3.4}$$

in which, $\beta(x)$ is an arbitrary function which is defined on [0,1] and satisfies:

$$\beta(x) = \begin{cases} 0 & if \ \ x \leq 0 \\ \beta(x) + \beta(1-x) = 1 & \forall x \in [0,1] \\ 1 & if \ \ x \geq 1 \end{cases} \tag{3.5}$$

Many functions satisfy the characteristics of Equation (3.5), and the most used function $\beta(x)$ in literature [28] is:

$$\beta(x) = x^4(35 - 84x + 70x^2 - 20x^3) \qquad \forall x \in [0,1] \tag{3.6}$$

The filter bank of the empirical wavelets can be constructed by adopting Fourier spectrum segment information into Equations (3.3) and (3.4). After the scaling function and empirical wavelets are derived, the detail coefficients are given as

$$W_x(n,t) = \int x(\tau)\Psi_n(\tau - t)d\tau = F^{-1}\left(\hat{X}(\omega)\overline{\widehat{\Psi}_n(\omega)}\right) \tag{3.7}$$

The approximation coefficients can be obtained by

$$W_x(0,t) = \int x(\tau)\emptyset_n(\tau - t)d\tau = F^{-1}\left(\hat{X}(\omega)\overline{\widehat{\emptyset}_n(\omega)}\right) \tag{3.8}$$

Then, the modes extracted from the vibration signal are described as

$$f_0(t) = W_x(0,t) * \emptyset_1(t) \tag{3.9}$$

$$f_k(t) = W_x(k,t) * \Psi_k(t) \tag{3.10}$$

and the reconstruction signal can be obtained as

$$\hat{x}(t) = W_x(0,t) * \emptyset_1(t) + \sum_{n=1}^{N} W_x(n,t) * \Psi_n(t) = F^{-1}\big(W_x(0,\omega)\widehat{\emptyset}_1(\omega) + \sum_{n=1}^{N} \widehat{W}_x(n,\omega) * \widehat{\Psi}_n(\omega)\big) \tag{3.11}$$

3.2.2 The improved EWT

As mentioned in the literature [24], it is a big challenge to employ Fourier Spectrum for determining the boundaries associated with EWT analysis when a signal is contaminated with significant noise and non-stationary components. Under this circumstance, an improved time-frequency analysis approach is worth of investigations to identify and track the real-time frequency components of the non-stationary signals. With an improved energy-concentration of the time-frequency representation, SET is employed to improve the effectiveness and accuracy in defining the boundaries for using EWT to perform the non-stationary signal decomposition.

3.2.3 Synchroextracting Transform (SET)

A multicomponent vibration signal $x(t)$, which consists of N non-stationary frequency components, is presented as

$$x(t) = \sum_{i=1}^{N} x_i(t) = \sum_{i=1}^{N} A_i(t) e^{j\int \omega_i(t)dt} \tag{3.12}$$

in which $A_i(t)$ and $\omega_i(t)$ represent the instantaneous amplitude and frequency of the *i*th time-varying mono-component, respectively. The different modes can be well separated based on a sufficient distance, i.e.,

$$\omega_{i+1}(t) - \omega_i(t) > 2\Delta \quad , j \in \{1, \dots, m-1\} \tag{3.13}$$

where Δ represents the frequency support of the window function. The Short Time Fourier Transform (STFT) representation $G_e(t,\omega)$ of the vibration signal $x(t)$ can be expressed as the following first-order approximation form [22, 26, 27]

$$G_e(t,\omega) \approx \sum_{i=1}^{N} A_i(t) * \hat{g}\big(\omega - \omega_i(t)\big)\ e^{j\int \omega_i(t)dt} \tag{3.14}$$

Then, the IF of the vibration signal is derived using Equation (3.14)

$$\omega(t) = \sum_{i=1}^{N} \omega_i(t) = -j * \frac{\partial G_e(t,\omega)}{G_e(t,\omega)} \tag{3.15}$$

In Equation (3.14), $\hat{g}$ is the Fourier transform of the window function $g \in L^2(R)$.

To generate an energy-concentrated time-frequency representation, Yu et al. [22] suggested to only retain the time-frequency information of the STFT results which is significantly related to the time-variant characteristics of a target signal. In this case, SET is expressed as

$$Te(t,\omega) = G_e(t,\omega) * \delta\big(\omega - \omega_i(t)\big) \tag{3.16}$$

In Equation (3.16), $\delta\big(\omega - \omega_i(t)\big)$ can be further expressed as

$$\delta\big(\omega - \omega_i(t)\big) = \begin{cases} 1, & \omega = \omega_i(t) \\ 0, & else \end{cases} \tag{3.17}$$

Combining Equations (3.14) - (3.17), SET can be deduced as

$$Te(t,\omega)_{\omega - \sum_{i=1}^{N} \theta'_i(t) = 0} = Ge(t,\omega)_{\omega - \sum_{i=1}^{N} \theta'_i(t) = 0} \approx \sum_{i=1}^{N} A_i(t) * \hat{g}(0)\ e^{j\int \omega_i(t)dt} \tag{3.18}$$

2.2.2 Time-varying system identification based on the improved EWT

For an *n* degree-of-freedom (DOF) time-variant system, the equation of motion is given as

$$\mathbf{M}(t)\ddot{u}(t) + \mathbf{C}\dot{u}(t) + \mathbf{K}u(t) = \mathbf{f}(t) \tag{3.19}$$

in which $\mathbf{M}$, $\mathbf{K}$, and $\mathbf{C}$ denote $n \times n$ time-variant mass, stiffness and damping matrices, respectively; $u(\mathrm{t})$, $\dot{u}(\mathrm{t})$ and $\ddot{u}(\mathrm{t})$ are displacement, velocity and acceleration responses of the time-variant system, respectively; $\mathbf{f}(t)$ is the external excitation force vector.

Equation (3.19) can be further transformed into modal spatial coordinates, which can be expressed as [1]

$$\ddot{q}_i(t) + 2h_{0i}\dot{q}_i(t) + \omega^2{}_{0i}q_i(t) = \frac{\emptyset_i^T \mathbf{f}(t)}{\boldsymbol{M_i}} \qquad (i = 1,2, \dots n) \tag{3.20}$$

where $\boldsymbol{M_i} = \emptyset_i^T \mathbf{M} \emptyset_i$ denotes the *i*th modal mass, $\emptyset_i$ is the *i*th mode shape vector. The natural frequency of the *i*th modal response is represented by ω_{0i}. When zero mean Gaussian white noise is assumed as the external excitation of the system, the IF of the *i*th modal response can be written as

$$\omega^2{}_i(t) = \omega^2{}_{0i}(t) - \frac{\frac{\emptyset_i^T \mathbf{f}(t)}{\boldsymbol{M_i}} q + H\left[\frac{\emptyset_i^T \mathbf{f}(t)}{\boldsymbol{M_i}}\right] H[q]}{[q^2 + (H[q])^2]} \tag{3.21}$$

where *H* denotes HT, and the second term of Eq. (21) is about a zero mean fast time-varying function. The natural frequency of the time-variant system can be obtained from the identified IF of its analytical signal by filtering out the fast varying component.

The measured dynamic response of the *l*-th DOF $u_l(t)$ of the time-varying system can be described as a function of modal responses

$$u_l(t) = \sum_{i=1}^{n} \phi_{li} q_i \tag{3.22}$$

where ϕ_{li} is the *l*-th coefficient of the *i*-th mode shape vector. The decomposed *i*th modal response $u_l{}^{(i)}(t)$ from the vibration signal measured from the *l*-th DOF can be represented as

$$u_l{}^{(i)}(t) = \phi_{li} q_i \tag{3.23}$$

The obtained mono-component signal $u_l{}^{(i)}(t)$ can be written as an analytical signal $Z_l{}^{(i)}(t)$

$$Z_l{}^{(i)}(t) = \phi_{li} q_i + \phi_{li} H[q_i] = \phi_{li} A_i e^{j \int \omega_i(t) dt} \tag{3.24}$$

From Equation (3.24), it indicates that the IF of the decomposed vibration signal equals to the IF of the modal response. The flow chart of time-varying system identification based on the improved EWT along with HT is shown in Figure 3-1.

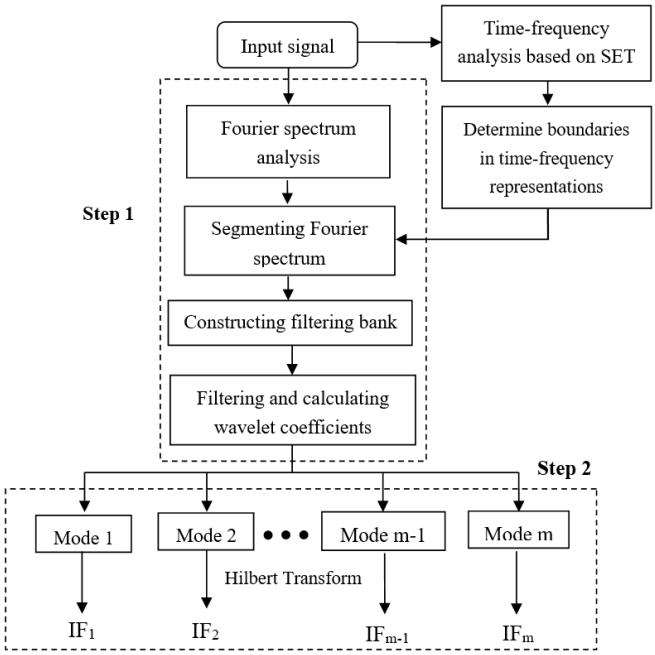

Figure 3-1 The flow chart of the proposed approach for time-varying system identification.

3.3 Numerical Studies

3.3.1 A simulation signal

In this section, a simulated signal $y(t)$, as defined in Equation (3.25), is used to investigate the effectiveness of using SET to determine the boundaries for EWT analysis. It consists of two time-variant frequency components $y_1(t)$ and $y_2(t)$ which are described in Equations (3.26) and (3.27), respectively.

$$y(t) = y_1(t) + y_2(t) + noise(t) \tag{3.25}$$

$$y_1(t) = 2\sin(14\pi t + 4\pi \arctan((2t-2)^2)) \tag{3.26}$$

$$y_2(t) = 2\sin(48\pi t + 20\pi \sin t) \tag{3.27}$$

To further validate the feasibility of using SET to improve the performance of EWT, a high-level noise, that is, 20% Gaussian white noise, is added to the simulated signal. The sampling duration is set as 5 seconds with a sampling rate of 120Hz. Figure 3-2 and Figure 3-3 show the time domain response and the Fourier Spectrum of the simulated signal,

respectively. It can be seen that the two frequency components are not obvious and therefore properly defining the filtering boundaries for EWT analysis may not be straightforward. SET is employed to track and determine the time-varying frequency components of the vibration signal. In order to verify the effectiveness of using SET, the classical time-frequency analysis technique, namely, WT, is also performed to identify the instantaneous frequencies of the signal. The time-frequency analysis results obtained from WT and SET are shown in Figures 3-4 (a) and (b), respectively. It can be observed that both WT and SET can effectively track the two time-variant frequency components of the non-stationary signal. However, as can be seen from Figure 3-4(b), SET provides a clearer trajectory and more concentrated energy distribution than WT. Based on the time-frequency analysis results from SET, it is clear to define a constant filtering boundary between these two frequency components. When the filtering boundaries are exactly determined, the Fourier Spectrum of the non-stationary signal can be segmented for EWT, and used to construct the filtering bank. Then, the individual modes can be effectively decomposed, and the obtained two time-varying IMFs are shown in Figure 3-5 (a) and Figure 3-6 (a), respectively. To further verify the effectiveness of the proposed approach, Variational Mode Decomposition (VMD) [28] is also performed to identify the time-varying components of the signal, and the decomposed two IMFs are shown in Figure 3-5 (b) and Figure 3-6 (b), respectively. By comparing the identified results in Figures 3-5 and Figure 3-6, it is clearly observed that the improved EWT is more reliable and accurate to identify the time-varying components of the signal. In addition, Figures 3-7 (a) and (b) display the Fourier spectrum of the extracted IMFs using two methods, respectively, it can be observed that the non-stationary simulated signal can be accurately decomposed by using the improved EWT approach, even under a significant noise effect.

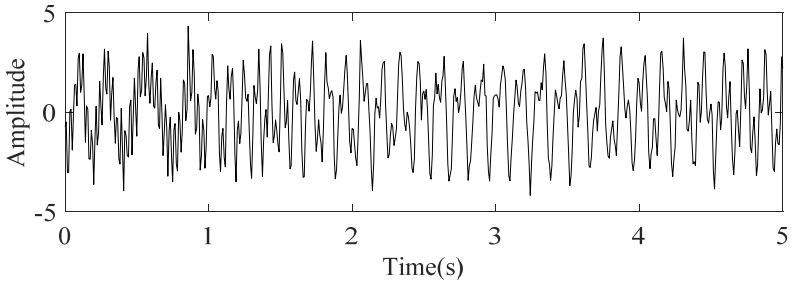

Figure 3-2 The simulated signal with 20% noise.

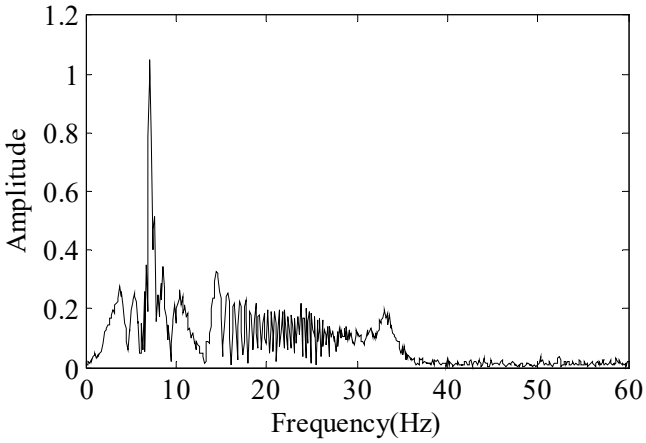

Figure 3-3 Fourier Spectrum of the simulated signal.

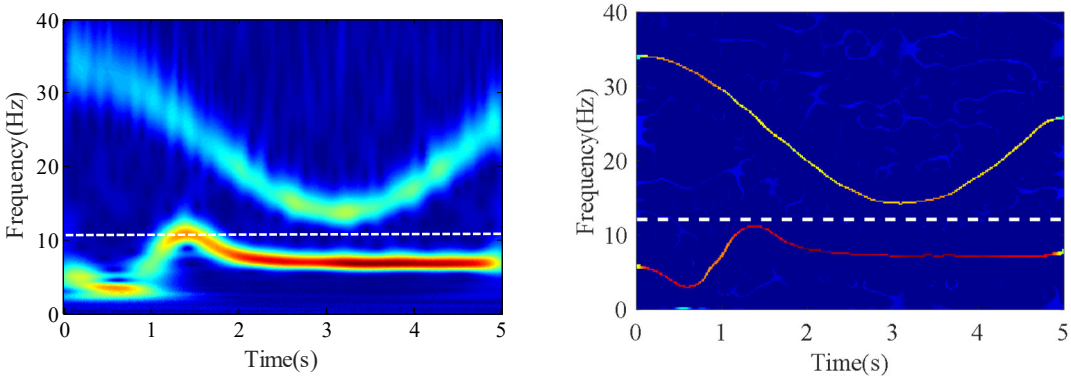

(a) (b)

Figure 3-4 Time-frequency analysis of the non-stationary signal using: (a) WT; (b) SET.

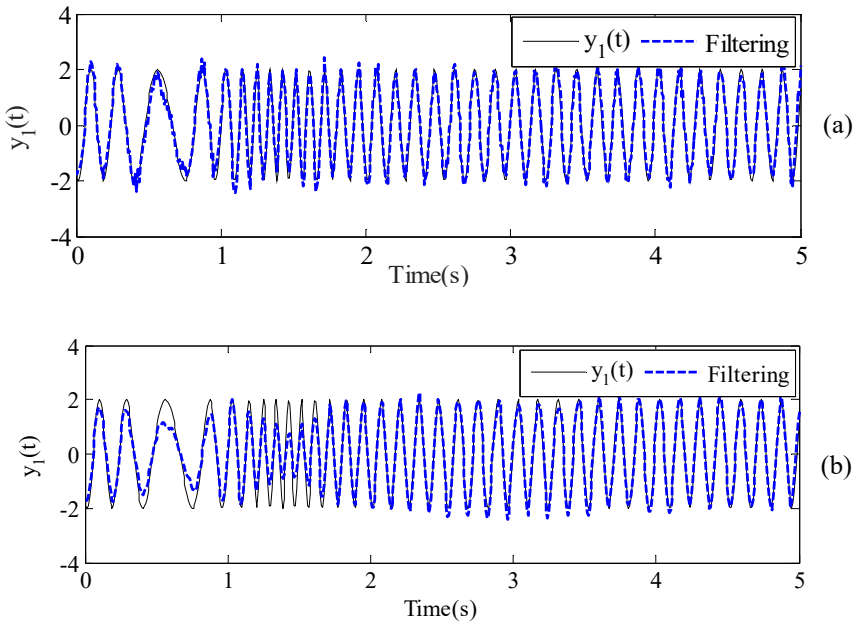

Figure 3-5 The decomposed first mode using: (a) Improved EWT; (b) VMD.

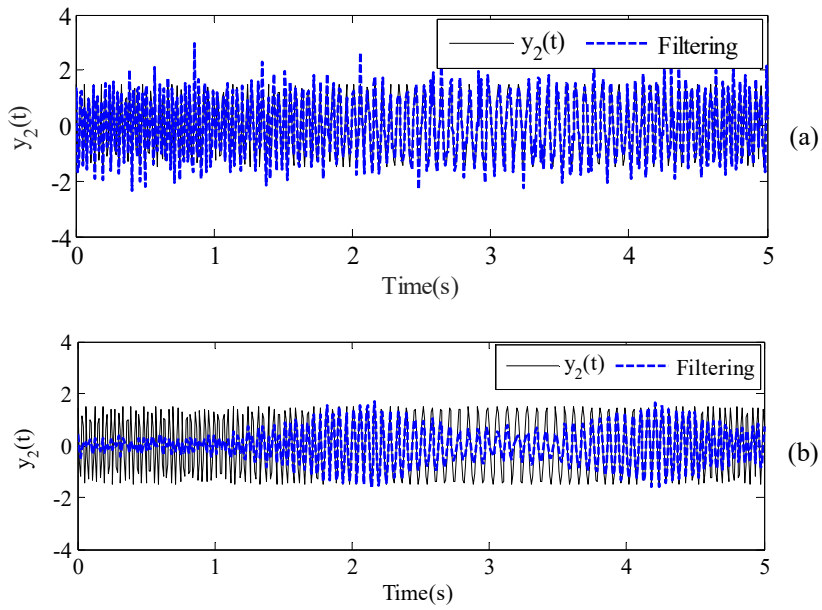

Figure 3-6 The decomposed second mode using: (a) Improved EWT; (b) VMD.

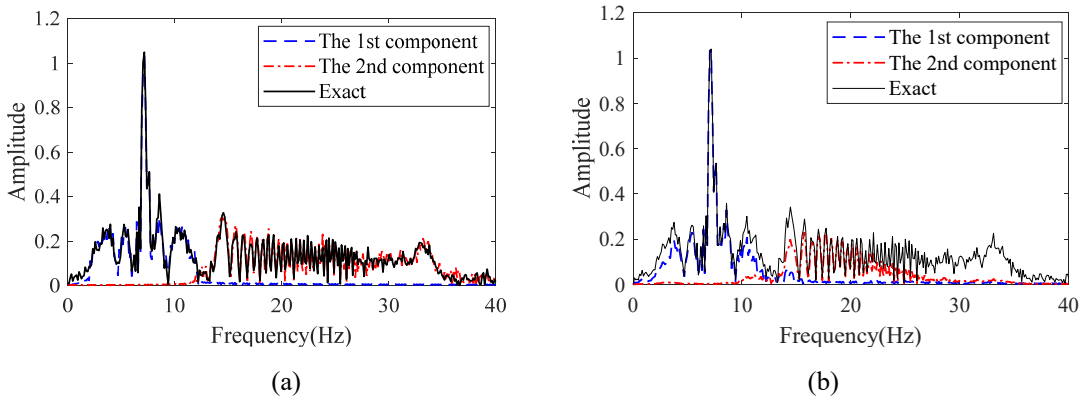

Figure 3-7 Fourier spectrum of the two decomposed IMFs using: (a) Improved EWT; (b) VMD.

3.3.2 Time-varying system identification of a two-storey shear building

Numerical studies on a two-storey shear building, as shown in Figure 3-8, are conducted to investigate the accuracy and effectiveness of using the proposed approach for time-varying system identification. The time-varying structure has two masses of m_1=2.50×10^5kg at the first floor, and m_2=1.70×10^5kg at the top floor. Two damping coefficients c_1=9.6×10^2 kN·s/m and c_2=3.2×10^2kN·s/m are assumed for these two stories, respectively. The stiffness of the first storey k_1 is defined to be periodically reduced from 2.10×10^5 kN·m to 1.404×10^5 kN·m during a period of t=4 to 16 seconds. That is, $k_1 = \{2.1 - 0.058(t-4) - 0.131\sin[0.5\pi(t-4)]\} \times 10^5$ kN·m. The stiffness of the second storey is set to be linearly reduced from 1.05×10^5 kN·m to 0.7×10^5 kN·m in a time duration between 4s and 8s.

3.3.3 Instantaneous frequency identification

In order to investigate the effectiveness and reliability of the proposed time-varying system identification approach, the following two excitations are considered in the numerical case studies.

Case 1: The 1940 EI Centro ground acceleration record as shown in Figure 3-9 (a) is selected as the external excitation to the two-storey building.

Case 2: The structure is excited by a Gaussian white noise process with zero mean and a standard deviation of 0.1g (g denotes the gravitational acceleration), as shown in Figure

3-9 (b).

For the above mentioned two cases, the displacement responses of the first floor are measured with a sampling rate of 50Hz. The recorded vibration signals for the two cases are shown in Figures 3-10 (a) and (b), respectively. Since the non-stationary characteristics of the structural dynamic responses are unknown in prior, SET is first performed to determine the filtering boundaries for EWT analysis. The SET results of these two cases are shown in Figures 3-11 (a) and (b), respectively. It is clearly seen from Figure 3-11 that a frequency interval can be defined between the instantaneous frequencies of these two time-varying frequency components. Therefore the filtering boundaries for the analysis of EWT can be well defined as three constant frequencies, 0.8Hz, 3.5Hz and 7.5Hz. Once the filtering boundaries are defined, the two time-varying frequency components of structural displacement responses can be exactly separated by the EWT approach. The decomposed signals for the two cases by using EWT are shown in Figures 3-12 (a) and (b), respectively. Two mono-components are well separated and identified from the vibration responses. The identified instantaneous frequencies of the two cases by using HT are presented in Figures 3-13 (a) and (b). Significant fluctuations are observed by comparing the results from HT with the exact values. By filtering out the rapidly varying component of the identified instantaneous frequencies using a low-pass filter, the average value of these instantaneous frequencies can accurately represent the time-varying frequency components of the structure.

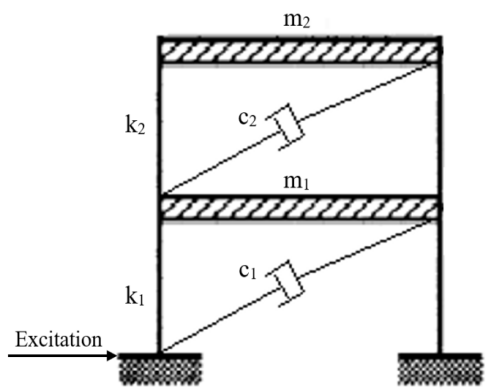

Figure 3-8 The two-storey shear building model.

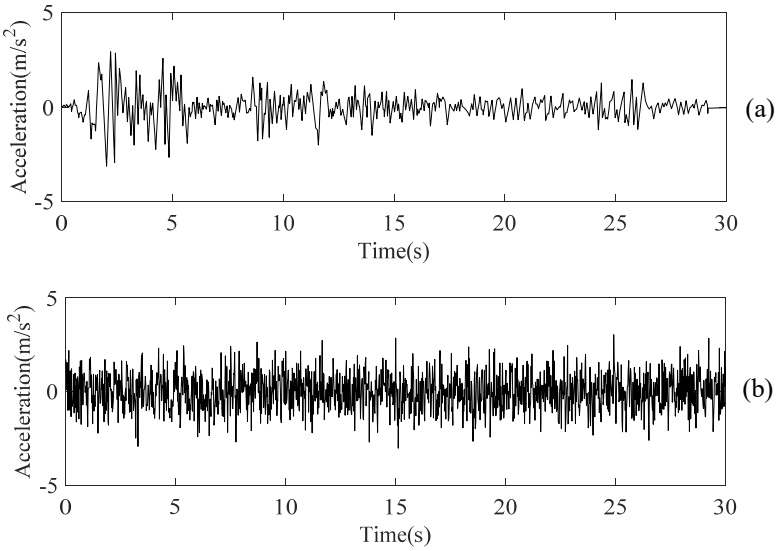

Figure 3-9 External excitations in two numerical cases: (a) El Centro earthquake; (b) Gaussian white noise.

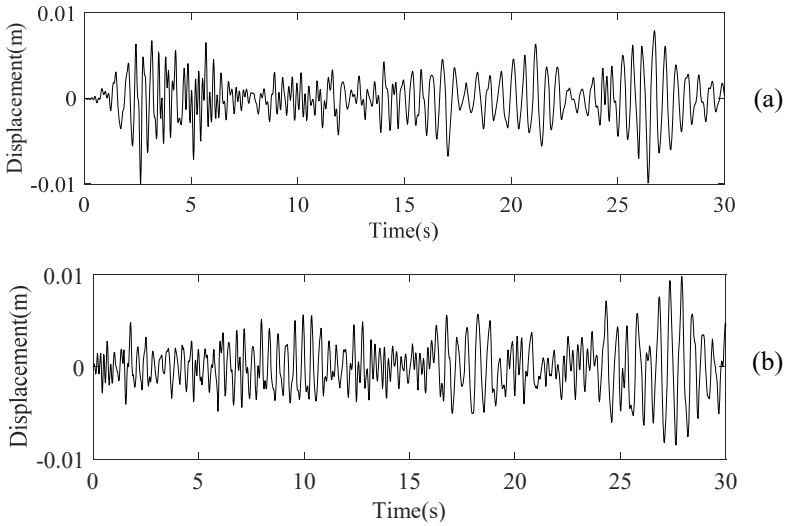

Figure 3-10 Displacement responses of the first floor: (a) under earthquake excitation; (b) under Gaussian white noise excitation.

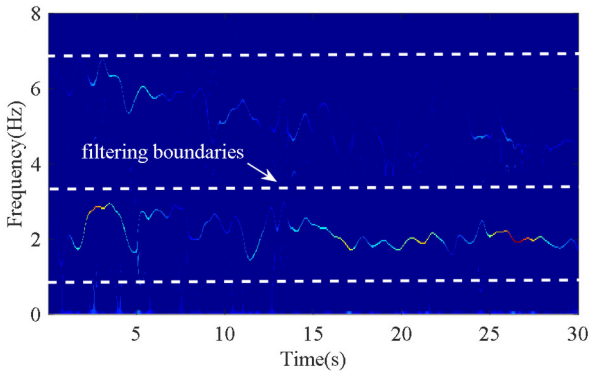

(a)

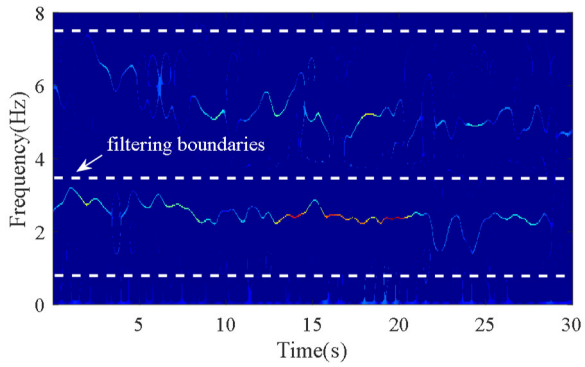

(b)

Figure 3-11 The detected filtering boundaries based on SET: (a) under earthquake excitation; (b) under Gaussian white noise excitation.

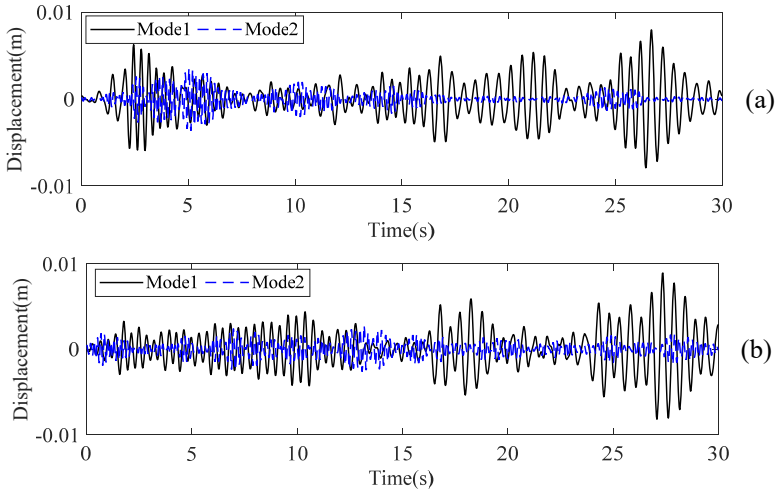

Figure 3-12 The decomposed two individual modes using the improved EWT: (a) under earthquake excitation; (b) under Gaussian white noise excitation.

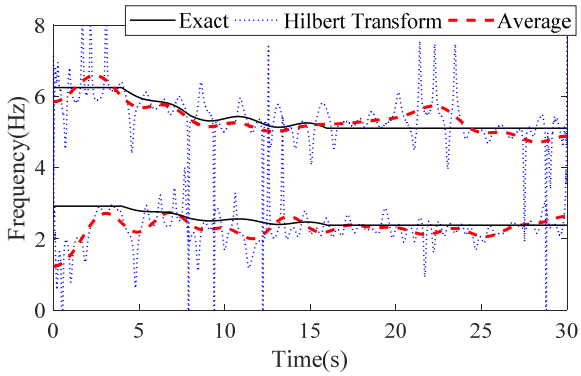

(a)

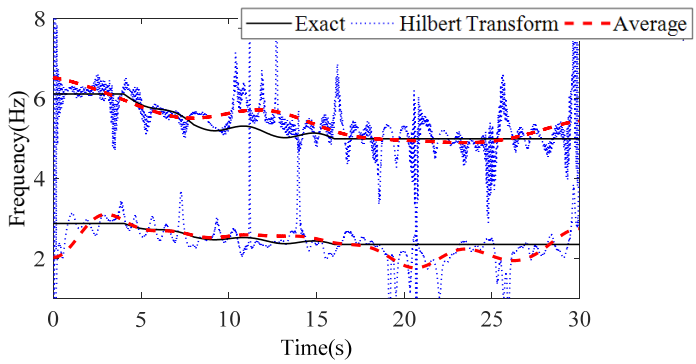

(b)

Figure 3-13 The identified instantaneous frequencies by the proposed approach: (a) under earthquake excitation; (b) under Gaussian white noise excitation.

3.3.4 Effects of measurement noise

To further investigate the performance and reliability of the proposed approach, 5% and 10% noises are added to the structural dynamic responses obtained in Case 1 and Case 2. The same procedure as above is followed to analyse the data. The extracted average frequency components from the two decomposed modes under the effects of the different noise levels are presented in Figures 3-14 (a) and (b), respectively. It can be observed that the identified instantaneous frequencies are close to the exact values even if under the effects of high-level noise. The noise level has a minor effect on the identification accuracy.

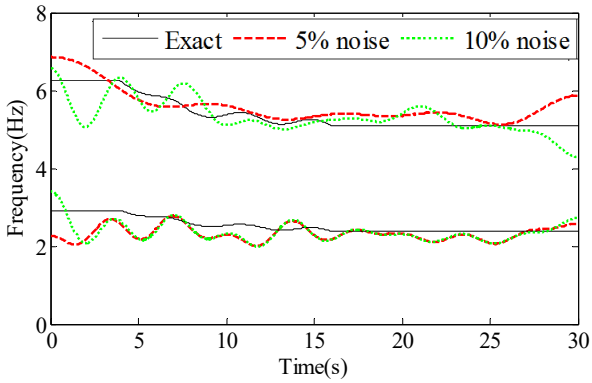

(a)

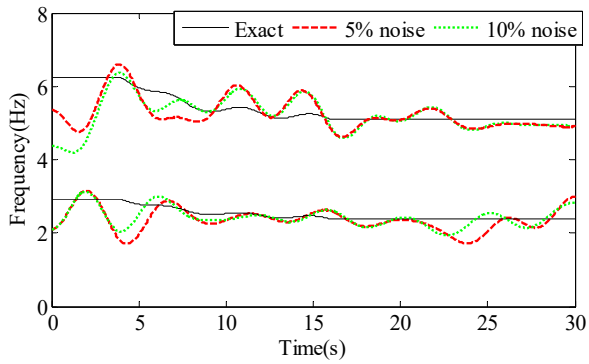

(b)

Figure 3-14 The identified instantaneous frequencies under different noise levels: (a) under earthquake excitation; (b) under Gaussian white noise excitation.

3.4. Experimental Investigations

3.4.1 A highway bridge

To further investigate the performance of using the proposed approach to identify the instantaneous frequency of real civil structures, experimental studies on an operational highway bridge are conducted. The target bridge consists of three spans, which is shown in Figure 3-15. The beams are 17.10m long in the 1st and 3rd spans, and the central-span beam is 16.96m long with two half joints at the ends. The half joints shown in Figure 3-15 (b) have been strengthened by using external vertical steel strengthening rods as well as the horizontal strengthening rods on the two sides of the joint. This half-joint arrangement is different from the typical arrangement as there is no bearing between the suspended and supporting nibs

while the joints are post-tensioned by an internal tendon crossing the joint. On the abutments and piers, the girders are tied by cast-in-situ infill panels, which are supported by two 4-column piers. The structural dynamic responses of the bridge under the operational traffic loads are recorded by a structural health monitoring system installed in 2014. Strain, displacement and acceleration responses at various locations of the bridge are measured. The acceleration responses of the bridge under the traffic loads are measured with two tri-axial accelerometers (S_1, S_2) at the mid-span of the bridge. The locations of the acceleration sensors are shown in Figure 3-16. A camera is installed to capture the traffic vehicles on the bridge when the monitoring system is activated, with a frame rate of 1Hz. The health monitoring system can be trigged to record the dynamic responses data of the bridge subjected to the traffic when the strain response in any of the strain rings reaches a pre-defined threshold (equals to $120\mu\varepsilon$). A two minutes window with 60 seconds pre-triggering and 60 seconds afterwards is applied to record the dynamic responses of an event with a sampling rate of 130Hz. Since only two accelerometers are installed at the mid-span of the bridge to record the vibration signals of the bridge, the natural frequencies of the structure under the different traffic loading and environmental conditions can be identified, however the mode shape could not be obtained in this case.

(a)

(b)

Figure 3-15 An operational highway bridge: (a) Bird view of the bridge; (b) The reinforced half joints.

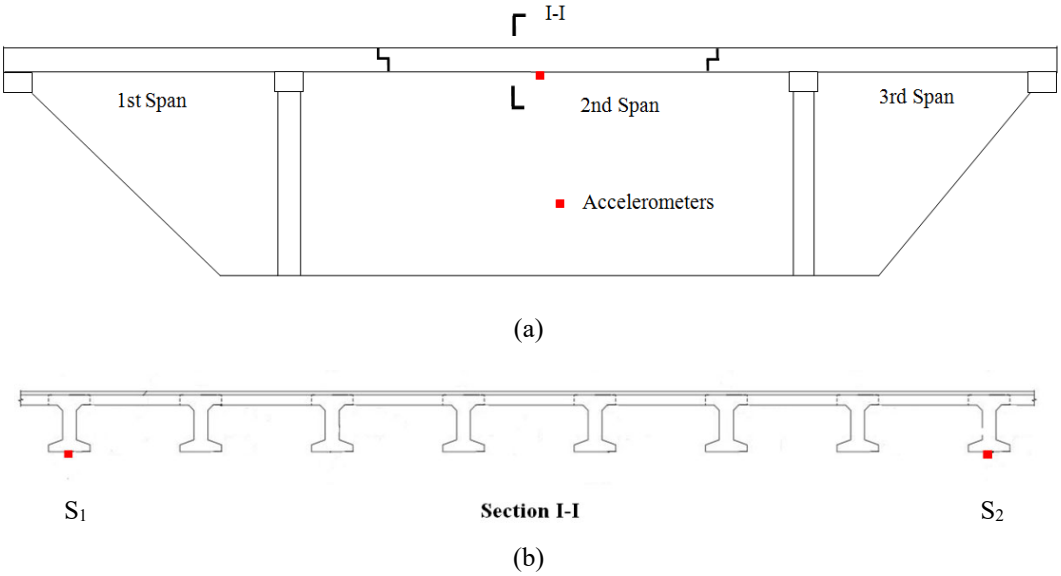

Figure 3-16 Locations of the installed accelerometers: (a) Elevation view of the bridge; (b) Cross section of the mid-span

3.4.2 Time-varying instantaneous frequency identification

In this section, modal identification of the bridge structure under the weak external excitation is conducted, and then the instantaneous frequencies identification of the bridge under heavy traffic loads is further discussed and investigated by using the proposed approach. Based on the images captured by the installed camera, a light weight traffic excitation case is selected for the first case. In this event, the traffic and the measured acceleration response from the accelerometer S_1 are presented in Figures 3-17 (a) and (b), respectively. It can be seen from the measured vibration signal that the maximum response amplitude of the vibration signal is approximately equal to 0.007g, which can be considered as a relatively small dynamic response measured from the highway bridge. Due to the light weight traffic and the mass of those vehicles is negligible as compared to that of the bridge, the acceleration signal is used for modal identification of the bridge structure to understand the vibration characteristics of the bridge. However, since the global mode shapes of the structure cannot be obtained by only using the responses at two locations from two accelerometers, a finite element model, as shown in Figure 3-18, developed based on the design drawings is employed to

approximately represent the bridge. The analytical modal frequencies and mode shapes obtained from the finite element model are shown in Figures 3-19 (a)-(d), respectively. By cross checking the frequencies and mode shapes, four main frequencies of the measured vibration signal are identified by using the fast Fourier Transform (FFT) as 5.78Hz, 7.88Hz, 12.20Hz, and 18.87Hz, respectively, as shown in Figure 3-20. In order to ensure the reliability of the identified modes, the phase information of each mode extracted from the vibration signals recorded by two accelerometers are compared in Figures 3-21(a)-(d), respectively. It can be seen from Figure 3-21 that the two vibration signals have similar phase information at the first and the third modes, however, the opposite phase is clearly observed at the second and the fourth modes. Compared with the mode shapes from the finite element model, it can be concluded that the first and third modes correspond to the bending modes of the bridge structure. However, the second and fourth modes are the torsional modes of the bridge. For bridges under traffic loads, higher modes are normally considered to have relatively lower contributions to the responses than the lower modes [29], however, it is observed that the third mode of the bridge at 12.20Hz has the highest energy in the Fourier Spectrum. The potential reason can be described as: with the roughness and damaged surface on the pavement of the deck, for example, as shown in Figure 3-22, the highway bridge is usually forced by the bouncing motion of the moving traffic loads [30-32], which may excite the high frequency components of the bridge.

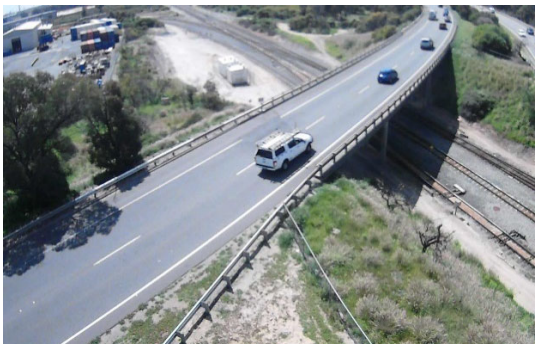

(a)

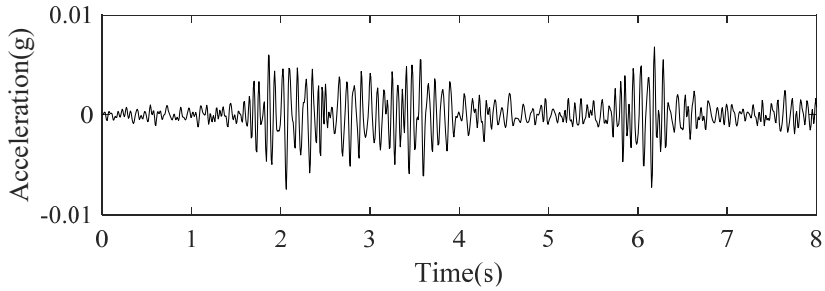

(b)

Figure 3-17 (a) The light weight traffic excitation; (b) the measured acceleration from sensor S_1.

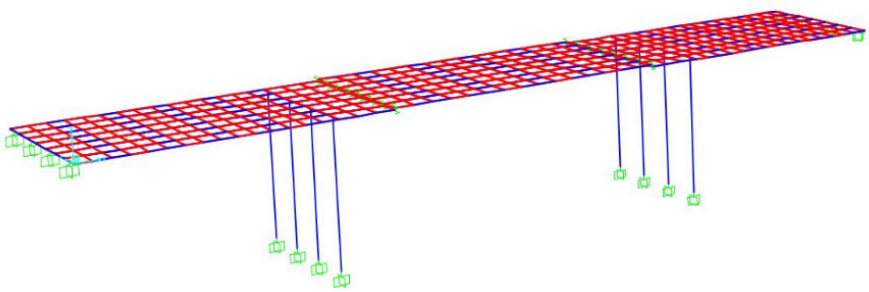

Figure 3-18 The finite element model of the bridge.

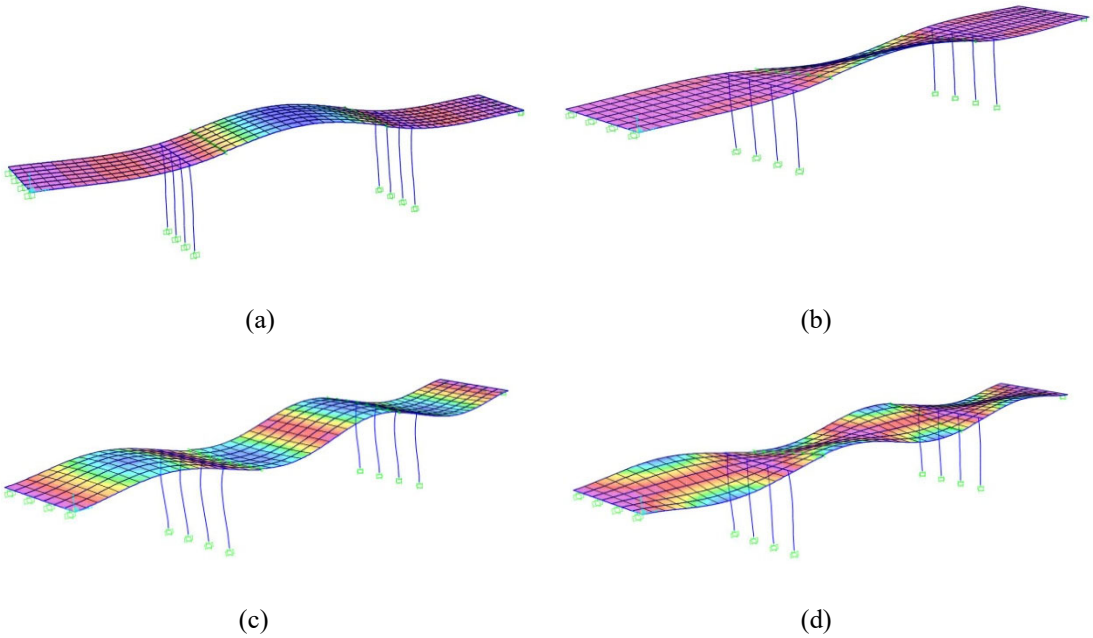

Figure 3-19 Modal information extracted from the FE model of the Bridge: (a) The first mode (f_1=5.82Hz); (b) The second mode (f_2=7.85Hz); (c) The third mode (f_3=12.85Hz); (d) The fourth mode (f_4=16.77Hz).

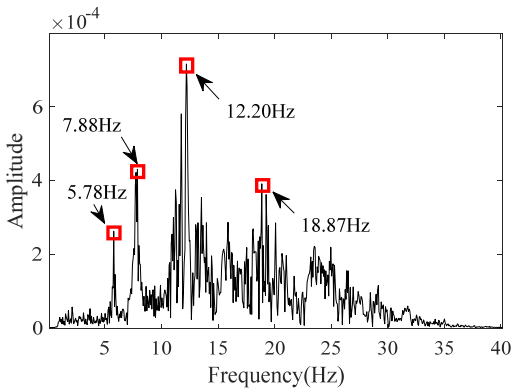

Figure 3-20 Fourier spectrum of the measured vibration signal

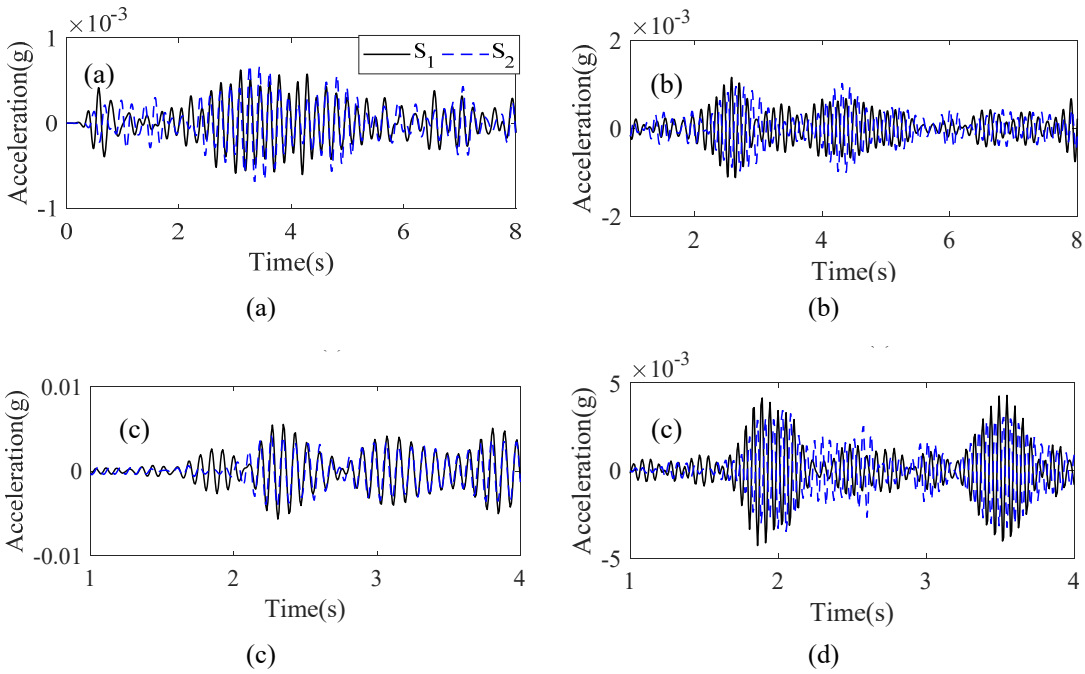

Figure 3-21 The phase information of each mode between two measured acceleration signals: (a) The first mode; (b) The second mode; (c) The third mode; (d) The fourth mode

Figure 3-22 The damaged surface of the bridge deck.

The natural frequencies of the bridge are verified with the finite element analysis. The instantaneous frequencies of the bridge under the heavy traffic loads are identified by using the proposed approach. The measured acceleration response under two heavy tank trucks is used to identify the time-varying IF of the structure. The traffic from the selected event and the corresponding vibration signal recorded from the accelerometer S_1 are shown in Figures 3-23 (a) and (b), respectively. Since the mass ratio between two heavy tank trucks and the bridge is more significant than the first case, the bridge is considered as a time-varying system when the vehicles are crossing the bridge. The maximum recorded acceleration signal on the bridge is equal to 0.048g, indicating a significant vibration. In order to identify the

varying modes of the acceleration signal, the time-frequency analysis based on SET is first performed to determine the frequency boundaries of the modes. The time-frequency analysis results from SET are shown in Figures 3-24 (a) and (b), and it is clearly observed that the filtering boundaries of EWT can be determined. To extract two bending modes from the non-stationary acceleration signal, the filtering boundaries of 4.8Hz, 6.8Hz, 9.5Hz and 14.2Hz are selected for EWT. It can be noted from Figure 3-24 (a) that the time resolution of the first two time-variant modes is low, and the main reason is the time series used in this study is too short, which would cause a low time resolution due to the requirement of frequency resolution. Once the two bending modes are accurately extracted from the non-stationary acceleration signal via EWT, the instantaneous frequencies of two modes can be identified and shown in Figures 3-25 (a) and (b), respectively. It can be observed from Figure 3-25 that these two identified instantaneous frequencies have a slow fluctuation trend when the two heavy trucks are crossing the bridge. As observed from Figure 3- 25 (a), the IF of the first bending mode is gradually changing from the 5.96Hz to 4.88Hz, and coming back to 5.64Hz at the end of the event. This demonstrates that the bridge under heavy trucks in this case is time-varying, due to the significant mass ratio between the two heavy trucks and the bridge [31-32], as well as the varying excitation locations. Due to the heavy mass of the vehicle, the total mass of the bridge-vehicle system increases and therefore the identified natural frequency decreases. As observed from Figure 3-25 (b), the IF of the second bending mode of the measured acceleration signal shows a similar variation pattern as the first bending mode. The maximum change rate of the IF is approximately equal to 19.5%, which indicates that the heavy traffic loads have a significant effect on the modal parameters of the highway bridge. Generally, it can be concluded that the proposed approach can well separate the two main time-varying modes from a non-stationary vibration signal, as well as track the IF of a time-varying bridge-vehicle system.

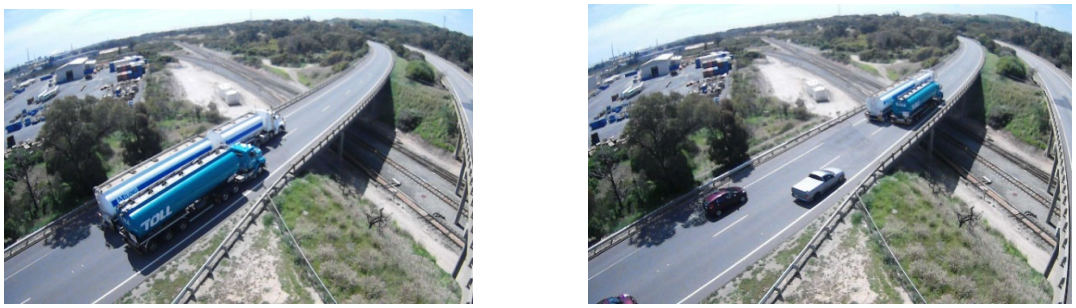

(a)

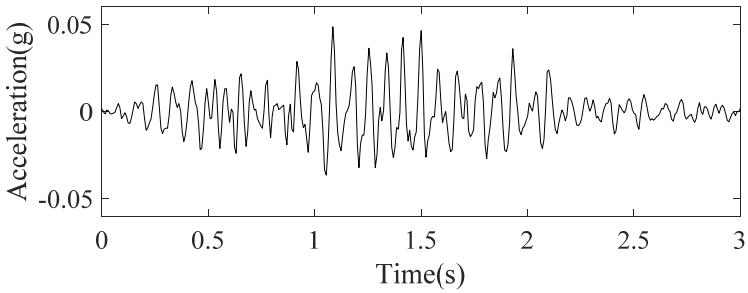

(b)

Figure 3-23 (a) The traffic loads on the bridge; (b) the corresponding measured acceleration from S_1

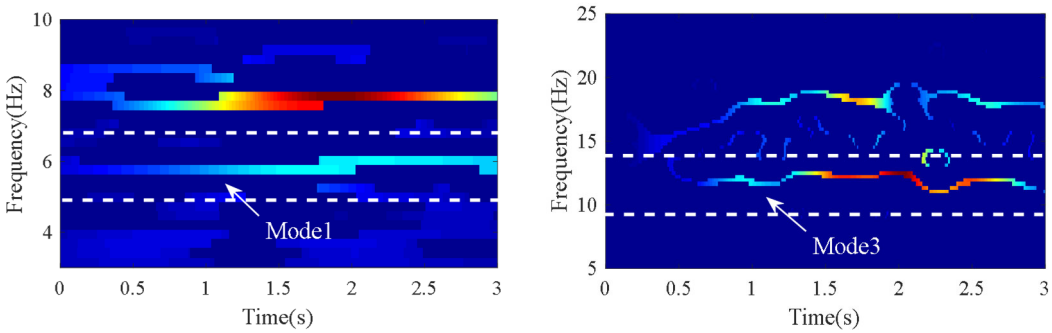

(a) (b)

Figure 3-24 The two identified bending modes based on the results of SET: (a) Mode1; (b) Mode3.

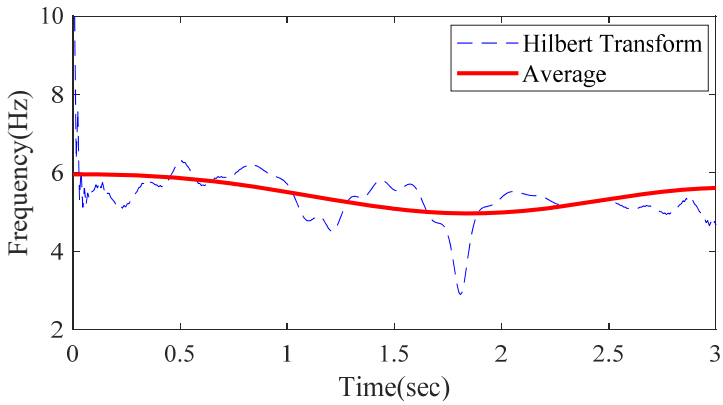

(a)

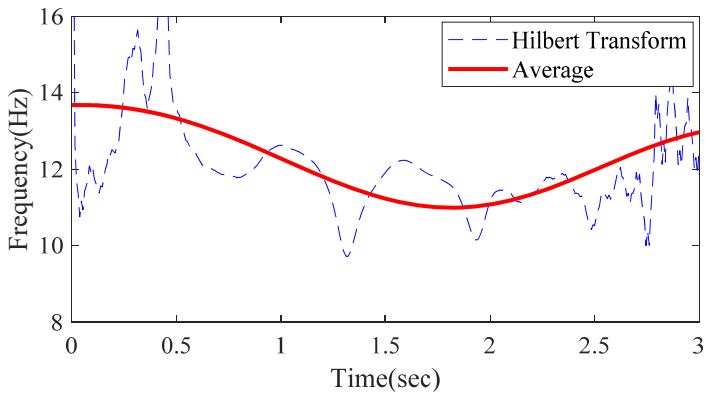

(b)

Figure 3-25 The identified instantaneous frequencies of two bending modes via the proposed approach: (a) The first bending mode; (b) The second bending mode.

3.5. Conclusions

This chapter proposes an improved EWT approach based on SET for the time-varying system identification. The time-frequency analysis of a vibration signal is performed by using SET to determine the filtering boundaries for EWT analysis instead of the ordinary Fourier Spectrum. An improved EWT method is developed to separate the vibration signal into several IMFs based on the defined filtering boundaries. When IMFs of a vibration signal are obtained, HT can be conducted to identify and extract the IF of each mode. The slowly varying part of the identified IF by HT is approximately equal to the IF of a time-varying system under the external excitations. Based on the numerical simulations and experimental validations, the following conclusions can be drawn:

(1) The improved EWT approach can be used to accurately decompose a non-stationary signal into several modes based on the predefined filtering boundaries from SET;

(2) The proposed approach is effective and accurate for time-varying system identification to obtain the instantaneous frequencies of structures, even under the significant noise effect.

References

[1] Wang Z.C., Ren W.X., Chen G.D. (2013). Time-Varying Linear and Nonlinear Structural Identification with Analytical Mode Decomposition and Hilbert Transform. *Journal of Structural Engineering ASCE*, 139(2): 06013001.

[2] Bao C.X., Hao H., Li Z.X., Zhu X.Q. (2009). Time-varying system identification using a newly improved HHT algorithm. *Computer and Structures*, 87(23-24): 1611-23.

[3] Huang Q., Xu Y.L., Liu H.J. (2015). An efficient algorithm for simultaneous identification of time-varying structural parameters and unknown excitations of a building structure. *Engineering Structures*, 98: 29-37.

[4] Tang H.S., Xue S.T., Chen R., Sato T. (2006). Online weighted LS-SVM for hysteretic structural system identification. *Engineering Structures*, 28(12): 1728-35.

[5] Lin J.W., Betti R., Smyth A.W., Longman R.W. (2001). On-line identification of nonlinear hysteretic structural system using a variable trace approach. *Earthquake Engineering and Structural Dynamics*, 30:1279-1303.

[6] Yang J.N., Huang H.W. (2007). Sequential non-linear least-squares estimation for damage identification of structures with unknown inputs and unknown outputs. *International Journal of Non-linear Mechanics*, 42(5): 789-801.

[7] Wang C., Ren W.X., Wang Z.C., Zhu H.P. (2013). Instantaneous frequency identification of time-varying structures by continuous wavelet transform. *Engineering Structures*, 52: 17-25.

[8] Wang Z.C., Ren W.X., Chen G.D. (2018). Time-frequency analysis and applications in time-varying nonlinear structural systems: A state-of-the-art review, *Advances in Structural Engineering*, 21(10):1562-84.

[9] Wang Z.C., Xin Y., Xing J.F., Ren W.X. (2017). Hilbert low-pass filter of non-stationary time sequence using analytical mode decomposition. *Journal of Vibration and Control*, 23(15): 2444-69.

[10] Smyth A.W., Masri S.F., Chaassiakos A.G., Caughey T.K. (2002). Development of adaptive modeling techniques for non-linear hysteretic system. *International Journal of Non-linear Mechanics*, 37(8):1435-51.

[11] Noel J.P., Kerschen G. (2017). Nonlinear system identification in structural dynamics: 10 more years of progress. *Mechanical Systems and Signal Processing*, 83(15): 2-35.

[12] Wang Z.C., Ren W.X., Chen G.D. (2012). A Hilbert transform method for parameter identification of time-varying structures with observer techniques. *Smart Material and Structures*, 21: 105007(9pp).

[13] Dziedziech K., Staszewski W.J. (2015). Wavelet-based modal analysis for time-variant systems. *Mechanical Systems and Signal Processing*, 50-51: 323-37.

[14] Klepka A., Uhl T. (2014). Identification of modal parameters of non-stationary systems with use of wavelet based on adaptive filtering. *Mechanical Systems and Signal Processing*, 47(1-2): 21-34.

[15] Ulker-Kaustell M., Karoumi R. (2011). Application of the continuous wavelet transform on the free vibrations of a steel-concrete composite railway bridge. *Engineering Structures*, 33(3): 911-919.

[16] Shi Z.Y., Law S.S. (2007). Identification of linear time-varying dynamical systems using Hilbert transform and empirical mode decomposition method. *Journal of Applied*

Mechanics, 74(2): 223-30.

[17] Wang Z.C., Chen G.D. (2012). Recursive Hilbert-Huang Transform Method for Time-Varying Property Identification of Linear Shear-Type Buildings under Base Excitations. *Journal of Engineering Mechanics ASCE*, 138(6): 631-39.

[18] Hou Z.K., Hera A., Shinde A. (2006). Wavelet-based structural health monitoring of earthquake excited structures. *Computer-Aided Civil and Infrastructure Engineering*, 21: 268-79.

[19] Daubechies I., Lu J.F., Wu H.T. (2011). Synchrosqueezed Wavelet Transforms: An Empirical Mode Decomposition-like Tool. *Applied and Computational Harmonic Analysis*, 30(2): 243-61.

[20] Liu J.L., Wang Z.C., Ren W.X., Li X.X. (2015). Structural time-varying damage detection using Synchrosqueezing wavelet transform. *Smart Structures and Systems*, 15(1): 119-33.

[21] Wang S., Chen X., Cai G., Chen B., Li X., He Z. (2014). Matching demodulation transform and synchrosqueezing in time-frequency analysis. *IEEE Transaction in Signal Processing*, 62(1): 69-84.

[22] Yu G., Yu M.J., Xu C.Y. (2017). Synchroextracting Transform. *IEEE Transactions on Industrial Electronics*, 64(10): 8042-54.

[23] Gilles J. (2013). Empirical Wavelet Transform. *IEEE Transactions on Signal Processing*, 61(16): 3999-4010.

[24] Xin Y., Hao H., Li J. (2019). Operational modal identification of structures based on improved empirical wavelet transform, *Structural Control & Health Monitoring*, 26: e2323.

[25] Amezquita-Sanchez J.P., Park H.S., Adeli H. (2017). A novel methodology for modal parameters identification of large smart structures using MUSIC, empirical wavelet transform, and Hilbert transform. *Engineering Structures*, 147: 148-59.

[26] Wang S.B., Chen X.F., Tong C.W., Zhao Z.B. (2017). Matching synchrosqueezing wavelet transform and application to aeroengine vibration monitoring. *IEEE Transactions on Industrial Electronics*, 66(2): 360-372.

[27] Thakur G., Wu H.T. (2011). Synchrosqueezing-based recovery of instantaneous frequency from nonuniform samples. *SLAM Journal of Mathematical Analysis*, 43(5): 2078-95.

[28] Ni P.H., Li J., Hao H., Xia Y., Wang X.Y., Lee J.M., Jung K.H. (2018). Time-varying system identification using variational mode decomposition. *Structural Control & Health Monitoring*, 25: e2175

[29] Kim J., Lynch J.P. (2012). Experimental analysis of vehicle-bridge interaction using a wireless monitoring system and a two-stage system identification technique. *Mechanical Systems and Signal Processing*, 28: 3-19.

[30] Cantieni R. (1992). Investigation of vehicle-bridge interaction for highway bridges In: Heavy vehicles and roads: technology, safety and policy London: Thomas Telford.

[31] Xiao F., Chen G.S., Hulsey J.L., Zatar W. (2017). Characterization of non-stationary properties of vehicle-bridge response for structural health monitoring. *Advances in Mechanical Engineering*, 9(5): 1-6.

[32] Cantero D., Hester D., Brownjohn J. (2017). Evolution of bridge frequencies and modes of vibration during truck passage. *Engineering Structures*, 152: 452-64.

CHAPTER 4 ENHANCED VIBRATION DECOMPOSITON METHOD BASED ON MULTISQUEEZING TRANSFORM AND ANALTICAL MODE DECOMPOSITION

ABSTRACT[3]

This chapter proposes an enhanced vibration decomposition approach based on Analytical Mode Decomposition (AMD) and Multisynchrosqueezing Transform (MSST). Although AMD based low-pass filter has been applied for signal decomposition with time varying cut-off frequencies, these cut-off frequencies are usually manually selected from the wavelet scalogram of the target signal. The process therefore significantly reduces the computational efficiency of using AMD based low-pass filter for non-stationary signal analysis. To overcome this problem, in this study, MSST with a time varying cut-off frequency detection algorithm is used to automatically define the time-varying bisecting frequencies for the AMD analysis. Once the time varying cut-off frequencies are identified, AMD can be used to adaptively decompose the non-stationary signal into individual components. To investigate the effectiveness of the proposed approach, termed as MSST-AMD, for vibration signal decomposition and its application, numerical studies on a non-stationary signal with overlapped frequency components are conducted. To further apply the proposed approach for structural vibration response analysis, a three-storey shear-type structure with varying stiffness subjected to earthquake excitations is simulated in this study for instantaneous modal parameter identification. In experimental verifications, the proposed MSST-AMD approach combined with a damage index is further extended to evaluate the damage severity of a structure under earthquake excitations. The results in both numerical simulations and experimental validations demonstrate that the proposed MSST-AMD approach is reliable and accurate for non-stationary signal analysis and vibration decomposition, which can be further used for instantaneous modal parameter identification and structural damage detection.

[3] Xin, Y., Li, J. & Hao, H. (2020). Enhanced Vibration Decomposition Method based on Multisynchrosqueezing Transform and Analytical Mode Decomposition. *Structural Control & Health Monitoring.* (Under review)

4.1 Introduction

One of critical issues in structural health monitoring is to accurately extract individual frequency components from the measured structural vibration signals, i.e. acceleration and displacement responses, etc., for effective structural condition monitoring. However, when civil engineering structures are excited by strong external loads, i.e. earthquake, hurricane, etc., the measured structural dynamic responses are often non-stationary or nonlinear over time [1-2]. Under these circumstances, the traditional time-domain and frequency-domain based methods [3-6] cannot be directly employed to track and identify the time-varying dynamic characteristics of structures during the vibration periods. To overcome this challenge, some advanced time-frequency analysis techniques are developed to identify the non-stationary structural dynamic characteristics from the measured vibration signals. The time-frequency methods for non-stationary signal analysis studied in the literature include Wigner-Ville distribution (WVD), Short Time Fourier Transform (STFT), Wavelet Transform (WT) and Hilbert Transform methods [7-10], etc.

One of the widely used time-frequency analysis techniques is the Hilbert Transform based method. For instance, Hilbert-Huang transform (HHT) has been applied for non-stationary signal analysis in many engineering fields [11-12]. To further enhance the original HHT method, some improved HHT methods have been developed [13-14]. To extract the individual frequency components, Feldman [15-16] developed a new signal decomposition method named as Hilbert vibration decomposition (HVD), and the method has been successfully applied in mechanical engineering vibration signal analysis. Recently, Chen and Wang [17] developed a new signal decomposition theorem, termed as analytical mode decomposition (AMD), which can adaptively decompose a multi-component signal into several individual components based on the predefined cut-off frequencies. For a signal with frequency modulation components, Wang et al. [18] further extended the AMD method for the time-varying or non-stationary vibration signal analysis. With the varying frequency components of the non-stationary signals, the time-varying cut-off frequencies need be selected between each two frequency components for signal decomposition, instead of using constant bisecting frequencies. Since the non-stationary signals simulated in the literature are assumed as the continuous time series, the AMD based low-pass filter can successfully extract the individual components based on the predefined time-varying cut-off frequencies. However, in real applications, the selection of the time-varying cut-off frequencies is not straightforward and the discretization of signals may cause the failure of the low frequency component extraction based on AMD theorem. To eliminate the effects of the signal discretization, Wang et al. [19] further extended the AMD theory for non-stationary discrete time series with two or more amplitude- and frequency-modulation components. Based on

the derivations, it is indicated that the AMD based one-step, two-step and four-step low-pass filters are reliable for non-stationary discrete signal analysis.

Although the AMD based low-pass filter have been successfully applied for non-stationary discrete signal analysis, the process of selecting the time-varying cut-off frequencies between each two individual components significantly reduces computational efficiency of the method [20] and even affects the accuracy. Unlike stationary or linear signals, the constant bisecting frequencies of AMD method can be directly defined from their frequency spectrum. When using AMD method for analysing non-stationary signals, the cut-off frequencies are usually predefined from its time-frequency representation and may be difficult to define accurately, due to the overlapping of the frequency components. As mentioned in literature [18], the time-varying cut-off frequencies of the AMD method can be selected from the time-frequency analysis of a signal by wavelet analysis. However, this process cannot be automatically conducted. Therefore, it will significantly increase the computational cost of using AMD-Hilbert spectral analysis for non-stationary signals.

To achieve automatic non-stationary signal decomposition by using AMD based low-pass filter, a high-resolution time-frequency representation of the non-stationary signal is required for defining the time-varying cut-off frequencies. However, restricted by the Heisenberg uncertainty principle, the time-frequency representations generated by the traditional methods, i.e. WT, S-transform and STFT could be blurry and cause imprecise analysis results for non-stationary signals. To overcome this issue, more recently, Daubechies et al. [21] proposed an energy-concentrated time-frequency analysis technique, termed as Synchrosqueezing Transform (SST), which can squeeze the discrete time-frequency coefficients into the instantaneous frequency trajectories. However, when the signal is contaminated by high-level noise, the unexpected frequency components of noise would also be gathered into the SST results, which may cause an imprecise time-frequency analysis results. Based on the theory of SST method, Yu et al. [22] further developed a Multisynchrosqueezing transform (MSST) method for non-stationary signal analysis, which is used to generate a more energy-concentrated time-frequency representation by performing multi-step SST operations. The identification results indicated that the MSST method can

accurately track the time-varying features of strong non-stationary signals.

In this study, MSST is employed to enhance AMD based low-pass filter for adaptive non-stationary signal analysis. For a discrete non-stationary signal, time-frequency analysis based on MSST is first performed to determine the number and locations of the individual frequency components, and a ridge detection algorithm is developed to automatically define the time-varying cut-off frequencies between each two individual components. Then, AMD based low-pass filter is used to extract the mono-components from the target signal. The instantaneous frequencies of the decomposed mono-components can be identified by using the ridge detection algorithm. A multi-component non-stationary signal with the overlapping of frequencies is simulated to validate the feasibility and accuracy of the proposed approach. Then, a three-storey shear building model with varying stiffness coefficients subjected to seismic excitations is further developed to investigate the effectiveness of using the enhanced method for structural dynamic response decomposition. The proposed approach is also extended and applied for structural damage detection combined with a damage index. Experimental studies on a 12-storey scaled reinforced concrete (RC) frame structure subjected to strong ground motions are conducted to validate the effectiveness of using the proposed improved signal decomposition approach for damage detection.

The remainder of this chapter is organized as follows. Section 2 briefly explains the theory of AMD and the derivations of MSST, and then a fundamental process of using the improved adaptive low-pass filter based on MSST and AMD for non-stationary signal analysis is developed. In Section 3, numerical study on a multi-component non-stationary signal with varying frequencies is first conducted to investigate the feasibility of using the proposed approach for vibration signal decomposition. Then a three-storey time-varying structure subjected to seismic excitations is built to validate the effectiveness of using the proposed approach for structural vibration signal analysis and instantaneous modal parameter identification. In Section 4, the proposed approach is further applied for time-varying structural damage detection. A damage index is defined based on the identified instantaneous frequencies of structural vibration responses. Then a 12-storey scaled RC frame structure under the various seismic excitations is used as an example to validate the effectiveness and

reliability of using the proposed signal decomposition approach for structural damage detection. Section 5 provides some discussions and conclusions.

4.2. Theoretical Background and Development

4.2.1 AMD based low-pass filter with time-varying cut-off frequencies

The AMD based low-pass filter for non-stationary signal analysis has been developed in the literature [18]. In this study, the time-varying cut-off frequencies are selected to extract the individual components from a non-stationary signal. The theorem of AMD with time-varying cut-off frequencies can be briefly described as: Let $x(t)$ represent a vibration signal of m time-varying individual components with frequencies:$\omega_i(t)$ $(i = 1,2, \dots, m), \omega_i(t) > 0$, it can be separated into m components $x_i{}^c(t)$ $(i = 1,2, \dots, m)$, whose frequency ranges satisfy: $|\omega_1(t)| < \omega_{c1}(t)$, $\omega_{c1}(t) < |\omega_2(t)| < \omega_{c2}(t), \dots, \omega_{c(m-2)}(t) < |\omega_{m-1}(t)| < \omega_{c(m-1)}(t)$, and $\omega_{c(m-1)}(t) < |\omega_m(t)|$. The decomposed individual components can also be expressed as

$$x(t) = \sum_{i=1}^{m} x_i{}^c(t) \tag{4.1}$$

$\omega_i(t)$ represents the instantaneous frequency of the ith decomposed signal $x_i{}^c(t)$, and $\omega_{ci}(t) \in (\omega_{i-1}(t), \omega_i(t))$ $(i = 1,2, \cdots, m)$ denotes m-1 time-varying cut-off frequencies. Each individual signal can be determined by

$$x_1^c = s_1(t), x_2^c = s_2(t) - s_1(t), \dots, x_m^c(t) = x(t) - s_{m-1}(t) \tag{4.2}$$

$$s_i(t) = \sin[\int_{-\infty}^{t} \omega_{ci}(\tau)\,\mathrm{d}\tau]\, H\left\{x(t)\cos\left[\int_{-\infty}^{t} \omega_{ci}(\tau)\,\mathrm{d}\tau\right]\right\}$$

$$-\cos\left[\int_{-\infty}^{t} \omega_{ci}(\tau)\,\mathrm{d}\tau\right] H\left\{x(t)\sin\left[\int_{-\infty}^{t} \omega_{ci}(\tau)\,\mathrm{d}\tau\right]\right\} \quad (i = 1, 2, \cdots, m) \tag{4.3}$$

in which $H[\cdots]$ represents Hilbert transform, $s_i(t)$ is the ith individual component of the target signal. Here, $s_i(t)$ is different from those decomposed mono-components described in Equation (4.1) due to the use of a filter.

Equation (4.3) suggests that using AMD can analytically extract the low-frequency component $s(t)$ of a non-stationary signal by selecting a time-varying cut-off frequency $\omega_c(t)$. The low-pass component $s(t)$ can be obtained as

$$s(t) = \sin\left(\int_{-\infty}^{t} \omega_c(\tau)\,\mathrm{d}\tau\right) H\left[x(t)cos\left(\int_{-\infty}^{t} \omega_c(\tau)\,\mathrm{d}\tau\right)\right] -$$

$$\cos\left(\int_{-\infty}^{t}\omega_c(\tau)\,\mathrm{d}\tau\right)H[x(t)\sin\left(\int_{-\infty}^{t}\omega_c(\tau)\,\mathrm{d}\tau\right)] \tag{4.4}$$

Equation (4.4) operates like a low-pass filter that passes any low frequency signal $s(t)$ but prevents the fast-varying signal in time domain. As mentioned in the above equations, the AMD based filter is well defined to extract the low-frequency components from a continuous multi-component signal. However, in real engineering application, the measured structural vibration signals are usually discrete due to the low sampling rate. To use AMD based low-pass filter for discrete time sequences analysis, Wang et al. [19] further extended the theoretical derivations of AMD to one-step, two-step, and four-step signal decomposition approaches according to the different sampling rates, termed as "DAMD". The corresponding descriptions of DAMD are described briefly below.

It is assumed that $u(t)$ denotes a discrete vibration signal with m time-varying components $u_i(t)$ $(i = 1,2,\dots,m)$, with instantaneous frequencies denoted as $\omega_i(t)$ $(i = 1,2,\dots,m)$. The sampling rate of the discrete signal is set as ω_s. The one-step AMD method can be used to extract the individual components of the original signal when the time-varying frequencies of all components in any time steps satisfy the following Conditions

$$0 < [\omega_1(t)]^{max} < [\omega_2(t)]^{max} < \cdots < [\omega_m(t)]^{max} < \frac{\omega_s}{4} \tag{4.5}$$

$$[\omega_m(t)]^{max} \leq \frac{\omega_s}{2} - [\omega_c(t)]^{max} \tag{4.6}$$

in which $[\omega_m(t)]^{max}$ is the maximum frequency value of the target signal, and $[\omega_c(t)]^{max}$ denotes the maximum value of the time-varying cut-off frequencies.

It can be noticed that the one-step AMD method is only effective when Equations (4.5) and (4.6) are simultaneously satisfied. However, when Equation (4.6) cannot be satisfied, the two-step AMD based low-pass filter is needed to perform the discrete non-stationary signal analysis. Similarly, the four-step AMD method is required when both conditions in Equations (4.5) and (4.6) are not satisfied, but the defined time-varying cut-off frequencies need to satisfy

$$\frac{\omega_s}{4} < [\omega_c(t)]^{max} < \frac{\omega_s}{2} \tag{4.7}$$

The extended AMD based filter can analytically extract the low-frequency components from a measured discrete signal with appropriate cut-off frequencies. Since the main objective of this study aims at developing an automatic AMD based low-pass filter for adaptive non-stationary signal decomposition, the signals used in the numerical and experimental studies are assumed to satisfy Equations (4.5) and (4.6).

4.2.2 An enhanced vibration decomposition based on MSST and AMD

In Section 2.1, AMD based low-pass filter with time-varying cut-off frequencies is introduced for non-stationary signal decomposition. For a non-stationary discrete signal, the frequencies of its individual components are usually varying over the vibration duration. This may cause the frequency overlapping of different frequency components in Fourier spectrum. Under these circumstances, the time-varying cut-off frequencies need to be selected carefully from the time-frequency representations of these signals. The scalogram of a non-stationary signal by wavelet analysis has been employed for the selection of time-varying cut-off frequencies in the literature [18]. However, with the restrictions of the Heisenberg uncertainty principles, the classical time-frequency analysis methods, i.e. WT, STFT and WVD, may not clearly track the nonlinear characteristics of a strong non-stationary signal. This could lead to an incorrect selection of the time-varying cut-off frequencies of the non-stationary signal from its time-frequency representation. Therefore, in this study, the MSST method combined with a developed ridge detection technique [23-24] is employed to enhance the AMD based low-pass filter for automatic non-stationary signal decomposition. The theoretic background of MSST is briefly described below.

It is assumed that a measured vibration signal $u(t)$, which consists of m time-varying frequency components, is written as

$$u(t) = \sum_{i=1}^{m} u_i(t) = \sum_{i=1}^{m} A_i(t) e^{j\int \omega_i(t)dt} \tag{4.8}$$

in which $A_i(t)$ and $\omega_i(t)$ are the instantaneous amplitude and frequency of the ith individual component, respectively. Different frequency components can be well decomposed under a sufficient distance, i.e.

$$\omega_{i+1}(t) - \omega_i(t) > 2\xi \qquad i \in (1,2,\cdots,m-1) \tag{4.9}$$

in which ξ is the frequency support of the window function.

The STFT based time-frequency representation of a vibration signal can be approximately expressed as [10]

$$G_{STFT}(t,\omega) \approx \sum_{i=1}^{m} A_i(t)\mathcal{F}\big(\omega - \omega_i(t)\big) e^{j\int \omega_i(t)dt} \tag{4.10}$$

where $\mathcal{F}(\cdots)$ represents the Fast Fourier transform (FFT).

To improve the time-frequency resolution of STFT approach, a SST based STFT approach is developed [25], which can be written as

$$Ts(t,\varphi) = \int_{-\infty}^{+\infty} G_{STFT}(t,\omega) * \delta\big(\varphi - \omega_i(t,\omega)\big)d\omega \tag{4.11}$$

in which $\delta(\cdots)$ denotes a frequency-reassignment operator, which is applied to squeeze the original STFT coefficients $G_{STFT}(t,\omega)$ into the corresponding instantaneous frequency trajectories. To further improve the time-frequency resolution, Yu et al. [22] proposed to execute a multi-step SST analysis, which can obtain a more energy-concentrated time-frequency results than one-step SST. The multi-step iterations of SST can be expressed as

$$\begin{aligned} Ts_{(2)}(t,\varphi) &= \int_{-\infty}^{+\infty} Ts(t,\varphi) * \delta\big(\varphi - \omega_i(t,\omega)\big)d\omega \\ Ts_{(3)}(t,\varphi) &= \int_{-\infty}^{+\infty} Ts_{(2)}(t,\varphi) * \delta\big(\varphi - \omega_i(t,\omega)\big)d\omega \\ &\vdots \\ Ts_{(l)}(t,\varphi) &= \int_{-\infty}^{+\infty} Ts_{(l-1)}(t,\varphi) * \delta\big(\varphi - \omega_i(t,\omega)\big)d\omega \end{aligned} \tag{4.12}$$

in which the lth SST operations $Ts_{(l)}(t,\varphi)$ can be translated as

$$Ts_{(l)}(t,\varphi) = \int_{-\infty}^{+\infty} G_{STFT}(t,\omega) * \delta\left(\varphi - \omega_i{}^{(l)}(t,\omega)\right) d\omega \tag{4.13}$$

In Equation (4.13), the lth iterations of $\omega_i(t,\omega)$ can be calculated as

$$\omega_i{}^{(l)}(t,\omega) = \theta_i{}'(t) + \left(\frac{\theta_i{}''(t)^2}{1+\theta_i{}''(t)^2}\right)^l \left(\omega - \theta_i{}'(t)\right) \tag{4.14}$$

From Equation (4.14), it can be noticed that the estimated instantaneous frequencies are closer to the real frequency components by executing multi-step SST iterations. It also indicates that the MSST based time-frequency representation is more suitable for the time-varying cut-off frequency selection of AMD method.

To enhance AMD based low-pass filter for non-stationary discrete signal decomposition, a ridge detection algorithm is required to reliably and accurately extract the time-varying cut-off frequencies from the squeezed time-frequency coefficients. In the literature [22], an

effective ridge detection algorithm is applied to identify the time-varying vibration characteristics of a non-stationary signal. In this study, this algorithm is further modified to identify the time-varying cut-off frequencies of a multi-component vibration signal. The process of this algorithm is described in Appendix 1. The time-varying cut-off frequencies of a non-stationary vibration signal can be automatically defined from the scalogram of performing MSST analysis. Then AMD based low-pass filter can adaptively extract the low-frequency components of the target signal by using these predefined cut-off frequencies. The proposed enhanced vibration decomposition approach based on MSST and AMD, termed as (MSST-AMD), is described in Figure 4-1.

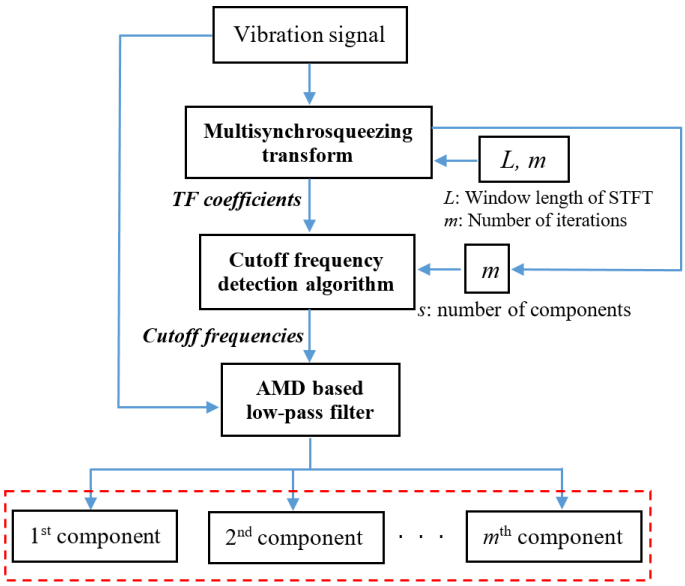

Figure 4-1 The enhanced vibration decomposition based on the proposed approach: MSST-AMD.

4.3 Numerical Studies

4.3.1 Numerical simulation 1

In this section, a multi-component vibration signal $y(t)$, as defined in Equation (4.15), is used to investigate the effectiveness of using the proposed MSST-AMD approach for adaptive non-stationary signal decomposition. The simulated non-stationary signal $y(t)$

consists of four frequency-modulated individual components $y_1(t)$, $y_2(t)$, $y_3(t)$ and $y_4(t)$, which are described by Equations (4.16)-(4.19), respectively.

$$y(t) = y_1(t) + y_2(t) + y_3(t) + y_4(t) + noise(t) \tag{4.15}$$

$$y_1(t) = \begin{cases} \cos[7\pi t + 2\sin(0.4\pi t)] & t \in [0,10\text{s}] \\ \cos\{7\pi t + 2\sin[0.5\pi(t-10)]\} & t \in (10,20\text{s}] \\ \mathrm{e}^{-0.005[5\pi(t-20)]}\cos\{5\pi t + 2\sin[0.4\pi(t-20)]\} & t \in (20,30\text{s}] \end{cases} \tag{4.16}$$

$$y_2(t) = \begin{cases} \cos[10\pi t + 2\sin(0.4\pi t)] & t \in [0,10\text{s}] \\ \cos\{10\pi t + 2\sin[0.5\pi(t-10)]\} & t \in (10,20\text{s}] \\ \mathrm{e}^{-0.005[8\pi(t-20)]}\cos\{8\pi t + 2\sin[0.4\pi(t-20)]\} & t \in (20,30\text{s}] \end{cases} \tag{4.17}$$

$$y_3(t) = \begin{cases} \cos[16\pi t + 2\sin(0.4\pi t)] & t \in [0,10\text{s}] \\ \cos\{14\pi t + 2\sin[0.4\pi(t-10)]\} & t \in (10,20\text{s}] \\ \mathrm{e}^{-0.005[13\pi(t-20)]}\cos\{13\pi t + 2\sin[0.5\pi(t-20)]\} & t \in (20,30\text{s}] \end{cases} \tag{4.18}$$

$$y_4(t) = \begin{cases} \cos[20\pi t + 2\sin(0.4\pi t)] & t \in [0,10\text{s}] \\ \cos\{18\pi t + 2\sin[0.5\pi(t-10)]\} & t \in (10,20\text{s}] \\ \mathrm{e}^{-0.005[16\pi(t-20)]}\cos\{16\pi t + 2\sin[0.5\pi(t-20)]\} & t \in (20,30\text{s}] \end{cases} \tag{4.19}$$

In this study, to further investigate the performance of the proposed method under the effects of noise, 5% Gaussian white noise is added to the original signal. Figure 4-2 shows the noisy signal, with a length of 30 seconds and a sampling rate of 100Hz. The theoretical instantaneous frequencies of these four individual components are shown in Figure 4-3. It is clearly observed from Figure 4-3 that the instantaneous frequencies of these individual components are varying and decaying over time. To validate the superiority of using MSST, the time-frequency representation of using MSST is compared with that of wavelet analysis. When using the wavelet transform for the non-stationary signal analysis, the Morlet wavelet is selected as a mother wavelet function to calculate the wavelet coefficients of the target signal. The center frequency is set as 2Hz with a bandwidth parameter equal to 8 s^2, and the analysis result is shown in Figure 4-4(a). It can be noticed from Figure 4-4 (a) that the wavelet analysis of the signal can track the trend of the abovementioned four individual

components of the original signal $y(t)$. Referring to the wavelet scalogram described in Figure 4-4 (a), the time-varying cut-off frequencies if using AMD need to be manually selected very carefully between every two mono-components to well separate the components. The process will significantly add the computational cost of using AMD based approach for non-stationary signal analysis [20]. Then MSST is employed to improve defining the low-pass filters for AMD in the multi-component signal analysis. The time-frequency analysis of the signal is performed by using one-step and ten-step MSST operations, respectively, and the corresponding results are presented in Figures 4-4(b) and (c). By comparing the results when using the WT and MSST methods, it can be found that MSST generates a more energy-concentrated time-frequency representation than the wavelet analysis. In addition, by comparing the analysis results from using one-step and ten-step MSST operations, it can be observed that the identified instantaneous frequency trajectories based on ten-step MSST is more accurate than those of the one-step MSST and wavelet analysis, especially at the first few seconds of the signal. Once the MSST based time-frequency analysis of the signal is conducted, the developed cut-off frequency detection algorithm described in Appendix 1 is applied to automatically determine the time-varying cut-off frequencies for the AMD based low-pass filter. Figure 4-5 shows the identified three time-varying cut-off frequencies between four individual modes. Based on these identified cut-off frequencies, four mono-components can be adaptively extracted from the original signal, and the decomposed components of $y_2(t)$ and $y_3(t)$ are exhibited in Figures 4-6 (a) and (b), respectively. It can be observed from Fig. 6 that the individual components of $y_2(t)$ and $y_3(t)$ are well separated by using MSST-AMD with the predefined cut-off frequencies. The corresponding instantaneous frequencies of these individual components are identified by using Hilbert transform, which are displayed in Figures 4-7(a) and (b), respectively. As observed from Figures 4-7(a) and (b), the end effects exist in these two decomposed individual components, which is caused by the finite length and incomplete cycle included in the non-stationary signal. However, for most the duration of the signal, the identified instantaneous frequency components are accurate. To further investigate the superiority of the proposed MSST-AMD approach, the identification results by using the proposed approach are compared with the S-transform based band-variable filter developed in the

literature [26]. The selected filtering window and the identified instantaneous frequencies of the second mono-component by the S-transform based filter are shown in Figures 4-8(a) and (b), respectively. By comparing the identified instantaneous frequencies as shown in Figure 4-7(a) and Figure 4-8(b), it can be observed that the identified results based on the MSST-AMD are more accurate than those of using the S-transform based filter. In addition, when using the S-transform based filter for non-stationary signal decomposition, the filtering windows need to be predefined from the S-transform based time-frequency analysis manually. Similarly, the computational efficiency may be significantly decreased and errors increase when the filtering boundaries are blurry between different individual components. However, the proposed MSST-AMD approach can automatically decompose a non-stationary signal into several individual components with a better accuracy.

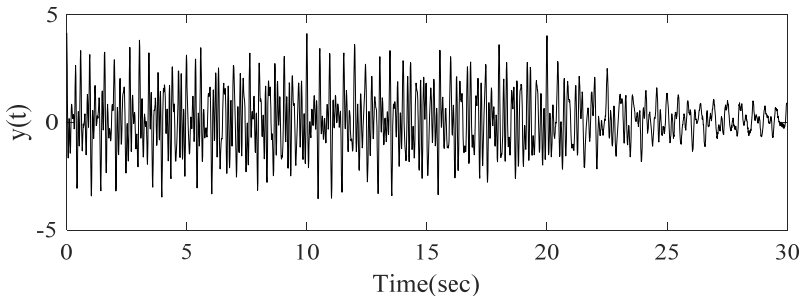

Figure 4-2 The simulated non-stationary signal with 5% Gaussian white noise.

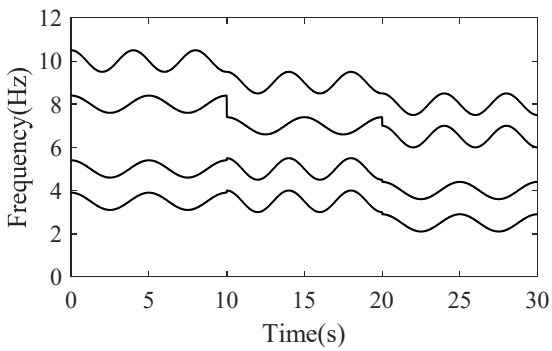

Figure 4-3 The theoretical instantaneous frequencies of the simulated noisy signal.

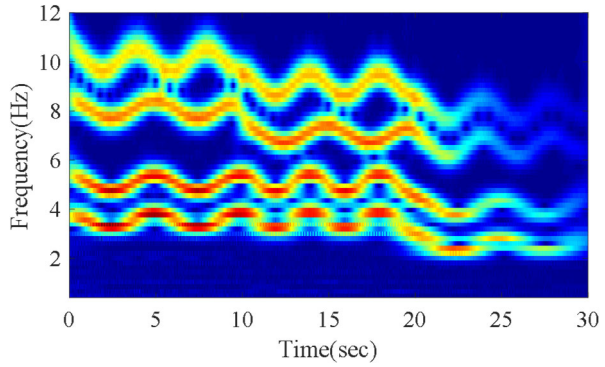

(a)

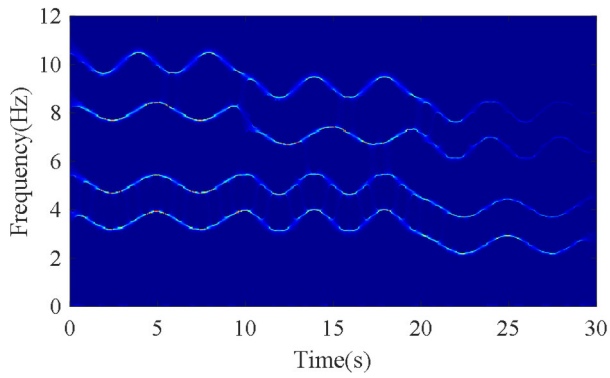

(b)

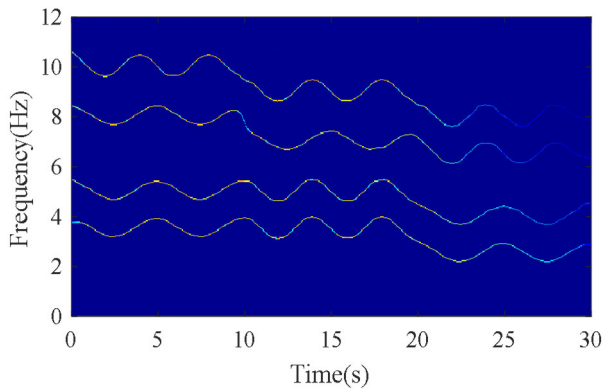

(c)

Figure 4-4 Time-frequency analysis results by using: (a) Wavelet analysis; (b) one-step MSST operation; (c) ten-step MSST operation.

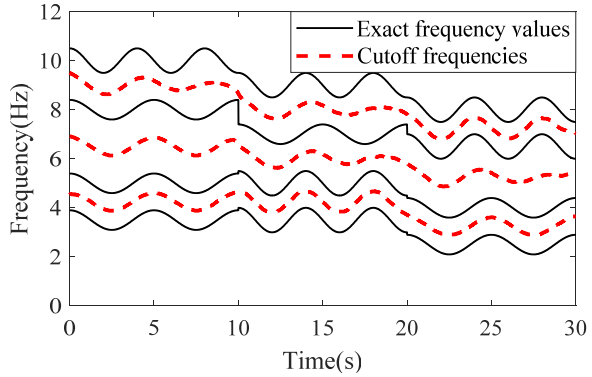

Figure 4-5 Automatically identified instantaneous frequencies and cut-off frequencies by using MSST-AMD.

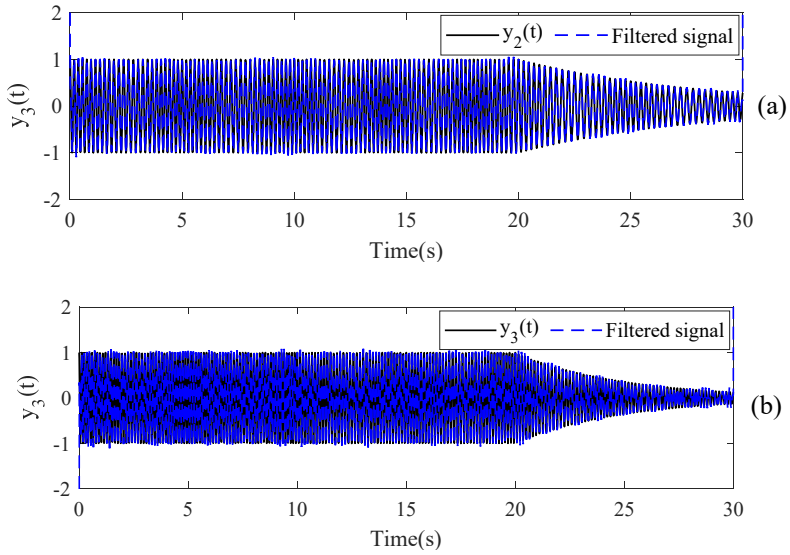

Figure 4-6 The decomposed mono-components based on the proposed MSST-AMD approach: (a) The 2nd mono-component; (b) The 3rd mono-component.

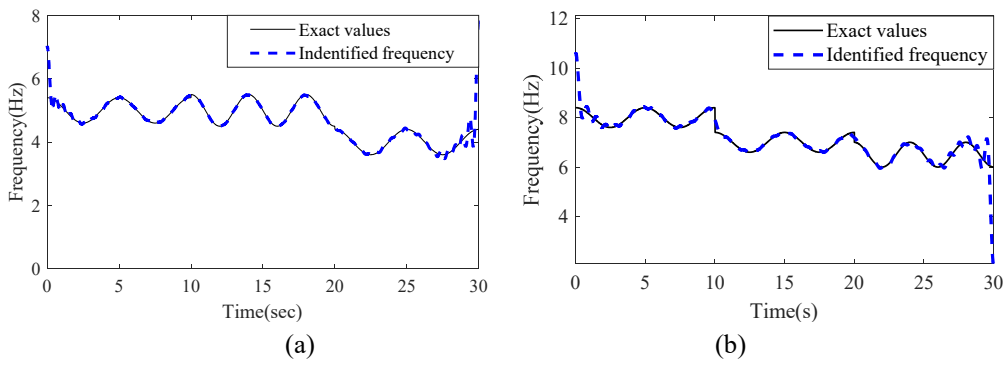

Figure 4-7 The identified instantaneous frequencies by using the proposed MSST-AMD approach with Hilbert transform: (a) The 2nd mono-component; (b) The 3rd mono-component.

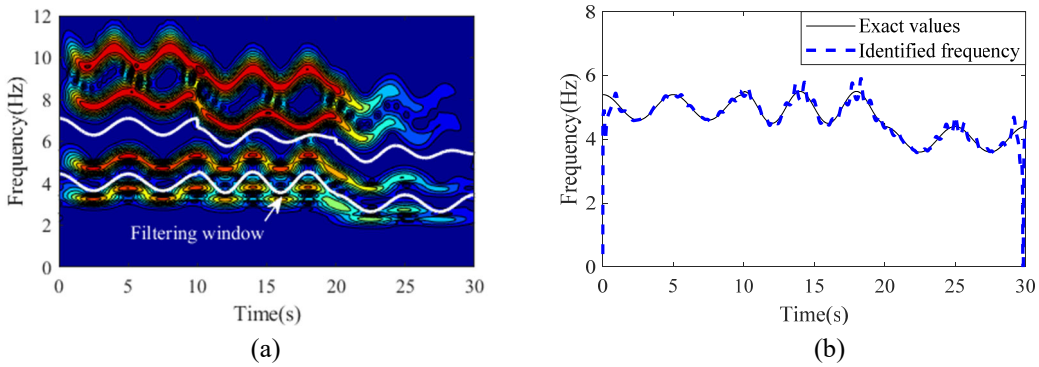

(a) (b)

Figure 4-8 Vibration signal analysis and decomposition by using the S-transform based filter: (a) The selected filtering window; (b) The identified instantaneous frequency of the 2nd mono-component.

4.3.2 Application of MSST-AMD approach for instantaneous modal identification of time-varying structures

In this section, the proposed MSST-AMD approach is further conducted to identify the instantaneous modal parameters of time-varying structures subjected to external excitations by combining with Hilbert transform. In the proposed procedure, the MSST-AMD approach is first used to decompose the measured vibration signals of a time varying structure into individual components, and then, Hilbert transform can further be performed to identify the instantaneous natural frequencies and mode shapes of the time varying structure.

To application of the proposed MSST-AMD approach for time-varying system identification, a three-storey shear-type building model, as shown in Figure 4-9, is modeled in MATLAB. In this building model, the mass m_i $(i = 1,2,3)$ of each floor of the building is defined as 2.50×10^5kg, 1.4×10^5kg and 0.7×10^5kg, respectively; the initial elastic stiffness k_i $(i = 1,2,3)$ of each floor is set as 2.1×10^5 kN/m, 1.05×10^5 kN/m and 0.5×10^5 kN/m, and the corresponding damping matrix element c_i $(i = 1,2,3)$ of each floor is assigned as 1.2×10^2kN.s/m, 0.8×10^2kN.s/m and 0.4×10^2kN.s/m, respectively. To simulate the time-varying dynamic behaviors of the structure subjected to external excitations, the time-varying stiffness coefficients of the 1st and the 2nd floors are designed as

$$k_1 = \begin{cases} 2.1\times10^5\text{kN}\cdot m & [0s,4s) \\ \{2.1-0.058(t-4)-0.131\sin[0.5\pi(t-4)]\}\times10^5\text{kN}\cdot m & (4s,16s] \\ 1.404\times10^5\text{kN}\cdot m & (16s,30s] \end{cases} \tag{4.20}$$

$$k_2 = \begin{cases} 1.05\times10^5\text{kN}\cdot m & [0s,4s) \\ \{-0.75\times10^4 t+1.3\times10^5\}\text{kN}\cdot m & (4s,8s] \\ 0.7\times10^5\text{kN}\cdot m & (8s,30s] \end{cases} \tag{4.21}$$

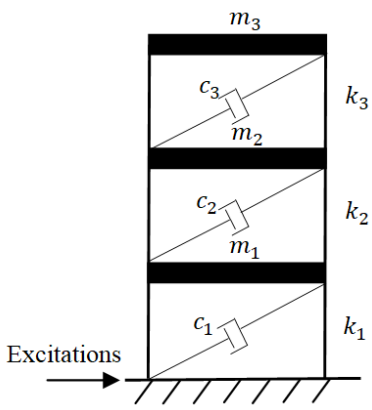

Figure 4-9 The time-varying building model

The 1940 El Centro ground acceleration record with time duration of 30 seconds is selected as the external excitation of the three-storey building model, which is shown in Figure 4-10. For a real structure, acceleration responses are usually measured for system identification [27]. Before using the proposed MSST-AMD approach for the instantaneous modal parameter identification of the building model, eigenvalue analysis is first performed to calculate the linear natural frequencies of the time-varying structure, which are 2.51Hz, 4.97Hz and 6.85Hz, respectively. Then, the simulated acceleration responses are used for structural instantaneous modal parameter identification. In this study, acceleration responses of the building structure are calculated by using the fourth-order Runge-Kutta method with a sampling rate of 50Hz. Based on the proposed MSST-AMD approach, the time-frequency representation of the measured acceleration response is first performed by using MSST. Based on the MSST analysis results and the proposed cut-off-frequency detection algorithm, time varying cutoff frequencies are automatically defined between each two modes, which is presented in Figure 4-11. Comparing with the frequency distribution of the measured acceleration response shown in Figure 4-11, it can be found that the identified time varying cut-off frequencies are reliable for individual mode extraction by using AMD based low-pass filter. Once the mono-components of structural vibration responses are decomposed by using AMD, the instantaneous frequencies of these three modes can be identified by using Hilbert Transform. The identified instantaneous frequencies and mode shapes of the structure subjected to earthquake excitations are shown in Figure 4-12. It can be observed from Figure 4-12 that the identified instantaneous frequency components by using Hilbert Transform are rapidly varying around the exact values over the vibration duration. To obtain the varying natural frequencies of this structure subjected to earthquake excitations, the rapidly-varying part is filtered out by using AMD with a suitable cutoff frequency [27]. By filtering out the fast time-varying components, the identified instantaneous frequencies of the structure are

shown in Figure 4-12. As can be seen from Figure 4-13, the identified instantaneous normalised mode shapes at time points A, B and C are presented, which correspond to the time points at 2.68 seconds, 6.24 seconds and 26.20 seconds of structural acceleration responses, respectively. As observed from Figure 4-12 and Figure 4-13, the results indicate that the proposed MSST-AMD approach can effectively identify the time-varying dynamic characteristics of a structure under earthquake excitations.

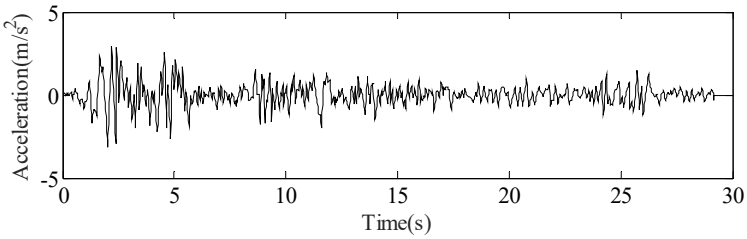

Figure 4-10 The applied earthquake excitation

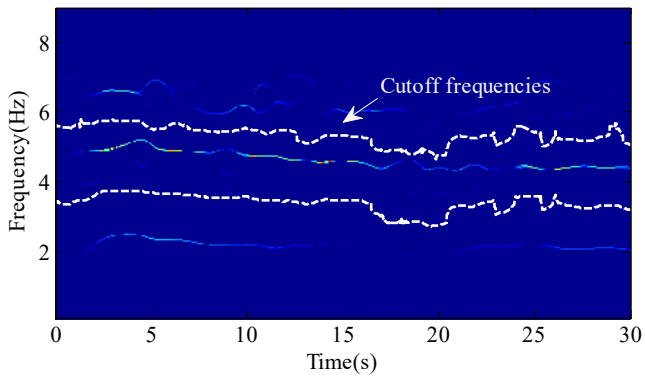

Figure 4-11 The identified cut-off frequencies by using MSST approach

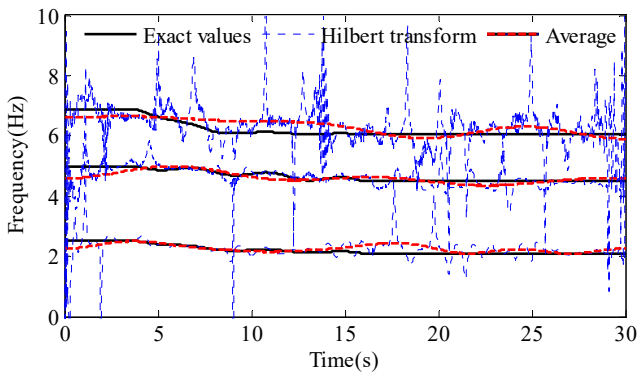

Figure 4-12 The identified instantaneous frequencies of the building model subjected to earthquake excitations

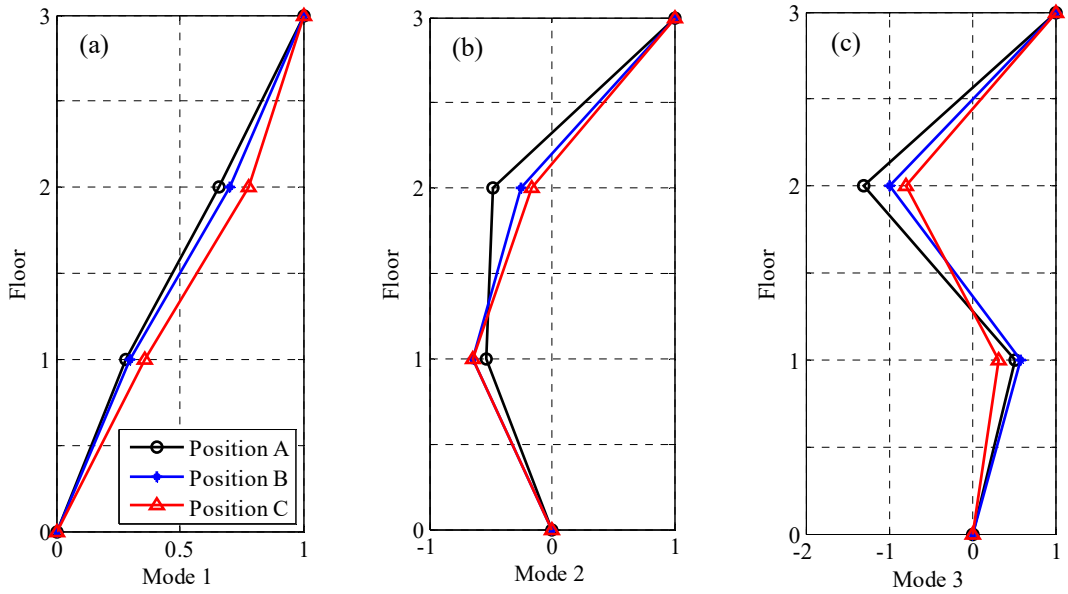

Figure 4-13 The identified normalised mode shapes of the building model subjected to earthquake excitations at different time points: (a) 1st mode; (b) 2nd mode; (c) 3rd mode.

4.4 Experimental Application

Experimental investigations and shake table tests on a 12-storey 1/10 scaled spatial RC frame model, as presented in Figure 4-14, are conducted to validate the feasibility of using the proposed MSST-AMD approach for vibration decomposition and structural damage detection. The total height of the testing model is 3.6m with 0.3m for each floor, and the dimension of this spatial RC frame structure is 0.6m×0.6m. The detailed geometrical dimensions and physical parameters of the RC structure can be found in [29]. The shake table tests were performed at Tongji University and the testing data were shared for benchmark studies. During the tests, 61 cases were tested to investigate the performance of the structure under various earthquake excitations. 23 accelerometers were employed to record the tri-axial dynamic responses of the RC structure subjected to the seismic excitations. However, in this research, only the measured acceleration responses at the top floor of the tested structure under the single-directional El Centro ground motion record are used to identify the time-varying dynamic characteristics during structural vibrations. In addition, to further evaluate the damage severity of the tested structure subjected to seismic

excitations, with the vibration decomposition results by using the proposed MSST-AMD approach, a damage index is applied for structural damage detection, which can be expressed as

$$DQ = \frac{1}{m}\sum_{i=1}^{m}\left[\frac{\int[\int_0^t \omega_i^r(\tau)\mathrm{d}\tau - \int_0^t \omega_i^d(\tau)\mathrm{d}\tau]^2 dt}{\int[\int_0^t \omega_i^r(\tau)\mathrm{d}\tau]^2 dt}\right]^{\frac{1}{2}} \tag{4.22}$$

in which m denotes the number of the decomposed individual components, $\omega_i^r(\tau)$ and $\omega_i^d(\tau)$ denote the identified ith instantaneous frequencies of this structure under the reference state and damaged case during the vibrations, respectively.

Based on Equation (4.22), it can be observed that the defined damage index reflects the instantaneous phase change of structural responses between the reference state and damaged state. Therefore, the damage index can be used to evaluate the damage severity of a structure subjected to different external excitations causing nonlinear vibration behavior. In this study, the damage index DQ is calculated by using the identified instantaneous frequencies of the decomposed fundamental mode from the measured acceleration responses at the top floor, under different structural conditions.

Four cases of the tested structure under the earthquake excitations are selected for this study, which are defined as EQ_1, EQ_2, EQ_3 and EQ_4, respectively. The corresponding input ground motions of the shake table tests were the regenerated El Centro seismic waves with four different peak ground accelerations (PGAs), which are equal to 0.258g, 0.388g, 0.517g and 0.775g, respectively. The measured acceleration responses at the top floor under four cases are shown in Figures 4-15 (a)-(d), respectively, and the associated Fourier spectra are presented in Figure 4-16. It can be found from Figure 4-16 that the measured natural frequency of the fundamental mode decreases from EQ_1 to EQ_4, and the main reason is that the tested structure has a substantial damage during the shake table testing. Based on the study in the literature [28], it can be noticed that the fundamental natural frequency of the tested structure under the health condition is 4.01Hz, which is higher than the identified result under EQ_1. However, according to the experimental report [29], no visible cracks are observed on the tested structure subjected to the EQ_1 excitation. The phenomenon is likely

due to the nonlinear dynamic behaviors of the RC structure during strong ground motion vibrations. To evaluate the structural damage conditions under significant ground motion excitations, the measured acceleration signals of the tested structure subjected to the EQ_1 excitation is considered as a reference state in this study. The other three states under EQ_2, EQ_3 and EQ_4 will be compared with the case under EQ1, to understand and identify the changes in structural conditions. Thus, totally three damage cases of the RC structure subjected to EQ_2, EQ_3 and EQ_4 excitations are studied. It shall be noted that the purpose of this comparison is to identify the changes in structural conditions.

Based on the vibration decomposition combined with the damage index *DQ*, the proposed MSST-AMD approach is first performed to extract the individual components from the measured acceleration data. Then the instantaneous frequencies of the first two decomposed mono-components under three different cases are further identified by using Hilbert Transform and are shown in Figures 4-17(a)-(c), respectively. It can be observed that the identified natural frequencies of the tested structure under external excitations are gradually reduced during the strong structural vibrations, which is caused from the increased damage severity of the tested structure. It should be noted that as mentioned above, there were a total of 61 testing cases in the study carried out in [29]. In this study, the four selected cases, i.e., EQ_1-EQ_4 are not the continuous testing cases. There were actually a number of testing cases in between any two subsequent cases selected for the analysis in this study. Therefore these identified instantaneous frequencies under different damage states in those three cases are not continuous, i.e., the end status of EQ_2 is not necessarily the starting status of EQ_3. Since the study analyses the instantaneous frequencies of the structure during each test/excitation and estimate the condition deterioration, this choice of testing cases does not affect the results. Based on the defined damage index in Equation (4.22), the calculated damage severity of the tested structure subjected to three earthquake excitations with different intensities are listed in Table 1. From Table 1, it can be observed that from EQ_2 to EQ_4, the damage severity of the structure is 0.29, 0.46 and 0.72, respectively. According to the experimental report [29], the structure has experienced a moderate damage under EQ_2 (PGA=0.388g), and the damage severity was further increased under EQ_3 (PGA=0.517g), and severe damage was observed under EQ_4 (PGA=0.775g). Therefore, as indicated in Table 1 the calculated damage index is reliable to define the severity of damage for three damage cases. Results in experimental investigations demonstrate that the proposed approach is effective and accurate for vibration signal decomposition, which can be further used for structural damage detection.

Table 4-1 The calculated damage index results under three damage cases

Case 1	Case 2	Case 3
0.29	0.46	0.72

Figure 4-14 The tested structure

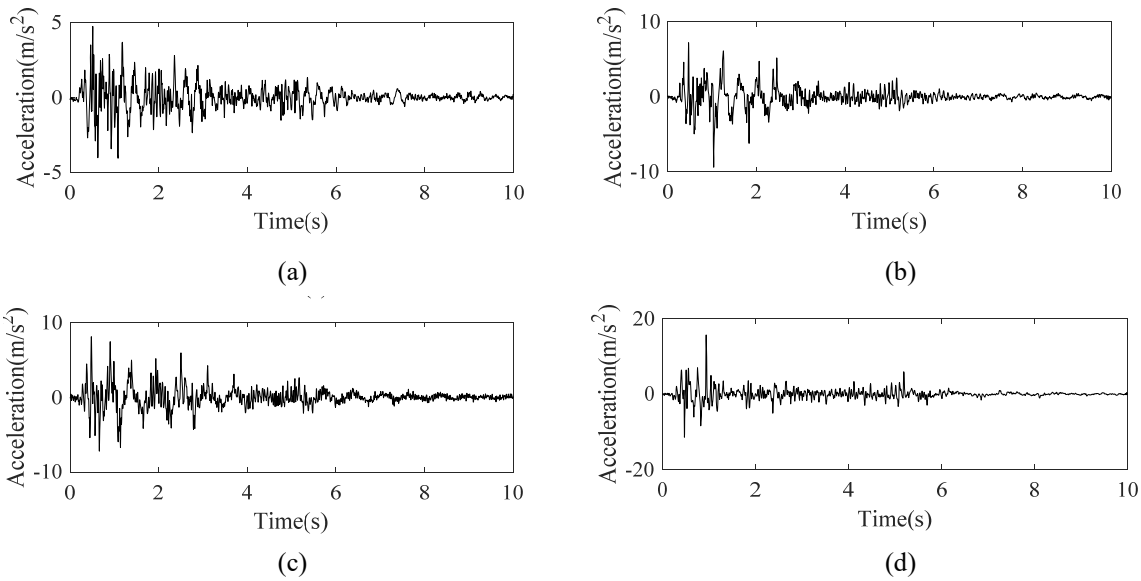

Figure 4-15 The measured acceleration signals under: (a) EQ_1; (b) EQ_2; (c) EQ_3; (d) EQ_4.

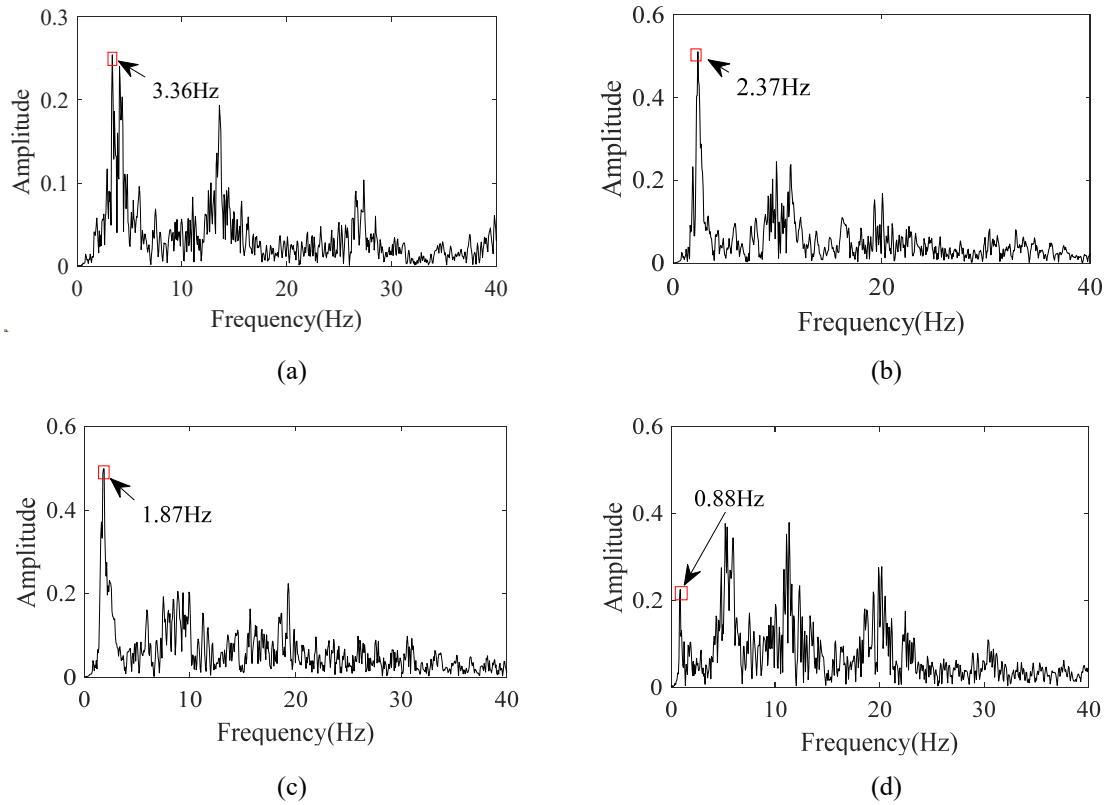

Figure 4-16 The Fourier spectrum of the measured acceleration data under: (a) EQ_1; (b) EQ_2; (c) EQ_3; (d) EQ_4.

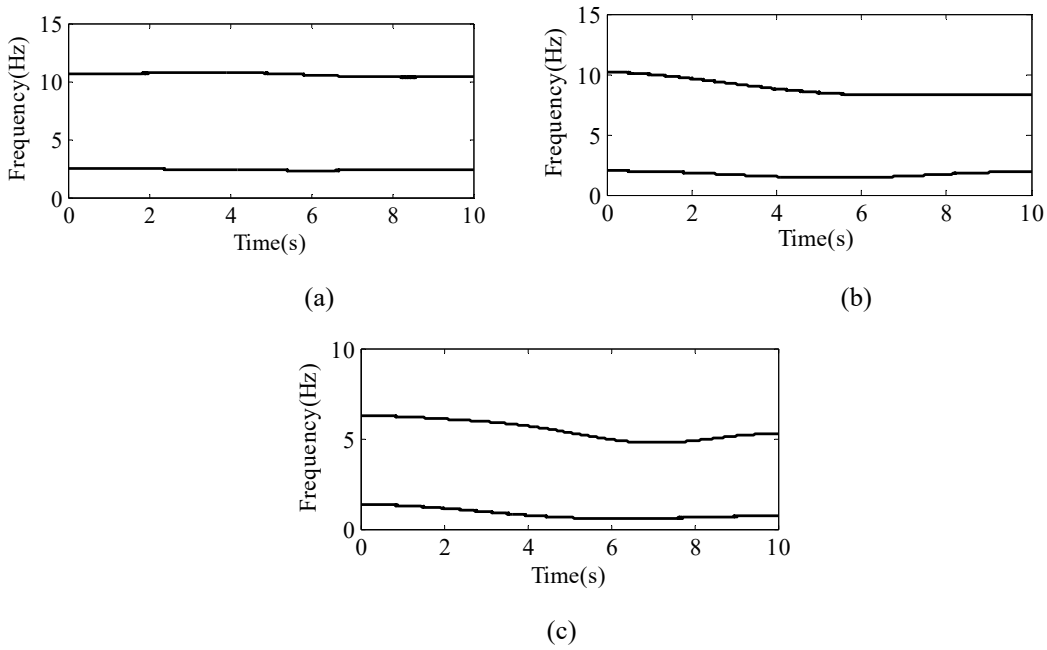

Figure 4-17 The identified instantaneous frequencies of the first two decomposed compoments under three damage cases: (a) Case 1; (b) Case 2; (c) Case 3.

4.5 Conclusions

This chapter proposes an enhanced vibration signal decomposition approach based on MSST and AMD for non-stationary signal analysis. To overcome the challenge of using AMD for non-stationary signal decomposition with overlapped frequency components, the proposed MSST-AMD approach can automatically decompose a signal into several mono-components, which can reduce the significant computational cost to define the time-varying cut-off frequencies of the AMD method. In this study, MSST is first performed to provide the accurate time-frequency representation, and then the developed cut-off frequency detection algorithm is employed to automatically define the time-varying cut-off frequencies between each two individual components. Once the time varying cut-off frequencies are determined, the proposed approach can be used to adaptively decompose the non-stationary signal into individual components. In addition, the proposed MSST-AMD method combined with a damage index is further used for structural damage detection under the earthquake excitations based on the identified instantaneous modal parameters. Numerical studies on a multi-component signals with overlapped frequency components are first conducted to validate the superiority of using the MSST-AMD for vibration signal decomposition. Then, numerical simulations on a three-storey building structure subjected to the seismic excitations are further performed to investigate the effectiveness of using the proposed MSST-AMD approach for structural vibration signal analysis and instantaneous modal parameter identification. In experimental application, the measured acceleration responses from a 12-storey scaled RC structure under various earthquake excitations are used for vibration decomposition with the proposed approach and structural damage detection with a defined damage index. Based on numerical simulations and experimental validations, the following conclusions can be drawn:

(1) The MSST based time-frequency representation with the proposed cut-off frequency detection algorithm can automatically define the time-varying cut-off frequencies of using AMD for non-stationary signal decomposition;

(2) The proposed MSST-AMD approach can effectively and accurately decompose a non-stationary signal into several mono-components, even under the significant noise effect; and

(3) Based on the vibration decomposition results by using the developed approach, structural damage detection is conducted by using a damage index. The results indicate that the proposed damage detection approach can successfully evaluate the damage severity of the structures subjected to the earthquake excitations.

References

[1] Beskhyroun S., Oshima T., Mikami S. (2010). Wavelet-based techniques for structural damage detection. *Structural Control & Health Monitoring*, 17 (5): 473-494.

[2] Ni P.H., Li J., Hao H., Xia Y., Wang X.Y., Lee J.M., Jung K.H. (2018). Time-varying system identification using variational mode decomposition. *Structural Control & Health Monitoring*, 25: e2175

[3] Ren W.X., Zong Z.H. (2004). Output-only modal parameter identification of civil engineering structures. *Structural Engineering and Mechanics*, 17(3-4): 429-444.

[4] Xin Y., Hao H., Li J. (2019). Operational modal identification of structures based on improved empirical wavelet transform. *Structural Control & Health Monitoring*, 26: e2323.

[5] Alamdari M.M., Anaissi A., Khoa N., Mustapha S. (2019). Frequency domain decomposition-based multisensor data fusion for assessment of progressive damage in structures. *Structural Control & Health Monitoring*, 26: e2299.

[6] Doebling S.W., Farrar C.R., Prime M.B. (1998). A summary review of vibration-based damage identification methods, *Shock and Vibration Digest*, 30(2): 91-105.

[7] Nagarajaiah S., Basu B. (2009). Output only modal identification and structural damage detection using time frequency & wavelet techniques, *Earthquake Engineering and Engineering Vibration*, 8(4): 583-605.

[8] Wang C., Ren W.X., Wang Z.C., Zhu H.P. (2013). Instantaneous frequency identification of time-varying structures by continuous wavelet transform. *Engineering Structures*, 50: 17-25

[9] Ren W.X., Sun Z.S. (2008). Structural damage identification by using wavelet entropy. *Engineering Structures*, 30(10): 2840-2849.

[10] Yu G., Yu M.J., Xu C.Y. (2017). Synchroextracting Transform. *IEEE Transactions on Industrial Electronics* 2017; 64(10): 8042-8054.

[11] Shi Z.Y., Law S.S. (2007). Identification of linear time-varying dynamical systems using Hilbert transform and empirical mode decomposition method. *Journal of Applied Mechanics*, 74: 223-30

[12] Yang J.N., Lei Y., Lin S., Huang N. (2004). Hilbert-Huang based approach for structural damage detection. *Journal of Engineering Mechanics*, 130(1): 85-95.

[13] Wang Z.C., Chen G.D. (2012). Recursive Hilbert-Huang Transform Method for Time-Varying Property Identification of Linear Shear-Type Buildings under Base Excitations. *Journal of Engineering Mechanics*, 138: 631-39.

[14] Bao C.X., Hao H., Li Z.X., Zhu X.Q. (2009). Time-varying system identification using a newly improved HHT algorithm. *Computer and Structures*, 87: 1611-23.

[15] Feldman M. (2006). Time-varying vibration decomposition and analysis based on the Hilbert transform. *Journal of Sound and Vibration*, 295: 518-530.

[16] Feldman M. (2011). Hilbert transform application in mechanical vibration. West Sussex: John Wiley & Sons, Ltd.

[17] Chen G.D., Wang Z.C. (2012). A signal decomposition theorem with Hilbert transform and its application to narrowband time series with closely-spaced frequency components. *Mechanical Systems and Signal Processing*, 28: 258-279.

[18] Wang Z.C., Chen G.D. (2013). Analytical mode decomposition of a time series with

overlapping and rapidly time-varying frequencies with Hilbert transform. *Smart Materials and Structures*, 22: 095003:1-14.

[19] Wang Z.C., Xin Y., Xing J.F., Ren W.X. (2017). Hilbert low-pass filter of non-stationary time sequence using analytical mode decomposition. *Journal of Vibration and Control*, 23(15): 2444-2469.

[20] Wang Z.C. (2011). Hilbert Transform application in signal analysis and non-parametric identification of linear and nonlinear systems. *Doctoral Dissertations*. 2012.

[21] Daubechies I., Lu J.F., Wu H.T. (2011). Synchrosqueezed Wavelet Transforms: An Empirical Mode Decomposition-like Tool. *Applied and Computational Harmonic Analysis*, 30: 243-61.

[22] Yu G., Wang Z.H., Zhao P. (2019). Multichrosqueezing Transform. *IEEE Transactions on Industrial Electronics* 2019; 66(7): 5441-55.

[23] Carmona R., Hwang W.L., Torresani B. (1999) Multiridge detection and time-frequency reconstruction. *IEEE Transactions on Signal Processing*, 47(2): 480-92.

[24] Meignen S., Pham D.H., McLaughlin S. (2017). On demodulation, ridge detection, and synchrosqueezing for multicomponent signals. *IEEE Transactions on Signal Processing*, 65(8): 2093-103.

[25] Oberlin T., Sylvain M., Perrier V. (2013). The Fourier-based Synchrosqueezing Transform. Hal-00916088.

[26] Ditommaso R., Mucciarelli M., Ponzo F.C. (2012). Analysis of non-stationary structural systems by using a band-variable filter. *Bulletin of Earthquake Engineering*, 10: 895-911.

[27] Xin Y., Hao H., Li J. (2019). Time-varying system identification by enhanced Empirical Wavelet Transform based on Synchroextracting Transform. *Engineering Structures*, 196: 109313.

[28] Gong M.S., Xie L.L., Ou J.P. (2008). Modal Parameter Identification of Structure Model using Shake Table Test Data. *The 14th World Conference on Earthquake Engineering*, Beijing, China.

[29] Lv X.L., Li P.Z., Chen Y.Q. (2004). Benchmark Test of a 12-storey Reinforced Concrete Frame Model on Shaking Table. Tongji University, Shanghai.

The [Xin, Y., Li, J. & Hao, H. Damage Detection in Initially Nonlinear Structures based on Variational Mode Decomposition. *International Journal of Structural Stability and Dynamics*. https://doi.org/10.1142/S0219455420420092] is unable to be reproduced here due to copyright restrictions.

The [Damage Detection in Initially Nonlinear Structures based on Variational Mode Decomposition] can instead be accessed via [https://doi.org/10.1142/S0219455420420092]

CHAPTER 6 BAYESIAN BASED NONLINEAR MODEL UPDATING USING INSTANTANEOUS CHARACTERSTICS OF STRUCTURAL DYAMIC RESPONSES

ABSTRUCT[4]

This chapter proposes a Bayesian based nonlinear model updating approach using the instantaneous amplitudes of the decomposed dynamic responses. Uncertainty quantification of the model updating results due to the measurement noise is conducted. The residual of the instantaneous amplitudes of the decomposed structural dynamic responses between the test structure and the analytical nonlinear model is used to construct the maximum likelihood function. Since nonlinear model parameters and simulated error variances of the instantaneous parameters are all unknown, the extended maximum likelihood estimation method is used to update these parameters. The uncertainty in the updated nonlinear model parameters can be evaluated by using the Cram-Rao lower bound theorem with the exact Fisher Information matrix. A numerical study on a three-storey building structure model under earthquake excitation is performed to verify the accuracy and performance of the proposed approach. An experimental verification on a high voltage switch structure under harmonic excitation is conducted to investigate the accuracy of using the proposed approach for nonlinear model updating. Both numerical and experimental results demonstrate that the proposed approach is reliable and accurate for nonlinear model updating, with the capacity of considering the uncertain noise effect in the measurements.

6.1 Introduction

Finite element model (FEM) has been extensively used for predicting the structural responses and structural identification in civil, aerospace and mechanical engineering community. Since FEM is built based on the idealized assumption of structural material

[4]This chapter was published in *Engineering Structures* with the full bibliographic citation as follows: Xin, Y., Hao, H., Li, J., Wang Z., Wan H. & Ren W. (2019). Bayesian based nonlinear model updating using instantaneous characteristics of structural dynamic responses. *Engineering Structures*, 183:459-474. https://doi.org/10.1016/j.engstruct.2019.01.043.

properties and boundary conditions from the original engineering design, it may not accurately represent the actual behaviors of an in-service structure. Therefore, it is very important to refine the FEM based on the measured structural responses, which is termed as finite element model updating (FEMU). The aim of FEMU is to build a high-fidelity FEM that is able to characterize the accurate structural behavior reliably. In the last several decades, FEMU has gained increasing attention from engineers and researchers, and various FEMU techniques have been developed [1-8].

Generally, the development of the deterministic FEMU methods is relatively mature, and numerous approaches have been successfully applied for linear and nonlinear model updating in the literature [9-16]. The main objective of the deterministic FEMU techniques is to minimize the difference between the quantitative structural characteristics obtained from the measured data and the analytical structural model by adjusting structural model parameters. Since the number of measured structural response parameters is always less than the actual structural parameters in a FEM, optimization analysis is needed in performing model updating. The accuracy of deterministic model updating results depends on the accuracy of the initial structural model and the accuracy of the structural response characteristics extracted from the measured data [17]. However, for deterministic FEMU methods, the effect of uncertainties on the model updating results needs to be carefully considered. The uncertainties in the model updating usually arise from measurement noise in the response data and the modeling errors in the structure. Accounting for the propagation effect of these uncertainties on the model updating process and investigating the effect on the model updating results have attracted significant attention in recent years [18-24].

One possible approach to deal with these uncertainties in FEMU is using a probabilistic framework based on the well-known Bayesian theorem [18-27]. The initial Bayesian approach for parameter estimation in model updating considering uncertainty was developed by Beck and Katafygiotis [28-29]. Behmanesh et al. [30-31] proposed a hierarchical Bayesian FEMU method for uncertainty quantification and damage identification of structural systems. Wan and Ren[32] proposed using an efficient Bayesian inference method with delayed rejection adaptive Metropolis (DRAM) algorithm to refine the FEM of a four-span pedestrian bridge considering the uncertainty in identified modal properties.

Most of the aforementioned studies on updating and identifying model parameters considering uncertainties are applicable for linear structural models. For the probabilistic nonlinear model updating, recursive filtering methods and batch estimation methods [33-35] have been developed in the past decades. However, the application of these methods is limited or only suitable for some highly idealized nonlinear models such as a single

degree-of-freedom (DOF) system, or simplified multi-DOF systems. Ebrahimian et al. [38] later used a batch Bayesian method for nonlinear FEMU with the measured dynamic responses, and the uncertainties of identified model parameters caused by measurement noise were further quantified by using the Cram-Rao lower bound (CRLB) method based on two different Fisher Information matrixes (FIM). Although the proposed FEMU method is effective for model parameter estimation with noisy responses, the measured response time series from real civil engineering structures, i.e. under ambient excitations, are usually very long, and it may significantly increase the computational cost when the whole measured data is used as target responses. To overcome this issue, Wang et al. [39-40] proposed a nonlinear model updating strategy based on instantaneous characteristics of decomposed dynamic responses. In this method, considering the slowly-varying characteristics of instantaneous parameters (compared with the original oscillating acceleration response), only a total of 15 local peaks of instantaneous amplitudes and frequencies of the decomposed dynamic responses were selected to construct the objective function for nonlinear model updating. The calibrated model can accurately predict the dynamic responses of structures. However, the uncertainty effect on the parameter identification is not quantified in these deterministic nonlinear model updating methods under the influence of measurement noise and modeling error.

This chapter proposes using a nonlinear model updating approach based on the instantaneous characteristics of the decomposed dynamic responses, to account for the uncertainty effect from the measurement noise. The instantaneous parameters of mono-components are firstly extracted from the response signal by using discrete analytical mode decomposed (DAMD) method and Hilbert Transform [41]. Then, the likelihood function associated with Bayesian method is built by using the instantaneous parameters extracted from analytical nonlinear models and testing structures. The nonlinear model parameter updating problem is formulated as the Maximum Likelihood Estimation (MLE).The optimization problem of MLE is solved with a gradient-based interior point algorithm [42-45], and the uncertainty quantification of the identified nonlinear model parameters is conducted by using the CRLB theorem [46-50]. To validate the accuracy and effectiveness of the proposed nonlinear model updating approach, a numerical study on a three-storey building structure model under earthquake excitation is conducted. An experimental verification on a real high voltage switch structure subjected to harmonic excitation is also performed to verify the proposed approach.

6.2 Theoretical Background

6.2.1 Instantaneous amplitude and frequency identification

The natural frequencies of a nonlinear structure usually change with time. Wang et al. [51] proposed AMD to analyse the time-varying vibration signals without selecting constant cutoff frequencies. However, in reality, the measured dynamic signals are discrete since the low sampling frequencies are selected. Wang et al. [41] further extended AMD for discrete time sequences, termed as "DAMD". Based on theoretical derivations, one-step, two step and four-step low-pass filters have been designed to extract the mono-components of non-stationary time sequences according to different sampling frequencies. The one-step low-pass filter is only effective when the following condition is satisfied

$$\text{Condition 1: } \omega_c(t) \leq \frac{\omega_s}{4} \text{ and } \omega_{max} \leq \frac{\omega_s}{2} - \omega_c^{max} \tag{6.1}$$

in which $\omega_c(t)$is a time-varying cutoff frequency; $\omega_c^{max}$is the maximum value of the time-varying cutoff frequency; ω_{max} and ω_s are maximum frequency and sampling frequency of a response signal, respectively.

Similarly, two-step low-pass filter is effective when Condition 2 is satisfied, and four-step filter is valid when Condition 3 is satisfied

$$\text{Condition 2: } \omega_c(t) \leq \frac{\omega_s}{4} \tag{6.2}$$

$$\text{Condition 3: } \frac{\omega_s}{4} < \omega_c(t) < \frac{\omega_s}{2} \tag{6.3}$$

In this study, since sampling frequencies satisfy Condition 1, the one-step low-pass filter is used to decompose mono-components of acceleration responses. The theorem of one-step low-pass filter with time-varying cutoff frequency is described below:

Let $x(t)$ denotes a real measured signal of n significant individual components with frequencies:$\omega_1(t), \omega_2(t), \cdots, \omega_n(t)$, which are all positive and in Lebesque space$L^2(-\infty, +\infty)$ of the real time variable t. It can be decomposed into n components $x_p^{(d)}(t)$ ($p=1,2,\ldots,n$) with the following frequency ranges $|\omega_1(t)| < \omega_{c1}(t)$, $\omega_{c1}(t) < |\omega_2(t)| < \omega_{c2}(t)$, $\cdots$, $\omega_{c(n-2)}(t) < |\omega_{n-1}(t)| < \omega_{c(n-1)}(t)$, and $\omega_{c(n-1)}(t) < |\omega_n(t)|$. This can also be expressed as

$$x(t) = \sum_{p=1}^{n} x_p^{(d)}(t) \tag{6.4}$$

in which $\omega_p(t)$ represents the frequency corresponding to the decomposed component $x_p^{(d)}(t)$, and $\omega_{cp}(t) \in \left(\omega_p(t), \omega_{p+1}(t)\right)$ $(p = 1,2,\cdots,n-1)$ are time-varying cutoff

frequencies. In this study, these time-varying cutoff frequencies can be determined by using wavelet transform. Each individual signal can be determined as

$$x_1^{(d)} = s_1(t), \cdots, x_p^{(d)}(t) = s_p(t) - s_{p-1}(t), \cdots, x_n^{(d)}(t) = x(t) - s_{n-1}(t) \quad (6.5)$$

$$s_p(t) = \sin[\int_{-\infty}^{t} \omega_{cp}(\tau)\,\mathrm{d}\tau]\, H\{x(t)\cos[\int_{-\infty}^{t} \omega_{cp}(\tau)\,\mathrm{d}\tau]\}$$

$$- \cos[\int_{-\infty}^{t} \omega_{cp}(\tau)\,\mathrm{d}\tau]\, H\{x(t)\sin\left[\int_{-\infty}^{t} \omega_{cp}(\tau)\,\mathrm{d}\tau\right]\}$$

$$(p = 1, 2, \cdots, n-1) \quad (6.6)$$

where H means the Hilbert transform, $s_p(t)$ is the pth mono-component of the original signal. Here, $\mathrm{s_p(t)}$ is different from the components $x_p^{(d)}(t)$ in Eq. 4 due to the use of a filter. Equation (6.6) can be considered as a low-pass filter that passes any low frequency signal $s(t)$but filters the fast-varying component $\bar{s}(t)$ in the time domain.

For an n DOF nonlinear system, the equation of motion can be written as

$$\mathbf{M}[\ddot{\mathbf{x}}(t)] + \mathbf{F_c}[\dot{\mathbf{x}}(t)] + \mathbf{F_s}[\mathbf{x}(t)] = \mathbf{f}(t) \quad (6.7)$$

in which $\mathbf{M}$ is the mass matrix,$\mathbf{F_c}[\dot{\mathbf{x}}(t)]$isthe damping force vector, $\mathbf{F_s}[\mathbf{x}(t)]$ is the nonlinear restoring force vector and $\mathbf{f}(t)$ is the excitation force vector. For a nonlinear structure, the nonlinear restoring force as function of time can be transformed into a multiplication form $\mathbf{K}(t)\mathbf{x}(t)$ with a new time-varying stiffness matrix $\mathbf{K}(t)$ and a system solution $\mathbf{x}(t)$with an overlapping spectrum [52]. Similarly, the nonlinear damping force can also be transformed into a function of time as a multiplication $\mathbf{C}(t)\dot{\mathbf{x}}(t)$ between the time-varying damping coefficient matrix $\mathbf{C}(t)$ and the velocity$\dot{\mathbf{x}}(t)$. Thus, the equivalent equation of motion of Equation (6.7) can be expressed as

$$\mathbf{M}(t)\ddot{\mathbf{x}}(t) + \mathbf{C}(t)\dot{\mathbf{x}}(t) + \mathbf{K}(t)\mathbf{x}(t) = \mathbf{f}(t) \quad (6.8)$$

where $\mathbf{M}(t)$, $\mathbf{C}(t)$ and $\mathbf{K}(t)$ are time-varying mass, damping, and stiffness matrices, respectively.

Dynamic responses of Equation (6.8) can be taken as a combination of several mono-components with time-varying frequency and amplitude [52].The measured response of the lth degree $x_l(t)$ can be expressed as the function of mono-component $x_l^{(i)}(t)$

$$x_l(t) = \sum_{i=1}^{n} x_l^{(i)}(t) \quad (6.9)$$

The analytical signal $Z_l^{(i)}$of the ith decomposed response $x_l^{(i)}(t)$ can be expressed as

$$Z_l^{(i)} = x_l^{(i)}(t) + H\left[x_l^{(i)}(t)\right] = A_i(t)e^{j\int \omega_i(t)dt} \tag{6.10}$$

in which$A_i(t)$and$\omega_i(t)$are the instantaneous amplitude and frequency of a decomposed non-stationary signal $Z_l^{(i)}$, respectively. In Equation (6.10), $A_i(t)$ represents the amplitude information of $Z_l^{(i)}$, and $\omega_i(t)$ reflects the instantaneous phase information of the decomposed signal. The instantaneous frequency and amplitude can be used to describe the characteristics of a non-stationary signal. In the study, instantaneous amplitudes of decomposed acceleration responses are used for nonlinear model updating. The accuracy of model updating results is evaluated by comparing both the instantaneous amplitudes and frequencies from the analytical nonlinear model and testing structure.

6.2.2 Bayesian approach for nonlinear model updating

In this section, instantaneous amplitudes extracted from measured acceleration responses are used for nonlinear model updating. The identified instantaneous parameters from the measured acceleration responses can be expressed as:

$$\hat{\mathrm{A}}_t = \left[\hat{\mathrm{A}}_1(t), \hat{\mathrm{A}}_2(t), \cdots, \hat{\mathrm{A}}_{N_m}(t)\right]^{\mathrm{T}} \tag{6.11}$$

where $\hat{\mathrm{A}}_{N_m}(t)$ is the instantaneous acceleration amplitude of the N_mth mono-component at the time instant *t*, where N_m denotes the number of mono-components.

The instantaneous amplitudes $\hat{\mathrm{A}}_t$ extracted from the measured acceleration responses may be different from those calculated from the analytical responses with the structural finite element model. The difference can be defined as:

$$\boldsymbol{\varepsilon}(\boldsymbol{\theta}, t) = \hat{\mathrm{A}}_t - \mathrm{A}_{acc}(\boldsymbol{\theta}, t) \tag{6.12}$$

$$\mathrm{A}_{acc}(\boldsymbol{\theta}, t) = \left[\mathrm{A}_1(\boldsymbol{\theta}, t), \mathrm{A}_2(\boldsymbol{\theta}, t), \cdots, \mathrm{A}_{N_m}(\boldsymbol{\theta}, t)\right]^T \tag{6.13}$$

in which $\boldsymbol{\theta}$ is the vector of nonlinear model parameters, $\mathrm{A}_{acc}(\boldsymbol{\theta}, t)$is the instantaneous amplitude vector identified from the analytical acceleration response, and $\boldsymbol{\varepsilon}(\boldsymbol{\theta}, t)$ represents the difference in the instantaneous amplitudes between the test and analytical results. Generally, the residual $\boldsymbol{\varepsilon}(\boldsymbol{\theta}, t)$ mainly stems from measurement noise and modeling error [17]. In this chapter, the uncertainty in the finite element modeling is not considered. The measurement noises in the recorded acceleration responses are assumed as stationary and independent Gaussian white noises with zero means. Therefore, the difference vector $\boldsymbol{\varepsilon}(\boldsymbol{\theta}, t)$ could also be considered as a Gaussian white noise process [17, 23]. Based on this assumption, the nonlinear model updating can be formulated as the following

optimization problem

$$\widehat{\boldsymbol{\theta}} = arg\min\left\{\sum_{i=1}^{N_m}\sum_{t=1}^{N_t}\mathrm{trace}\left(\varepsilon^i(t)\varepsilon^i(\boldsymbol{\theta},t)^{\mathrm{T}}\right)\right\}$$

$$= arg\ \min\left\{\sum_{i=1}^{N_m}\sum_{t=1}^{N_t}\left\|\hat{\mathrm{A}}_i(t) - \mathrm{A}_i(\boldsymbol{\theta},t)\right\|\right\} \tag{6.14}$$

Solving the optimization problem as shown in Equation (6.14) can be derived based on Bayesian framework and the maximum likelihood estimation methods when a Gaussian white noise simulation error is assumed [17, 20, 23, 26]. Therefore, the unknown model parameters $\boldsymbol{\theta}$ in Equation (6.14) can be considered as stochastic variables based on Bayesian strategy for parameter estimation. External excitation information on the structures is assumed available for the nonlinear model updating in this study. Therefore, a posterior probability density function (PDF) of the nonlinear model parameters can be expressed as

$$p\left(\boldsymbol{\theta}\middle|\hat{\mathrm{A}}_t\right) \propto cp\left(\hat{\mathrm{A}}_t\middle|\boldsymbol{\theta}\right)p(\boldsymbol{\theta}) \tag{6.15}$$

where $p\left(\hat{\mathrm{A}}_t\middle|\boldsymbol{\theta}\right)$ is called the likelihood function and used to represent the contribution of the instantaneous parameters in a posterior joint PDF of nonlinear model parameters [28, 29]. $p(\boldsymbol{\theta})$ is a prior PDF of nonlinear model parameters which is assigned based on the prior information and available knowledge on the nonlinear parameters. c is a constant which is used to ensure $\int p\left(\boldsymbol{\theta}\middle|\hat{\mathrm{A}}_t\right)d\boldsymbol{\theta} = 1$.

In the Bayesian framework for nonlinear model updating, model parameters $\boldsymbol{\theta}$ are usually estimated by maximizing the posterior PDF of $\boldsymbol{\theta}$, and the estimation strategy can be expressed as

$$\widetilde{\boldsymbol{\theta}} = arg\max\left\{p\left(\boldsymbol{\theta}\middle|\hat{\mathrm{A}}_t\right)\right\} = arg\max\left\{\prod_{i=1}^{N_m}\prod_{t=1}^{N_t}N\left(\hat{\mathrm{A}}_i(t)\middle|\boldsymbol{\theta}\right)\right\} \tag{6.16}$$

To estimate the nonlinear parameters more effectively, Equation (6.16) is usually transformed as a minimization problem. Therefore, the parameters $\boldsymbol{\theta}$ in Equation (6.16) can be further calculated by minimizing a negative natural logarithm of a posterior PDF as follows

$$\widetilde{\boldsymbol{\theta}} = arg\min\left\{-\ln\left(p\left(\boldsymbol{\theta}\middle|\hat{\mathrm{A}}_t\right)\right)\right\} = arg\min\left\{-\ln\left(p\left(\hat{\mathrm{A}}_t\middle|\boldsymbol{\theta}\right)\right) - \ln\left(p(\boldsymbol{\theta})\right)\right\} \tag{6.17}$$

where $\ln\left(p\left(\hat{\mathrm{A}}_t\middle|\boldsymbol{\theta}\right)\right)$ is a log-likelihood function. In the Bayesian framework for model

updating, since the known information about nonlinear model parameters $\boldsymbol{\theta}$ is usually limited, the prior PDF of the model parameters $p(\boldsymbol{\theta})$ can be assumed as a uniform PDF [20]. In Equation (6.17), if $p(\boldsymbol{\theta})$is assumed as a uniform PDF, and its natural logarithm will tend to a constant. Therefore, the problem of maximizing a posterior PDF will be turned to a problem of minimizing the negative log-likelihood function, the estimation process is called the maximum likelihood estimation (MLE) of $\boldsymbol{\theta}$ [20, 28]:

$$\widetilde{\boldsymbol{\theta}} = arg\min\left\{-\ln\left(p\left(\hat{\mathrm{A}}_t|\boldsymbol{\theta}\right)\right)\right\} = arg\min - \left\{\Gamma\left(\boldsymbol{\theta}, \hat{\mathrm{A}}_t\right)\right\}$$

$$\Rightarrow \widetilde{\boldsymbol{\theta}} = arg\max\{L(\boldsymbol{\theta})\} \quad \text{and} \quad \Gamma\left(\boldsymbol{\theta}, \hat{\mathrm{A}}_t\right) = \ln\{L(\boldsymbol{\theta})\} \tag{6.18}$$

where $L(\boldsymbol{\theta})$ can be further expressed as

$$L(\boldsymbol{\theta}) = \prod_{i=1}^{N_m}\prod_{t=1}^{N_t}\frac{1}{(2\pi)^{N_m N_t/2}|\boldsymbol{\Sigma}_{\boldsymbol{\varepsilon}}|^{1/2}}e^{-\frac{1}{2}\left(\hat{\mathrm{A}}_i(t)-A_i(\boldsymbol{\theta},t)\right)^T\boldsymbol{\Sigma}_{\boldsymbol{\varepsilon}}^{-1}\left(\hat{\mathrm{A}}_i(t)-A_i(\boldsymbol{\theta},t)\right)} \tag{6.19}$$

in which $L(\boldsymbol{\theta})$ denotes the simplified likelihood function, and diagonal matrix $\boldsymbol{\Sigma}_{\boldsymbol{\varepsilon}}$ represents the covariance matrix of the simulation error vector. As described, the residuals in the instantaneous amplitudes extracted from acceleration responses between measured data and the analytical nonlinear model can be considered as a Gaussian white noise process with $\boldsymbol{\varepsilon}\sim N(0, \boldsymbol{\Sigma}_{\boldsymbol{\varepsilon}})$. MLE of $\boldsymbol{\theta}$ in Equation (6.17) can be alternatively expressed as

$$\widehat{\boldsymbol{\theta}} = arg\min\left\{\frac{N_m N_t}{2}\ln(|\boldsymbol{\Sigma}_{\boldsymbol{\varepsilon}}|) + \frac{1}{2}\sum_{i=1}^{N_m}\sum_{t=1}^{N_t}\left(A_i(t) - A_i(\boldsymbol{\theta},t)\right)^T\boldsymbol{\Sigma}_{\boldsymbol{\varepsilon}}^{-1}\left(A_i(t) - A_i(\boldsymbol{\theta},t)\right)\right\} \tag{6.20}$$

In Equations (6.19) and (6.20), the variance matrix $\boldsymbol{\Sigma}_{\boldsymbol{\varepsilon}}$ can be represented as

$$\boldsymbol{\Sigma}_{\boldsymbol{\varepsilon}} = \begin{bmatrix} \sigma^2_{(1,1)} & 0 & 0 & \cdots & \cdots & \cdots & 0 \\ 0 & \ddots & & & & & \vdots \\ \vdots & & \sigma^2_{(1,N_t)} & & & & \vdots \\ \vdots & & & \ddots & & & \vdots \\ \vdots & & & & \sigma^2_{(N_m,1)} & & 0 \\ \vdots & & & & & \ddots & 0 \\ 0 & \cdots & \cdots & \cdots & \cdots & 0 & \sigma^2_{(N_m,N_t)} \end{bmatrix}_{N_m N_t \times N_m N_t}$$

where $\sigma^2_{(N_m,N_t)}$ is the simulation error variance of instantaneous parameters of the $N_m{}^{\text{th}}$ mono-component. For the covariance matrix $\boldsymbol{\Sigma}_{\boldsymbol{\varepsilon}}$ in Equations (6.19) - (6.20), the simulation error variance $\sigma^2_{(N_m,N_t)}$ is unknown. Therefore it is considered as an unknown parameter in nonlinear model updating. Since the simulation error variance for each mono-component is

consistent and the variance matrix $\boldsymbol{\Sigma_\varepsilon}$ is a diagonal matrix, another N_m unknown variables are included in the optimization process. To estimate all the unknown parameters including $\boldsymbol{\theta}$ and $\boldsymbol{\sigma}^2$, an extended MLE method is used in the study, which is expressed as the following objective function and an optimization problem

$$G\left(\boldsymbol{\theta},\ \sigma_{N_m}^2\right) = \frac{N_m N_t}{2}\ln(|\boldsymbol{\Sigma_\varepsilon}|) + \frac{1}{2}\sum_{m=1}^{N_m}\sum_{t=1}^{N_t}\left(\boldsymbol{\varepsilon}^m(\boldsymbol{\theta},t)\right)^T\boldsymbol{\Sigma_\varepsilon}^{-1}\left(\boldsymbol{\varepsilon}^m(\boldsymbol{\theta},t)\right)$$

$$\Rightarrow \left(\widehat{\boldsymbol{\theta}},\hat{\sigma}_{N_m}^2\right) = \arg min\left(G\left(\boldsymbol{\theta},\ \sigma_{N_m}^2\right)\right) \tag{6.21}$$

in which the objective function consists of two parts. The first part $\frac{N_m N_t}{2}\ln(|\boldsymbol{\Sigma_\varepsilon}|)$ is a regularization term penalizing the estimation of large values for the simulation error variance. The second part represents the difference in the instantaneous amplitudes of the decomposed dynamic responses between nonlinear model and real structure, which is weighted inversely by the estimated error variances. The parameter estimation problem in Equation (6.21) can be transformed into a constrained nonlinear optimization problem by setting a feasibility range for the nonlinear model parameters and the initial error variances (i.e., $\boldsymbol{\theta}_{min} \leq \boldsymbol{\theta} \leq \boldsymbol{\theta}_{max}$ and $\sigma_{min}^2 \leq \sigma^2 \leq \sigma_{max}^2$). This optimization problem is solved by using a gradient-based interior point method [42-43], and the optimization algorithm is available in the MALAB optimization toolbox [53]. To obtain the optimal model parameters $\boldsymbol{\theta}$ and simulation error variances σ^2, the gradient of the objective function is calculated as

$$\frac{\partial \boldsymbol{G}}{\partial \boldsymbol{\theta}} = -\sum_{m=1}^{N_m}\sum_{t=1}^{N_t}\left(A_m(t) - A_m(\boldsymbol{\theta},t)\right)^T\boldsymbol{\Sigma_\varepsilon}^{-1}\left(\frac{\partial A_m(\boldsymbol{\theta},t)}{\partial \boldsymbol{\theta}}\right) \tag{6.22}$$

$$\frac{\partial \boldsymbol{G}}{\partial \sigma_j} = \frac{N_m N_t}{2\sigma_j} - \frac{1}{2}\sum_{m=1}^{N_m}\sum_{t=1}^{N_t}\frac{\left(A_m(t)-A_m(\boldsymbol{\theta},t)\right)^2}{\sigma_j^2}, \qquad j = 1,2,\ldots,N_m N_t \tag{6.23}$$

6.2.3 Uncertainty quantification of the identified nonlinear model parameters

In Section 2.2, nonlinear model parameters $\boldsymbol{\theta}$ and error variances of the instantaneous acceleration amplitudes $\sigma_{N_m}^2$ are defined as variables to be adjusted in the defined objective function $G\left(\boldsymbol{\theta},\ \sigma_{N_m}^2\right)$. In the proposed Bayesian approach based nonlinear model updating framework, the nonlinear parameters and the simulation error variances, namely $\boldsymbol{\theta}$and $\sigma_{N_m}^2$, can be obtained by using the above described optimization algorithm. Compared with the stochastic parameter estimation by using Monte Carlo Markov Chain (MCMC), the

optimization algorithm based on MLE method may not be directly employed to calculate the covariance matrix of the identified nonlinear model parameters.

To overcome this limitation, a Cramer-Rao lower bound (CRLB) approach [50] is used to quantify the uncertainty effect based on the obtained $\widehat{\boldsymbol{\theta}}$ and $\hat{\sigma}_{N_m}^2$ from the MLE of $G(\boldsymbol{\theta},\ \sigma_{N_m}^2)$. In this study, CRLB of the parameter estimation uncertainty is estimated based on the exact FIM. The derivation of the uncertainty quantification process can be expressed as [38, 48, 49]

(1) The model parameters $\boldsymbol{\theta}$ and simulation error $\sigma_{N_m}^2$ can be combined as $\mathbf{H} = [\boldsymbol{\theta};\ \sigma_{N_m}^2]$, the FIM for MLE of Equations (6.22) and (6.23) can be expressed as:

$$\mathbf{FI}(\boldsymbol{\theta},\ \sigma_{N_m}^2) = \begin{bmatrix} (\mathbf{FI}_{\boldsymbol{\theta\theta}})_{N_\theta \times N_\theta} & (\mathbf{0})_{N_\theta \times N_\varepsilon} \\ (\mathbf{0})_{N_\theta \times N_\varepsilon} & (\mathbf{FI}_{\sigma\sigma})_{N_\varepsilon \times N_\varepsilon} \end{bmatrix} \tag{6.24}$$

where the sub-matrices $(\mathbf{FI}_{\boldsymbol{\theta\theta}})_{N_\theta \times N_\theta}and(\mathbf{FI}_{\sigma\sigma})_{N_\varepsilon \times N_\varepsilon}$can be derived as

$$(\mathbf{FI}_{\theta\theta})_{N_\theta \times N_\theta} = \boldsymbol{E}\left[\left(\frac{\partial G(\boldsymbol{\theta},\sigma_{N_m}^2)}{\partial \boldsymbol{\theta}}\right)^T \left(\frac{\partial G(\boldsymbol{\theta},\sigma_{N_m}^2)}{\partial \boldsymbol{\theta}}\right)\right] = \boldsymbol{E}\left[\sum_{m=1}^{N_m}\sum_{t=1}^{N_t}\left[\left(\frac{\partial A_m(\boldsymbol{\theta},t)}{\partial \boldsymbol{\theta}}\right)^T \boldsymbol{\Sigma_\varepsilon}^{-1}(A_m(t) - A_m(\boldsymbol{\theta},t))\right]\boldsymbol{\Sigma_\varepsilon}^{-1}\sum_{m=1}^{N_m}\sum_{t=1}^{N_t}\left[(A_m(t) - A_m(\boldsymbol{\theta},t))^T \boldsymbol{\Sigma_\varepsilon}^{-1}\left(\frac{\partial A_m(\boldsymbol{\theta},t)}{\partial \boldsymbol{\theta}}\right)^T\right]\right] = \sum_{m=1}^{N_m}\sum_{t=1}^{N_t}\left[\left(\frac{\partial A_m(\boldsymbol{\theta},t)}{\partial \boldsymbol{\theta}}\right)^T \boldsymbol{\Sigma_\varepsilon}^{-1}\left(\frac{\partial A_m(\boldsymbol{\theta},t)}{\partial \boldsymbol{\theta}}\right)\right] \tag{6.25}$$

$$(\mathbf{FI}_{\sigma\sigma})_{N_\varepsilon \times N_\varepsilon} = \frac{N_m N_t}{2}\begin{bmatrix} \frac{1}{\sigma_{11}^2} & & & & & & \\ & \ddots & & & & & \\ & & \frac{1}{\sigma_{1N_t}^2} & & & & \\ & & & \ddots & & & \\ & & & & \frac{1}{\sigma_{N_m 1}^2} & & \\ & & & & & \ddots & \\ & & & & & & \frac{1}{\sigma_{N_m N_t}^2} \end{bmatrix}_{N_m N_t \times N_m N_t} \tag{6.26}$$

(2) According to CRLB method, if $\widehat{\mathbf{H}} = [\widehat{\boldsymbol{\theta}}; \hat{\sigma}_{N_m}^2]$is an unbiased estimate of $\mathbf{H}$ based on the measured instantaneous data $\boldsymbol{A}_{acc}(t)$, and has a log-likelihood functionln$(L(\boldsymbol{\theta}))$, which is differentiable with respect to the vector of theoretical values $\mathbf{H}_{real}$, the covariance matrix of the estimated parameters satisfies

$$\boldsymbol{E}_{(\boldsymbol{A_{acc}}|\mathbf{H})}\left[(\widehat{\mathbf{H}} - \mathbf{H}_{real})(\widehat{\mathbf{H}} - \mathbf{H}_{real})^T\right] \geq \mathbf{FI}^{-1}(\mathbf{H}_{real}) \tag{6.27}$$

Therefore, based on Equations (6.24) - (6.27), the FIM can be further extended as

$$\begin{bmatrix} \boldsymbol{E}\left[\left(\widehat{\boldsymbol{\theta}}-\boldsymbol{\theta}\right)(\boldsymbol{\Theta}-\boldsymbol{\theta})^T\right] & \boldsymbol{E}\left[\left(\widehat{\boldsymbol{\theta}}-\boldsymbol{\theta}\right)(\widehat{\boldsymbol{\sigma}}^2-\boldsymbol{\sigma}^2)^T\right] \\ \boldsymbol{E}[(\widehat{\boldsymbol{\sigma}}^2-\boldsymbol{\sigma}^2)(\boldsymbol{\Theta}-\boldsymbol{\theta})^T] & \boldsymbol{E}[(\widehat{\boldsymbol{\sigma}}^2-\boldsymbol{\sigma}^2)(\widehat{\boldsymbol{\sigma}}^2-\boldsymbol{\sigma}^2)^T] \end{bmatrix} \geq \begin{bmatrix} \mathbf{FI}_{\boldsymbol{\theta\theta}}{}^{-1} & \mathbf{O} \\ \mathbf{O} & \mathbf{FI}_{\sigma\sigma}{}^{-1} \end{bmatrix} \tag{6.28}$$

in which $\boldsymbol{E}[X] = \boldsymbol{E}_{(\boldsymbol{A_{acc}}|\mathbf{H})}[X] = \int X\boldsymbol{p}(\boldsymbol{A_{acc}}|\boldsymbol{H})\, d\boldsymbol{A_{acc}}$. Thus, the lower bound for the covariance matrix of the estimated nonlinear model parameters $\boldsymbol{\theta}$ is given as

$$\boldsymbol{Cov}(\boldsymbol{\theta}) \geq \mathbf{FI}_{\boldsymbol{\theta\theta}}{}^{-1} \tag{6.29}$$

In these equations, since the nonlinear model parameters $\widehat{\boldsymbol{\theta}}$ and simulation error variances $\hat{\sigma}_{N_m}^2$ estimated by using MLE method converge gradually to the true values $\boldsymbol{\theta}$and $\sigma_{N_m}^2$, respectively. The covariance matrix of model parameters estimation approximately converges to the CRLB obtained by using $\widehat{\boldsymbol{\theta}}$ and$\hat{\sigma}_{N_m}^2$. Therefore, the uncertainty of the calibrated nonlinear model parameters can be quantified with Equation (6.29).

6.3 Numerical Verification

A numerical study is conducted in this section to investigate the accuracy and effectiveness of using the proposed approach for nonlinear model updating and uncertainty quantification.

6.3.1 Instantaneous parameters identification

A three-storey four-bay building structure model, as shown in Figure 6-1, is considered in finite element analysis using software Opensees [54] for numerical study. In this simulation, all beams and columns of the FEM are modeled by using displacement-based beam-column elements with fiber section, and the detailed section dimensions of the FEM are designed according to ASTM standards. As can be seen from Figure 6-1, the Wide Flange Beams with the dimensions of W24×94 and W27×114 are used to define the sections of beams and columns, respectively. In order to simulate the nonlinear dynamic response of the structure under earthquake excitation, a modified Giuffré-Menegotto-Pinto nonlinear material constitutive model in Opensees is used to define the material of the structure, and the stress-strain relationship of the material is described in Figure 6-2. It can be observed from Figure 6-2 that the hysteretic characteristics of the material model is determined by three parameters f_y, E and b, which denote the initial yield strength, Young's modulus and the strain-hardening ratio, respectively. Besides these parameters, another three secondary parameters which control the transition from elastic to plastic branches are assumed as known constants in this simulation. Therefore, totally six material parameters $f_y^{\mathrm{Beam}}, E^{\mathrm{Beam}}, b^{\mathrm{Beam}}, f_y^{\mathrm{Col}}, E^{\mathrm{Col}}$, and b^{Col} are considered as the unknown

nonlinear model parameters of the FEM. For these six parameters, $f_y^{\mathrm{Beam}}, E^{\mathrm{Beam}}$ and b^{Beam} are the material parameters of steel beams, and the nonlinear behaviors of the steel columns are defined by $f_y^{\mathrm{Col}}, E^{\mathrm{Col}}$ and b^{Col}. The theoretical values of these six hysteretic material parameters are set as: $f_y^{Beam} = 165\mathrm{MPa}$, $E^{Beam} = 2.0\mathrm{GPa}$, $b^{Beam} = 0.16$, $f_y^{\mathrm{Col}} = 345\mathrm{MPa}$, $E^{Col} = 2.0\mathrm{GPa}$, $b^{Col} = 0.08$. The detailed physical dimensions, sensor locations and load arrangements on the numerical model are shown in Figure 6-1. As can be seen in Figure 6-1, the distribution loads on three floors are defined as $q_1 = 22.5\mathrm{kN/m}$, $q_2 = 24.5\mathrm{kN/m}$, $q_3 = 24.5\mathrm{kN/m}$, respectively. Three accelerometers S_1, S_2 and S_3 installed on the floors are used to record the acceleration responses of the building model under earthquake excitation. The longitudinal component of the 1994 Northridge earthquake recorded at the Oxnard Boulevard station, as shown in Figure 6-3, is selected as the applied external excitation on the model. The nonlinear dynamic responses of the structure are calculated by using Newmark and Newton Raphson algorithm with a sampling rate of 240Hz. The acceleration response in the horizontal direction obtained from the sensor location S_3 as shown in Figure 6-1 is assumed as the measured dynamic response, which will be used for the signal decomposition. Figure 6-4 shows the measured time domain response. The moment-curvature hysteretic loops extracted from the responses of columns and beams are shown in Figures 6-5 (a) and (b), respectively. By using the procedure described in Section 2.1, the identified instantaneous amplitudes of the first and second mono-components from the acceleration response on the top floor are shown in Figure 6-6(a) and Figure 6-6(b), respectively. The identified instantaneous frequencies of the first two mono-components are shown in Figure 6-7 with the slowly-varying components of the identified instantaneous frequencies denoted with solid lines, which represent the nonlinear structural behavior and can be obtained by filtering out the fast-varying part with DAMD method.

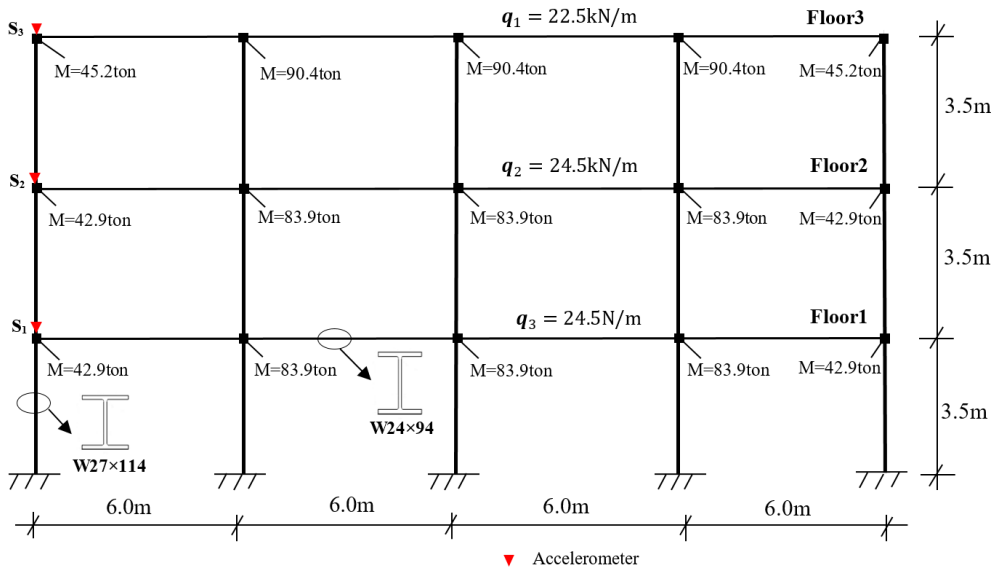

Figure 6-1 A three-storey four-bay building structure model

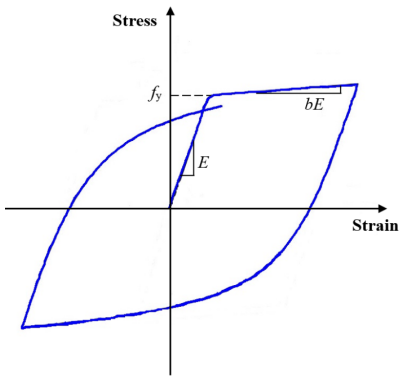

Figure 6-2 The stress-strain relationship of the hysteretic material model.

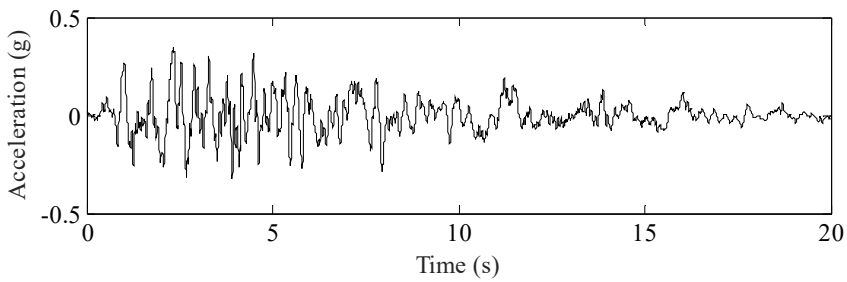

Figure 6-3 Acceleration record of Northridge earthquake

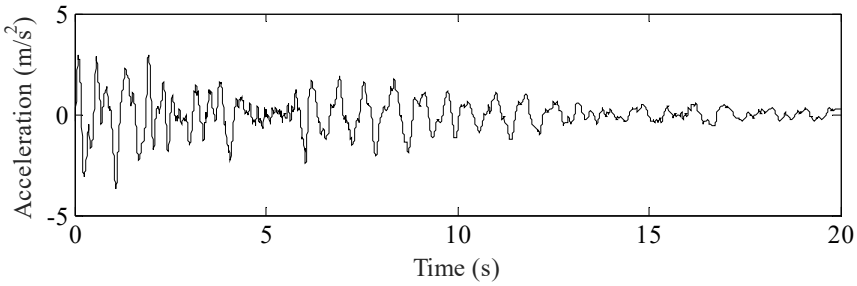

Figure 6-4 Acceleration response at the top floor

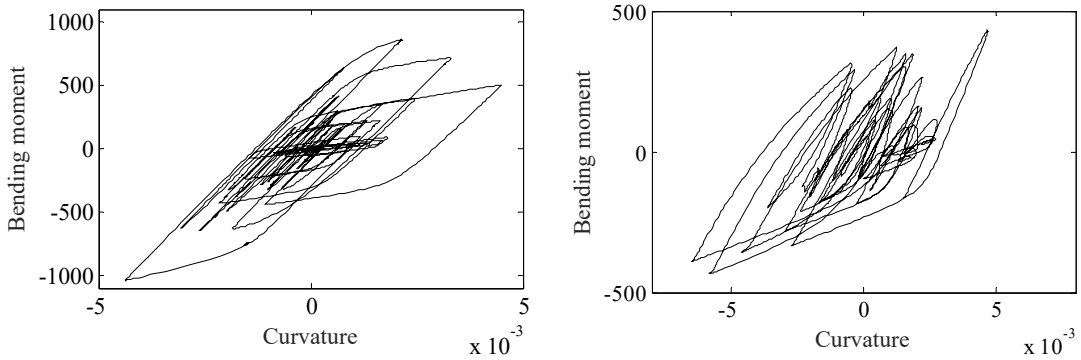

(a) (b)

Figure 6-5 The moment-curvature hysteretic loops under earthquake excitation: (a) Column elements; (b) Beam elements.

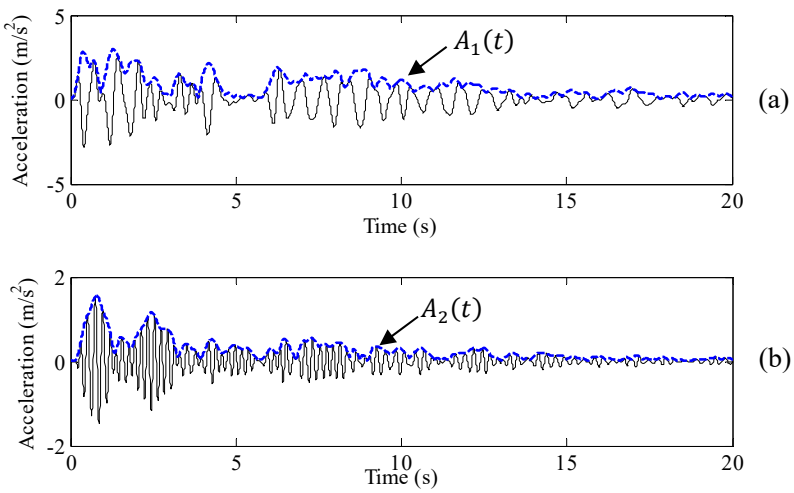

Figure 6-6 The identified instantaneous amplitudes of the first two mono-components of acceleration response at the top floor: (a) The first component; (b) The second component.

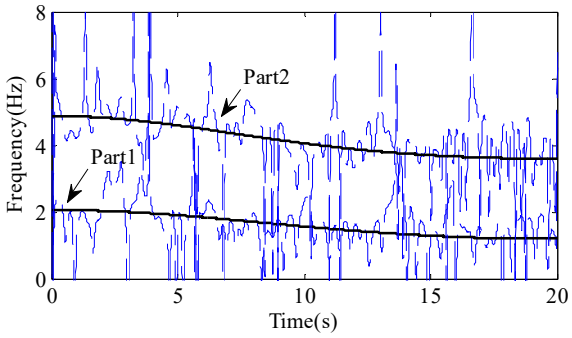

Figure 6-7 The identified instantaneous frequencies of the first two mono-components (Part1: the first main component; Part 2: the second main component).

6.3.2 Bayesian based nonlinear model updating

In this section, the identified instantaneous amplitudes of the measured acceleration responses are used for nonlinear model updating. Before investigating the performance of nonlinear model updating with these selected data points, the assumption made in Section 2.2 with the difference vector $\varepsilon^{m}(\theta, t)$ considered as a Gaussian white noise process when the white noises are smeared in the measured data will be validated first. The simulated acceleration response on the top floor added with 5% Gaussian white noise is used in the identification analysis. The obtained PDFs of the measurement noise extracted from the acceleration responses and the corresponding instantaneous amplitudes have the same statistical characteristics, as shown in Figures 6-8(a) - 6-8(f). This validates that the residual in the identification instantaneous amplitudes of the decomposed acceleration response can also be considered as a Gaussian white noise process with $\varepsilon \sim N(0, \Sigma_{\varepsilon})$.

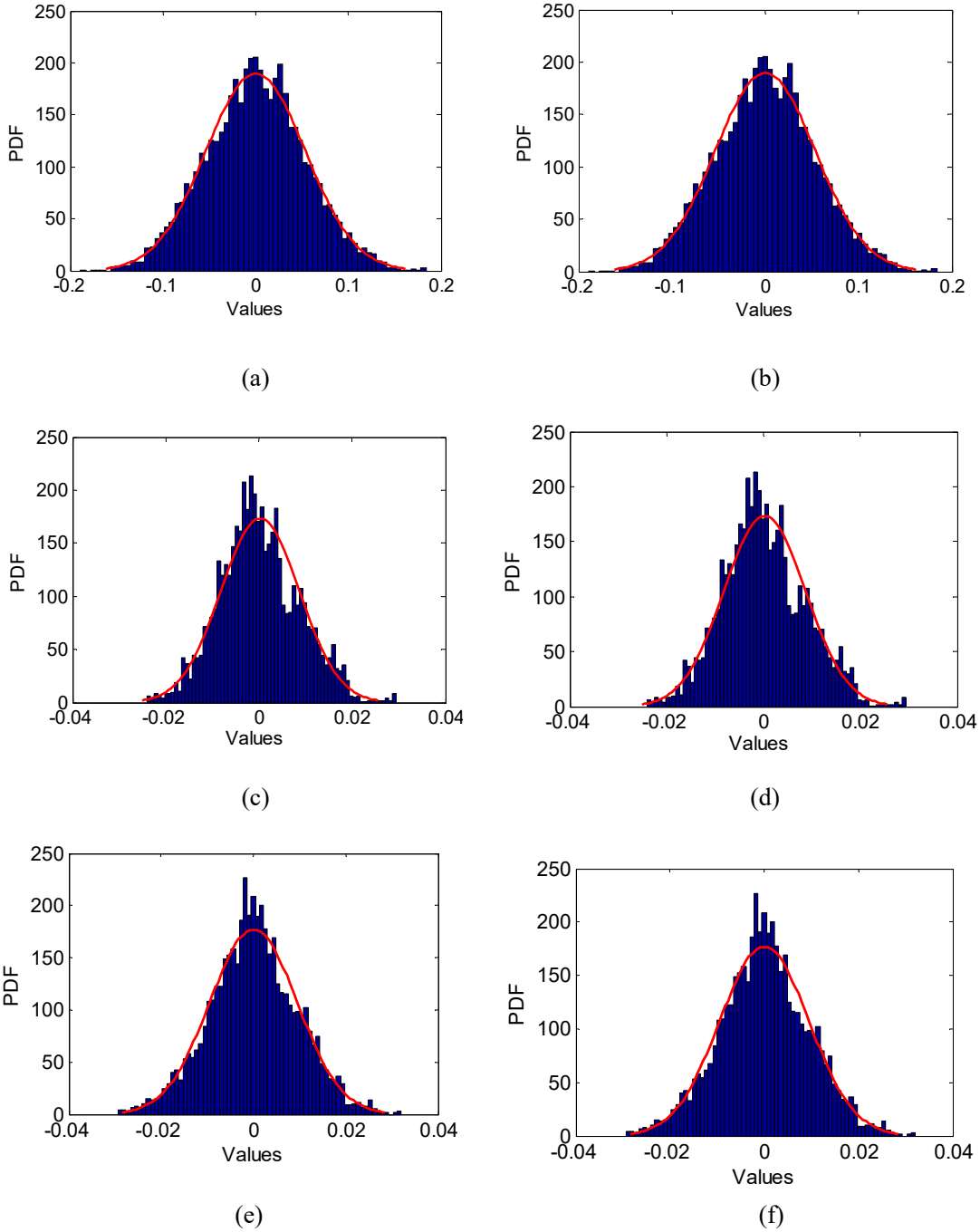

Figure 6-8 PDFs of the measurement noise extracted from the acceleration responses and the corresponding instantaneous amplitudes: (a) Acceleration response; (b) Instantaneous amplitude of the acceleration response; (c) The first component of acceleration response; (d) Instantaneous amplitude of the first component of acceleration response; (e) The second component of acceleration response; (f) Instantaneous amplitude of the second component of acceleration response.

Since the amplitudes of acceleration responses slowly vary with time by comparing with the oscillation of the time histories, it is not necessary to select all the measured data points as the input to the proposed approach for nonlinear model updating. This will improve the

computational efficiency of the proposed approach. However, if the selected data points are too few, it may make the selected time series lose the original statistical characteristics. In this study, the identification error analysis and computational cost comparison with different numbers of selected data points will be conducted to investigate the robustness of the proposed approach. Four cases are considered as follows

Case 1: 1% data points uniformly selected from the extracted instantaneous amplitudes

Case 2: 5% data points uniformly selected from the extracted instantaneous amplitudes

Case 3: 10% data points uniformly selected from the extracted instantaneous amplitudes

Case 4: the full data points of the instantaneous amplitudes are selected for model updating

In addition, since a measured dynamic response consists of a finite number of mono-components, if all mono-components of the vibration signal are also considered as the inputs of the proposed method, the unknown parameters of the objective function used for nonlinear model updating will be large, which may cause a numerical problem. Therefore, studies with different number of mono-components are conducted to verify the reliability of the proposed approach. Three cases are considered as follows

Case 5: a primary mono-component of acceleration response are selected

Case 6: two main mono-components of acceleration response are selected

Case 7: three mono-components of acceleration response are selected

Similar as studies conducted in Section 3.1, the same six material parameters f_y^{Beam}, E^{Beam}, b^{Beam}, f_y^{Col}, E^{Col}, and b^{Col} are identified in this study. To reliably evaluate the accuracy of the model updating results, two error indices R_ω and R_{acc} are defined as

$$R_\omega = \frac{\left\|\omega^{\mathrm{predict}}(t)-\omega(t)\right\|_2}{\|\omega(t)\|_2} \times 100\% \tag{6.32}$$

$$R_{acc} = \frac{\left\|A^{\mathrm{predict}}(t)-A(t)\right\|_2}{\|A(t)\|_2} \times 100\% \tag{6.33}$$

in which $\omega^{\mathrm{predict}}(t)$ and $\omega(t)$ represent the slowly-varying parts of the instantaneous

frequencies obtained from the analytical and testing models, respectively; $A^{predict}(t)$ and $A(t)$ are the acceleration amplitudes of the analytical and testing models, respectively. $\|\cdots\|_2$ represents the l_2 norm.

The initial model parameter values are arbitrarily set as: $\theta_{\text{initial}} = [0.1{f_y}^{\text{Col}}, 0.1E^{\text{Col}}, 1.8b^{\text{Col}}, 1.8{f_y}^{\text{Beam}}, 0.2E^{\text{Beam}}, 1.7b^{\text{Beam}}]$, and the range of these six model parameters is defined as: $0.001\theta^{\text{ture}} \leq \theta \leq 2\theta^{\text{ture}}$. It can be observed from Figure 6-8 that the statistical characteristics of measurement noise in different mono-components are similar, the error variance σ_1^2 is selected as the baseline variance in the proposed method for nonlinear model updating. The initial simulation error variance is assumed as $8.45\sigma_1$, and the feasible domain of the simulation error variance is defined as: $0.01\sigma_1 \leq \sigma \leq 100\sigma_1$.

The obtained nonlinear hysteretic model parameters $\hat{\boldsymbol{\theta}}$ and $\hat{\sigma}_1$ for the above seven cases are listed in Table 1, respectively. The corresponding error indices are presented in Table 2, respectively. As observed from Case 1 to Case 4 in Table 1, these six nonlinear model parameters can be accurately identified based on the proposed approach. It can also be observed that the defined two error indices are smaller than 6%, when more than 1% data points are selected. The uncertainty quantification results of these identified parameters when considering 5% noise effect are shown in Table 2. It is noteworthy from Table 2 that the covariance in the identification results of six parameters is gradually becoming stable when the selected data points are more than 10%.The maximum covariance is 1.26% among all the parameter identification results, indicating that the proposed approach is reliable and robust. As can be seen from Case 5 to case 7 in Table1, it can be found that the proposed method can also effectively calibrate the nonlinear model by using a primary component of acceleration response with a good accuracy. In addition, from the comparison of the estimated covariance of the identified nonlinear parameters in Table 2, it is noteworthy that the values of covariance of the Cases 5-7 are significantly smaller than those of the Cases 1-4. The main reason is that since a finite number of the mono-components are used for nonlinear model updating in Cases 5-7, the effect of measurement noise only within the filter window is considered. In other words, the proposed nonlinear model updating approach aims to accurately calibrate the main components of the measured dynamic responses. Considering

these main components can approximately represent the dynamic features of a measured response, it indicates that the proposed method is robust against measurement noise.

To validate that the proposed approach can significantly save the computational cost, the computational time for each case is listed in Table 1, by using a Dell desktop workstation with an Intel(R) Core(TM) i7-6700(3.4GHz) processor and 64GB RAM. As can be seen from Table 1, it can be found that the required computational time is significantly decreasing when a less number of data points are used for nonlinear model updating. The main reason could be that using a less number of data points will significantly decrease the complexity of nonlinear parameters estimation by using the proposed method. It can be observed from Table 2 that the nonlinear model updating using a primary component of acceleration response with 10% data points is reliable and accurate.

The convergence process of the six nonlinear material parameters and the error covariance in Cases1-4 are shown in Figures 6-9(a)-(g). It can be observed that when more data points are used, a less number of iterations are required in the optimization analysis and a better accuracy in the identification results is achieved. To balance the computational cost and accuracy, 10% data points uniformly selected from the instantaneous amplitudes of decomposed acceleration response is a good option for nonlinear model updating. In addition, to validate the reliability of the proposed approach, the identified nonlinear parameters with three sets of different initial parameter values are listed in Table 3. It can be clearly seen from Table 3 that the identification results are consistent even if the initial parameters are far away from the true values. These results demonstrate that the selection of initial nonlinear model parameter values has no effect on the identification results.

Table 6-1 Identified parameters of the nonlinear hysteretic model with different numbers of data points

Case	Column parameters			Beam parameters			σ_1 $/\sigma_1{}^{real}$	Running time(s)
	f_y/f^{real}	E/E^{real}	b/b^{real}	f_y/f^{real}	E/E^{real}	b/b^{real}		
Exact	1.00	1.00	1.00	1.00	1.00	1.00	1.00	/
Case1	1.02	1.01	0.93	1.01	1.10	1.00	1.59	2.86
Case2	0.99	1.03	0.96	1.00	1.01	1.04	1.36	3.34
Case3	0.99	1.02	0.95	1.00	1.01	1.04	1.01	5.61
Case4	0.99	1.02	0.96	1.00	1.00	1.04	1.01	821.01
Case5	1.01	1.00	0.95	0.99	1.01	1.03	1.02	5.61
Case6	1.00	1.04	0.95	0.99	1.01	1.07	1.01	15.53
Case7	0.99	1.01	0.99	1.00	1.01	1.09	0.99	40.01

Table 6-2 Uncertainty quantification of identified nonlinear model parameters with different numbers of selected data points

Case	Error index (%)		Column parameters			Beam parameters		
	R_{acc}	R_ω	$Cov_{f_y}(\%)$	$Cov_E(\%)$	$Cov_b(\%)$	$Cov_{f_y}(\%)$	$Cov_E(\%)$	$Cov_b(\%)$
Case1	12.42	2.89	1.85	1.80	5.70	2.31	1.95	3.49
Case2	5.87	0.16	0.71	0.83	2.39	1.07	0.75	1.55
Case3	4.89	0.06	0.37	0.43	1.25	0.55	0.39	0.82
Case4	4.38	0.06	0.37	0.41	1.26	0.55	0.39	0.81
Case5	4.91	0.08	0.06	0.07	0.19	0.08	0.06	0.12
Case6	4.89	0.08	0.05	0.06	0.17	0.07	0.05	0.11
Case7	5.21	0.07	0.05	0.05	0.17	0.07	0.05	0.11

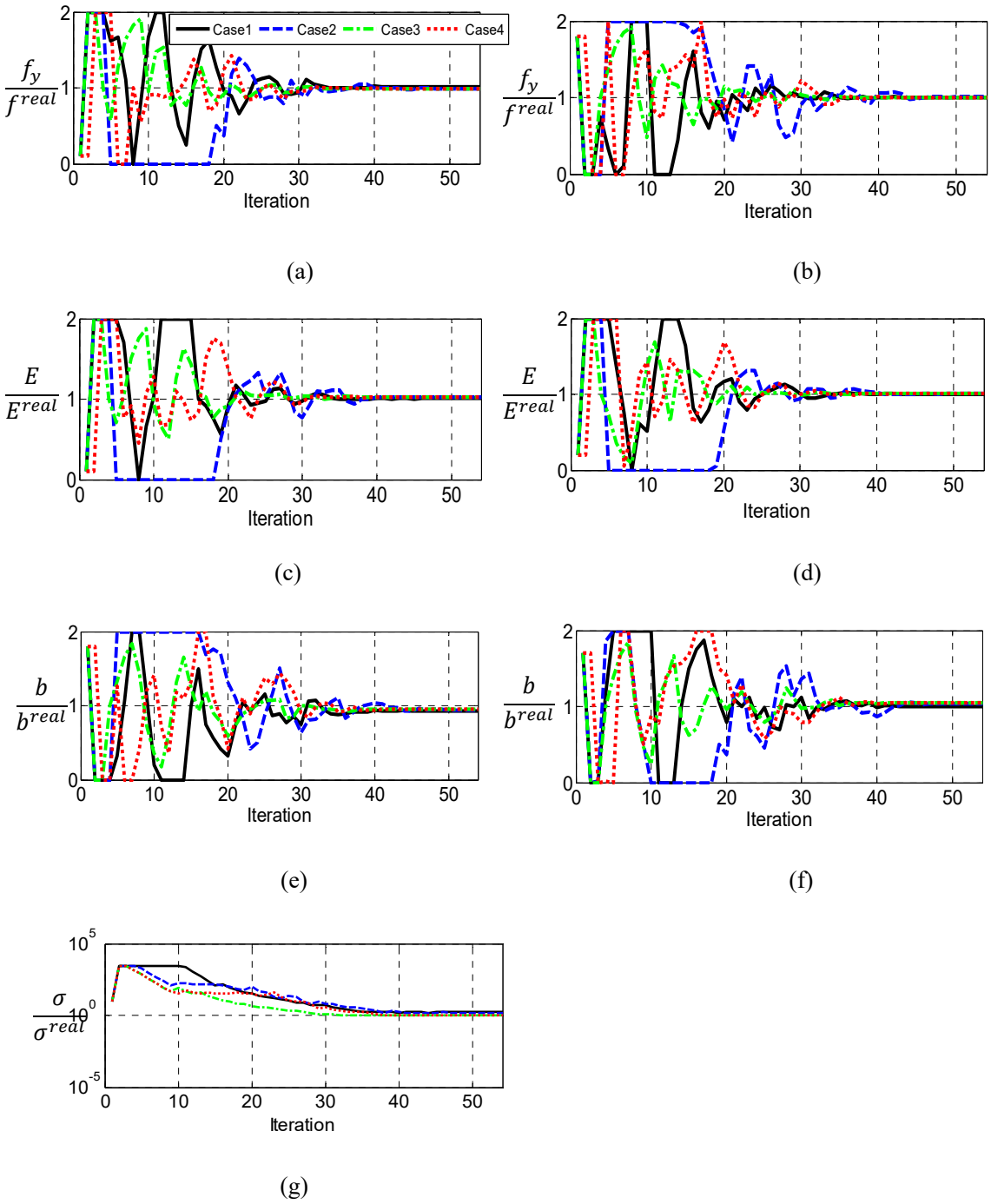

Figure 6-9 The convergence processes of model parameters and error variances with different numbers of data points: (a) Initial yield strength for column elements; (b) Young's modulus for column elements; (c) The stain-hardening ratio for column elements; (d) Initial yield strength for beam elements; (e) Young's modulus for beam elements; (f) The stain-hardening ratio for beam elements; (g) The standard error variance.

To further study the noise effect, the simulated accelerations with 5%, 10% and 20% white noises are used for the identification analysis, respectively. The same six nonlinear material

parameters$f_y^{\mathrm{Beam}}, E^{\mathrm{Beam}}, b^{\mathrm{Beam}}, f_y^{\mathrm{Col}}, E^{\mathrm{Col}}$, and $b^{\mathrm{Col}}$are identified. The updated nonlinear parameters and error variance are presented in Table 4. It can be seen from Table 4 that the proposed approach can accurately identify the nonlinear model parameters when measurement noise levels are 5% and 10% with the maximum relative error in the identified parameters less than 10%. For the case with 20% noise, the maximum value of the identification error indices is less than 15% and the maximum relative error in the parameter identification is 11% for the parameter $\mathrm{b}^{\mathrm{Beam}}$.The estimated errors and the uncertainty quantification results of these six parameters are listed in Table 5 when different noise levels are considered. From Table 5, it can be found that the covariance of the parameter identification results gradually increase with the measurement noise level, which is reasonable and expected. The convergence processes of the six nonlinear material parameters in these three cases are shown in Figures 6- 10 (a)-(g). A large number of iterations is usually required for the case with a higher noise in the measurement data. A comparison between the acceleration responses with 5% noise effect and the analytical response calculated with the updated parameters are shown in Figure 6- 11(a). The extracted instantaneous frequencies of the first mono-component are shown in Figure 6-11(b). These results also validate that an accurate parameter identification is achieved with the proposed approach.

Table 6-3 Identified parameters of the nonlinear hysteretic model with different initial values

Case		Column parameters			Beam parameters			σ/σ^{real}
		f_y/f^{real}	E/E^{real}	b/b^{real}	f_y/f^{real}	E/E^{real}	b/b^{real}	
Exact		1.00	1.00	1.00	1.00	1.00	1.00	1.00
Case1	Initial values	0.10	0.10	1.80	1.80	0.20	1.70	8.45
	Updated values	1.01	1.00	0.95	0.99	1.01	1.03	1.02
Case2	Initial values	0.20	0.18	0.10	0.30	1.90	0.10	16.60
	Updated values	1.01	1.00	0.95	0.99	1.01	1.03	1.02
Case3	Initial values	0.12	0.33	0.15	1.88	1.98	2.00	100.00
	Updated values	1.01	1.00	0.95	0.99	1.01	1.03	1.02

Table 6-4 Identified parameters of the nonlinear hysteretic model with different noise level

Case	Column parameters			Beam parameters			$\sigma_1/\sigma_1{}^{real}$
	f_y/f^{real}	E/E^{real}	b/b^{real}	f_y/f^{real}	E/E^{real}	b/b^{real}	
Exact	1.00	1.00	1.00	1.00	1.00	1.00	1.00
5%	1.01	1.00	0.95	0.99	1.01	1.03	1.02
10%	0.99	1.03	0.92	1.00	1.01	1.03	0.98
20%	1.00	1.02	0.98	0.96	1.00	1.11	1.08

Table 6-5 Uncertainty quantification of identified nonlinear model parameters with different noise level

Case	Error index (%)		Column parameters			Beam parameters		
	R_{acc}	R_ω	$Cov_{f_y}(\%)$	$Cov_E(\%)$	$Cov_b(\%)$	$Cov_{f_y}(\%)$	$Cov_E(\%)$	$Cov_b(\%)$
5%	4.91	0.08	0.06	0.07	0.19	0.08	0.06	0.12
10%	8.24	1.56	0.09	0.11	0.31	0.14	0.10	0.21
20%	13.26	2.55	0.24	0.27	0.81	0.35	0.24	0.53

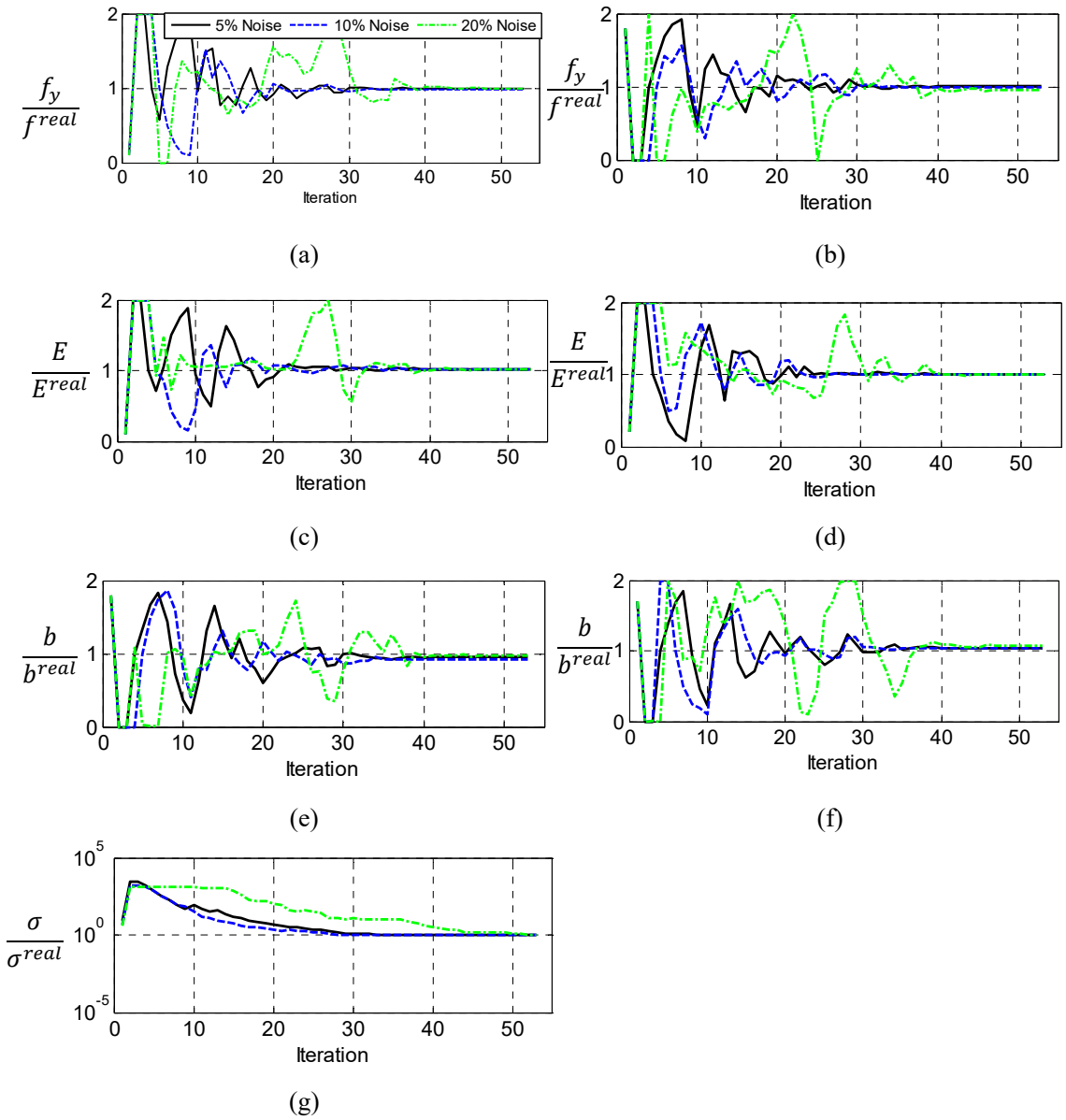

Figure 6-10 The convergence processes of model parameters and error variances under different measurement noise levels: (a) Initial yield strength for column elements; (b) Young's modulus for column elements; (c) The stain-hardening ratio for column elements; (d) Initial yield strength for beam elements; (e) Young's modulus for beam elements; (f) The stain-hardening ratio for beam elements; (g) The standard error variance.

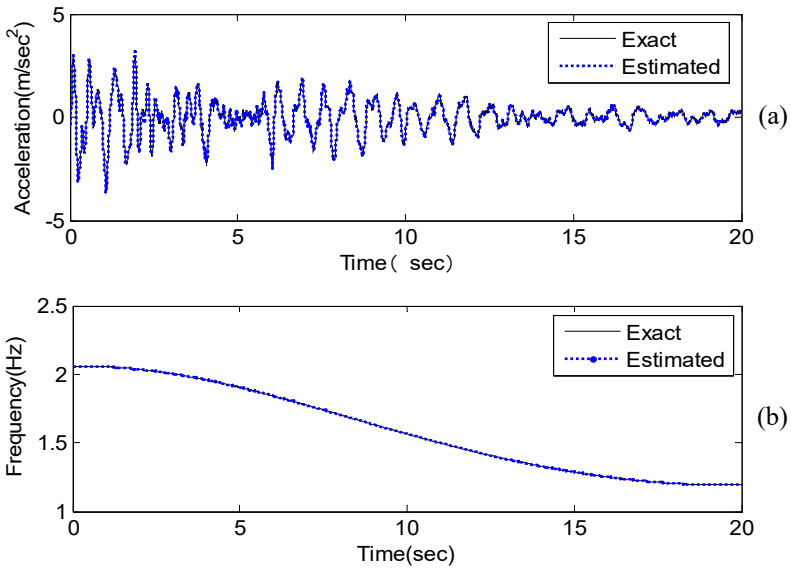

Figure 6-11 Comparison of the calculated acceleration response and identified instantaneous frequency of the first mono-component from the exact analytical and updated nonlinear models with 5% measurement noise: (a) Acceleration response; (b) Instantaneous frequency.

6.4 Experimental verification

6.4.1Nonlinear structural model and experimental setup

To further validate the effectiveness and accuracy of the proposed approach for nonlinear model updating, a high voltage switch structure with three pillars, as shown in Figure 6-12, under the harmonic excitation is tested in the laboratory and used as an example for nonlinear model updating. The experimental setup consists of three porcelain pillars and a steel I-beam which are bolted on the shake table. A wood truss is built and used as a transverse support for the test structure. The pillar is bolted to the I-beam by using a steel hollow square tube as supports. 3 accelerometers as shown in Figure 6-12 are used to record structural dynamic responses. The response signal recorded from accelerometer 3 at the base of the shake table is taken as the known external excitation on the testing model, and measured response of accelerometer 2 is used for nonlinear model updating. More details of this shake table test setup can be referred to [55].

In experimental tests, the bottom supports of the three-pillar model are gradually fractured under continuous harmonic excitation. The damage type of the experimental structure is considered as shear and bending failure of the bottom supports. In a previous study [40], the fractured support of the rightmost pillar as shown in Figure 6-13 is assumed as the main cause of the nonlinearity in the testing structure. The calibrated nonlinear joint model can be

effectively used to predict the dynamic responses of the test structure. However, the previous study neglected the damage of the other two supports, which may also contribute to the nonlinearity of the experimental structure. Considering this, to comprehensively include all the possible nonlinearities in the test structure and reduce the modeling errors, a more detailed nonlinear model with three joints, as shown in Figure 6-14, is built by using OpenSees.

In this new nonlinear model, three bottom supports are defined as nonlinear joint models. Each joint model is simulated by using a spring element with two bilinear steel material models in Opensees. Each bilinear material model includes three parameters, namely, F, E and b, representing the initial yield strength, Young's modulus and the strain-hardening ratio, respectively. These two bilinear material models are defined in the shear and torsional directions of the spring element, respectively. Linear elastic beam elements are used to model three ceramic pillars and all the beams, which are defined based on the true physical parameters of the experimental structure. In addition, with the feasible characteristics of the upper beam-column connections, four linear spring elements as shown in Figure 6-14 are employed to approximately simulate the dynamic characteristics of these connections. The damping ratio is measured as 3% based on the test results under a low level harmonic excitation [56]. A sinusoidal modulated harmonic loading is applied as the base excitation with a sampling frequency of 250 Hz. The measured excitation from accelerometer 3 is shown in Figure 6-15, and the measured acceleration at the right top is used for identification, as shown in Figure 6-16. Before the model updating of nonlinear joints, structural model is assumed as linear and stiffness parameters are updated with the response surface based model updating method [5]. The first two natural frequencies of the updated linear model are 7.68 Hz, and 13.9 Hz, respectively.

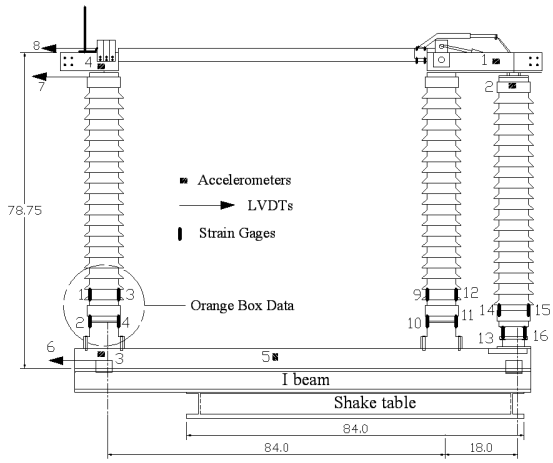

(a)

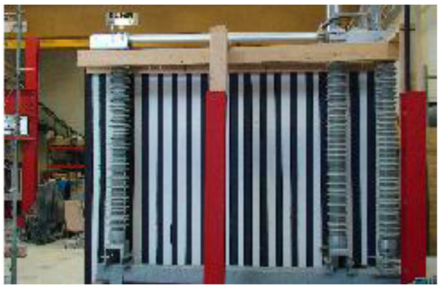

(b)

(c)

Figure 6-12 Experimental setup and testing structural model: (a) Testing model on the shake table and sensor setup; (b) Wood truss system; (c) The data acquisition system.

(a)

(b)

Figure 6-13 Failure of the structure: (a) The fractured bottom support; (b) The detailed damage of the bottom support.

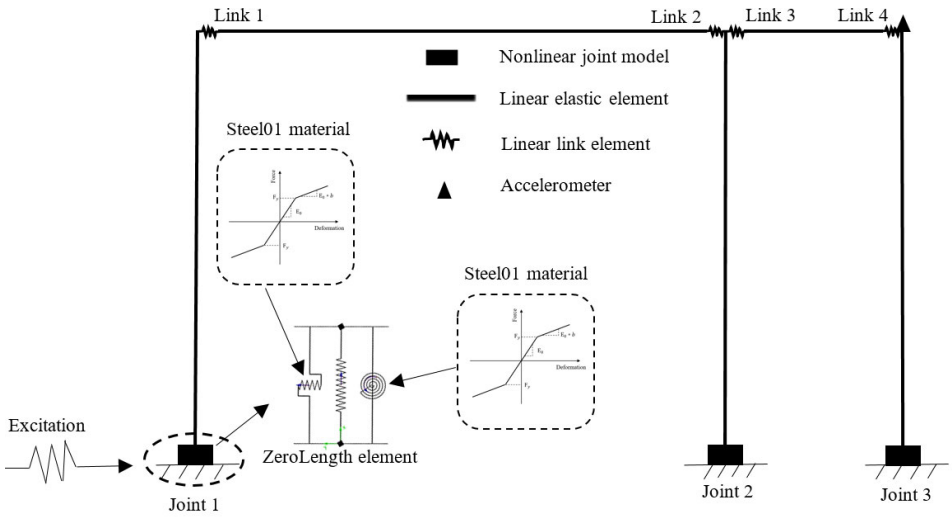

Figure 6-14 The nonlinear finite element model of testing structure in Opensees

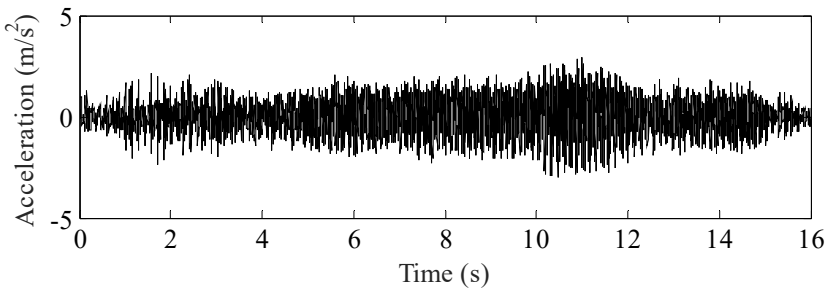

Figure 6-15 The measured external excitation at the base of the shake table

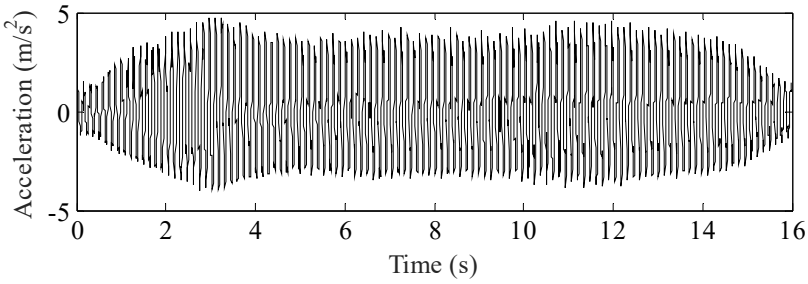

Figure 6-16 The measured acceleration response from accelerometer 2.

6.4.2 Nonlinear model updating

Since the nonlinear characteristic of every joint model is defined with six bilinear material parameters, 18 bilinear material parameters are totally selected as nonlinear model parameters to be identified. For example, six material parameters F_1, E_1, b_1, F_2, E_2 and b_2 are used to define the nonlinear characteristics of the first joint model of the left column in Figures 6-13. F_1, E_1 and b_1 are the nonlinear

material parameters of the first joint model in the shear direction, and F_2, E_2 and b_2 are the nonlinear material parameters in the torsional direction. Similarly, nonlinear characteristics of the second and third joint models can be defined with parameters F_3, E_3, b_3, F_4, E_4, b_4 and F_5, E_5, b_5, F_6, E_6, b_6, respectively. The initial values of three nonlinear joint models are defined based on the behaviors of ceramic structures and the bilinear material properties. The identifications by using 5% and 10% points are conducted. The results indicate that 5% data points is sufficient to update the experimental nonlinear structure under the harmonic excitation. Therefore 5% data points of the instantaneous amplitudes of decomposed acceleration response are used for the nonlinear model updating. The updated bilinear material parameters are presented in Table 6, and the corresponding error indices and error variance are summarized in Table 7, respectively. It can be observed that these two error indices are less than 8%, indicating that a very good agreement can be obtained between the acceleration responses and the instantaneous frequencies from the updated model and the testing model. The uncertainty quantification results of the identified nonlinear model parameters are listed in Table 8. As can be seen from Table 7, the identified σ_1 equals to 0.46, which represents an unpractical noise level within a limited filter window for the experimental structure. The reason caused the phenomena may be that the modeling errors and measurement noise effect in the real experimental tests are more significant. The acceleration and slow-varying portion of the instantaneous frequency calculated from the updated nonlinear model and the measured data are compared and shown in Figures 6-17(a) and (b), respectively.

The above numerical and experimental results demonstrate that a good accuracy in nonlinear model parameter identification is achieved, and the variances in the identification results due to the noise effects are evaluated. The main advantages of the proposed nonlinear model updating approach are summarized as: (1) Only the commonly measured acceleration responses are used for nonlinear model updating, which is a direct and effective approach; (2) The error in the identified instantaneous amplitudes of decomposed acceleration responses between the analytical model and measured data can be used to account for the variance of identified model parameters due to uncertainty effect. The proposed Bayesian based nonlinear model updating approach can well identify the nonlinear model parameters accurately, even under a significant noise effect. The uncertainty quantification is conducted to consider the noise effect on the identification results.

Table 6-6 The initial values and updated parameters for the nonlinear joint models

Nonlinear Joint	Parameter location	$F_i(10^2\text{N})$ Updated values (Initial values)	$E_i(10^5\text{N})$ Updated values (Initial values)	b_i Updated values (Initial values)
1st joint	Shear	1.25(0.90)	4.21(2.50)	0.68(0.50)
	Torsional	1.20(0.90)	3.50(2.50)	0.62(0.50)
2nd joint	Shear	1.05(0.90)	4.25(2.50)	0.62(0.50)
	Torsional	1.41(0.90)	3.56(2.50)	0.84(0.50)
3rd joint	Shear	1.13(0.90)	2.22(2.50)	0.64(0.50)
	Torsional	1.24(0.90)	2.48(2.50)	0.74(0.50)

Table 6-7 The error indices for the tested nonlinear structure after updating

$\mathbf{E}_{acc}(\%)$	$\mathbf{E}_{\omega}(\%)$	σ_1
7.61	0.48	0.46

Table 6-8 The uncertainty quantification of update nonlinear joint model parameters

	$COV_{F_i}(\%)$	$COV_{E_i}(\%)$	$COV_{b_i}(\%)$	$COV_{F_j}(\%)$	$COV_{E_j}(\%)$	$COV_{b_j}(\%)$
1st joint	0.38	1.35	3.21	1.08	1.56	1.02
2nd joint	0.52	2.66	3.35	1.55	1.83	0.89
3rd joint	0.46	1.37	1.88	0.84	1.01	1.82

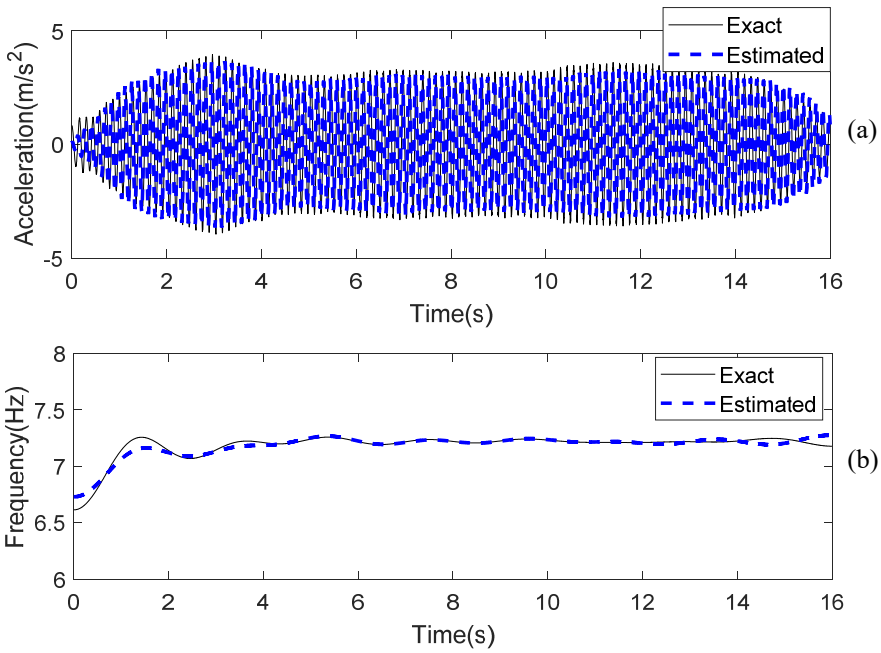

Figure 6-17 Comparison of the acceleration response and identified instantaneous frequency of the first mono-component from the measured data and the updated nonlinear model: (a) Acceleration response; (b) Instantaneous frequency.

6.5 Conclusions

This chapter proposes a nonlinear model updating approach based on the instantaneous characteristics of the decomposed structural dynamic responses. The instantaneous frequencies and amplitudes of decomposed acceleration response are extracted by using DAMD method. The Bayesian theory is used to quantify the covariance of the updated nonlinear model parameters by using an extended MLE based on the instantaneous amplitudes of decomposed acceleration responses. The uncertainty quantification in the calibrated nonlinear model parameters is conducted by using the CRLB theorem. Numerical studies on a three-story four-bay nonlinear building model and experimental verification on a high voltage switch structure are performed to verify the accuracy and performance of the proposed approach. Both numerical and experimental results demonstrate that the proposed approach can accurately update the nonlinear model parameters, and is capable of quantifying the uncertain noise effect in the measurements on the nonlinear model updating results.

Based on the numerical and experimental studies, the following conclusions and discussions are provided:

(1) The proposed approach can effectively update the nonlinear model with a high accuracy, even with significantly noisy data.

(2) In the study, measurement noise is considered as the uncertainty factor in nonlinear model updating. The propagation of the uncertainty effect in the identification process is investigated and the quantified covariance results in the updated nonlinear parameters are given.

(3) The computational efficiency is significantly improved since a less number of data points are used for nonlinear model updating based on the proposed nonlinear model updating approach.

(4) The proposed approach aims to calibrate the main components of the measured dynamic responses, indicating that it is robust when the measurement noise level is high.

(5) Modeling errors may have a significant effect on the structural identification and model updating of nonlinear structures. The quantification of the uncertainty effect sourced from the modeling errors will be further studied.

References

[1] Friswell M.I., Mottershead J.E. (1995). Finite element model updating in structural dynamics. The Netherlands: Kluwer Academic Publishers.

[2] Fritzen C.P., Jannewein D., Kiefer T. (1998). Damage detection based on model updating methods. *Mechanical Systems and Signal Processing*, 12: 163-86.

[3] Jaishi B., Ren W.X. (2005). Structural finite element model updating using ambient vibration test results. *Journal of Structural Engineering ASCE*, 131(4): 617-28.

[4] Lam H.F., Hu J., Yang J.H. (2017). Bayesian operational modal analysis and Markov chain Monte Carlo-based model updating of a factory building. *Engineering Structures*, 132:314-336.

[5] Ren W.X., Fang S.E., Deng M.Y. (2011). Response surface-based finite-element-model updating using structural static responses. *Journal of Engineering Mechanics ASCE*, 137(4): 248-257.

[6] Brownjohn J.M.W., Xia P.Q., Hao H., Xia Y. (2001). Civil structure condition assessment by FE model updating: Methodology and case studies. *Finite Elements in Analysis and Design*, 37(10):761-775.

[7] Li J., Law S.S., Ding Y. (2012). Substructure damage identification based on response reconstruction in frequency domain and model updating, *Engineering Structures*, 41: 270-284.

[8] Cunha J., Foltête E., Bouhaddi N. (2008). Evaluation of stiffness of semi-rigid joints in pultruded profiles from dynamic and static data by using model updating technique. *Engineering Structures*, 30(4): 1024-1036.

[9] Asgarieh E., Moaveni B., Stavridis. (2014). Nonlinear finite element model updating of an infilled frame based on identified time-varying modal parameters during an earthquake. *Journal of Sound and Vibration*, 333:6057-6073.

[10] Li J., Hao H., Chen Z. (2015). Damage identification and optimal sensor placement for structures under unknown traffic-induced vibrations. *Journal of Aerospace Engineering ASCE*, 30(2): B4015001.

[11] Song W., Dyke S.J., Harmon T. (2008). Application of nonlinear model updating for a reinforced concrete shear wall. *Journal of Engineering Mechanics ASCE*, 139(5): 635-649.

[12] Noel J.P., Kerschen G. (2017). Nonlinear system identification in structural dynamics: 10 more years of progress. *Mechanical Systems and Signal Processing*, 83:2-35.

[13] Kurt M., Moore K.J., Eriten M., McFarland D.M., Bergman L.A., Vakakis A.F. (2017). Nonlinear model updating applied to the IMAC XXXII Round Robin benchmark system. *Mechanical Systems and Signal Processing*, 88:111-122.

[14] Teughels A., Maeck J., Roeck De. (2002). Damage assessment by FE model updating using damage functions. *Computers and Structures*, 80:1869-1879.

[15] Asgarieh E., Moaveni B., Barbosa A., Chatzi E. (2016). Nonlinear model calibration of a shear wall building using time and frequency data features. *Mechanical Systems and Signal Processing*, 85:236-251.

[16] Park Y.S., Kim S., Kim N., Lee J.J. (2017). Finite element model updating considering boundary conditions using neural networks. *Engineering Structures*, 150: 511-519.

[17] Simoen E., Papadimitriou C., Lombaert G. (2013). On prediction error correlation in Bayesian model updating. *Journal of Sound and Vibration*, 332: 4136-4152.

[18] Strauss A., Frangopol D.M., Kim S. (2008). Use of monitoring extreme data for the performance prediction of structures: Bayesian updating. *Engineering Structures*, 30: 3654-3666.

[19] Yin T., Jiang Q.H., Yuen K.V. (2017). Vibration-based damage detection for structural connections using incomplete modal data by Bayesian approach and model reduction technique. *Engineering Structures*, 132: 260-277.

[20] Simoen E., Roeck G.D., Lombaert G. (2014). Dealing with uncertainty in model updating for damage assessment. *Mechanical Systems and Signal Processing*, 56-57: 123-149.

[21] Yuen K.V., Kuok S.C. (2011). Bayesian methods for updating dynamic models. *Journal of Applied Mechanics*, 64(1): 010802-1-010802-18.

[22] Lam H.F., Yang J.H., Au S.K. (2015). Bayesian model updating of a coupled-slab system using field test data utilizing an enhanced Markov chain Monte Carlo simulation algorithm. *Engineering Structures*, 102: 144-155.

[23] Jesus A., Brommer P., Zhu Y.J., Laory I. (2017). Comprehensive Bayesian structural identification using temperature variation. *Engineering Structures*, 141: 75-82.

[24] Au S.K. (2012). Connecting Bayesian and frequentist quantification of parameter uncertainty in system identification. *Mechanical Systems and Signal Processing*, 29: 328-342.

[25] Cheung S.H., Beck J.L. (2009). Bayesian model updating using hybrid monte carlo simulation with application to structural dynamic models with many uncertain parameters. *Journal of Engineering Mechanics ASCE*, 135(4): 243-255.

[26] Jang H.W., Smyth A. (2017). Bayesian model updating of a full-scale finite element model with sensitivity-based clustering. *Structural Control & Health Monitoring*, 24: e2004.

[27] Lam H.F., Yang J.H., Au S.K. (2017). Markov chain Monte Carlo-based Bayesian method for structural model updating and damage detection. *Structural Control & Health Monitoring*, 24: e2004.

[28] Beck J.L., Katafygiotis L.S. (1998). Updating Models and their Uncertainties. I: Bayesian Statistical Framework. *Journal of Engineering and Mechanics ASCE*, 124(4): 455-461.

[29] Katafygiotis L.S., Beck J.L. (1998). Updating Models and their Uncertainties. II: Model Identification. *Journal of Engineering and Mechanics ASCE*, 124(4): 463-467.

[30] Behmanesh I., Moaveni B. (2016). Accounting for environmental variability, modeling errors, and parameter estimation uncertainties in structural identification. *Journal of Sound and Vibration*, 374: 92-110.

[31] Behmanesh I., Moaveni B., Lombaert G., Papadimitriou C. (2015). Hierarchical Bayesian model updating for structural identification. *Mechanical Systems and Signal Processing*, 64-65: 360-376.

[32] Wan H.P., Ren W.X. (2015). Stochastic model updating utilizing Bayesian approach and Gaussian. *Mechanical Systems and Signal Processing*, 70-71: 245-268.

[33] Lin J., Zhang Y. (1994). Nonlinear structural identification using extended Kalman filter. *Computers and Structures*, 52: 757-764.

[34] Wu M., Smyth A.W. (2007). Application of the unscented Kalman filter for real-time nonlinear system identification. *Structural Control & Health Monitoring*, 14: 971-990.

[35] Calabrese A., Strano S., Terzo M. (2018). Adaptive constrained unscented Kalman filtering for real-time nonlinear structural system identification. *Structural Control & Health Monitoring*, 25: e2084.

[36] Chatzi E.N., Smyth A.W., Masri S.F. (2010). Experimental application of on-line parametric identification for nonlinear hysteretic systems with model uncertainty. *Structural Safety*, 32: 326-337.

[37] Omrani R., Hudson R.E., Taciroglu E. (2013). Parametric identification of nondegrading hysteresis in a laterally and torsionally coupled building using an unscented Kalman filter. *Journal of Engineering and Mechanics ASCE*, 139: 452-468.

[38] Ebrahimian H., Astroza R., Conte J.P., De Callafon R.A. (2017). Nonlinear finite element model updating for damage identification of civil structures using batch Bayesian estimation. *Mechanical Systems and Signal Processing*, 84: 194-222.

[39] Wang Z.C., Xin Y., Ren W.X. (2015). Nonlinear structural model updating based on instantaneous frequencies and amplitudes of the decomposed dynamic responses. *Engineering Structures*, 100: 189-200.

[40] Wang Z.C., Xin Y., Ren W.X. (2016). Nonlinear structural joint model updating based on instantaneous characteristics of dynamic responses. *Mechanical Systems and Signal Processing*, 76-77: 476-496.

[41] Wang Z.C., Xin Y., Xing J.F., Ren W.X. (2017). Hilbert low-pass filter of non-stationary time sequence using analytical mode decomposition. *Journal of Vibration and Control*, 23(15): 2444-2469.

[42] Byrd R., Gould N., Nocedal J., Waltz R. (2004). An active-set algorithm for nonlinear programming using linear programming and equality constrained sub-problems. *Mathematical Programming*, 100: 27-48.

[43] Scheinberg K. (2006). An effective implementation of an active set method for SVMS. *Journal of Machine Learning Research*, 7: 2237-2257.

[44] Ding Z., Yao R., Li J., Lu Z.R. (2018). Structural damage identification based on modified Artificial Bee Colony algorithm using modal data. *Inverse Problems in Science and Engineering*, 26(3): 422-442.

[45] Moon T.K., Stirling W.C. (2000). Mathematical Methods and Algorithms for Signal Processing. Prentice, Upper Saddle River, NJ.

[46] Hald A. (1999). On the History of Maximum Likelihood in Relation to Inverse Probability and Least Squares. *Statistical Science*, 14(2): 214-222.

[47] Goodwin G.C., Payne R.L. (1977). Dynamic System Identification: Experiment Design and Data Analysis, Academic Press, New York, NY.

[48] Kay S.M. (1993). Fundamental of Statistical Signal Processing Volume 1: Estimation Theory, Prentice Hall, Upper Saddle River, NJ.

[49] Tichavsky P., Murray C.H., Nehorai A. (1998). Posterior Cramér-Rao bounds for discrete-time nonlinear filtering. *IEEE Transactions on Signal Processing*, 46: 1386-1396.

[50] Au S.K., Li B.B. (2018). Posterior uncertainty, asymptotic law and Cramér-Rao bound. *Structural Control & Health Monitoring*, 25: e2113.

[51] Wang Z.C., Chen G.D. (2013). Analytical mode decomposition of time series with decaying amplitudes and overlapping instantaneous frequencies. *Smart Materials and Structures*, 22: 095003(14pp).

[52] Feldman M. (1994). Non-linear system vibration analysis using Hilbert transform-I: free vibration analysis method. *Mechanical Systems and Signal Processing*, 8(2): 119-127.

[53] Matlab Optimization Toolbox, User's Guide, R2017a.

[54] Mazzoni S., Scott M.H., Mckenna F., Fenves G.L., et al. (2006). Open system for earthquake engineering simulation-user manual. Pacific Earthquake Engineering Research Center, University of California, Berkeley, California.

[55] Wang Z.C., Ren W.X., Chen G.D. (2013). Time-varying system identification of high voltage switches of a power substation with slide-window least-squares parameters estimations. *Smart Materials and Structures*, 22(6).

CHAPTER 7 CONCLUSIONS AND RECOMMENDATIONS

7.1 Main conclusions

This research mainly focuses on developing the vibration based approaches for operational modal identification, time-varying system identification and nonlinear structural damage detection under normal and extreme operational conditions. The corresponding conclusions and findings made in this thesis can be summarized below:

1. Chapter 2 develops an improved EWT approach for structural operational modal identification based on SAR power spectrum. Firstly, a SAR power spectrum of the measured response is calculated to define the boundaries of frequency components for the subsequent EWT analysis. Then, the EWT can be applied to decompose the measured response into a number of IMFs. When the IMFs are obtained, structural modal information such as natural frequencies, mode shapes and damping ratios can be identified by using Hilbert transform and RDT. Based on the numerical simulations and experimental results, three conclusions can be obtained as 1) SAR power spectrum can effectively determine the boundaries of frequency components associated with EWT analysis, even for signals with significant noise effect; 2) Closely-spaced modes can be effectively identified and decomposed by using the improved EWT approach; 3) Operational modal identification based on the proposed approach is accurate and reliable to identify modal parameters of structures under ambient vibration, i.e. natural frequencies, mode shapes and damping ratios.
2. Chapter 3 presents an enhanced EWT method based on SET for time-varying system identification. In this method, SET is first conducted to analyse the frequency components of a non-stationary vibration signal measured from a time-varying system, and then, the filtering boundaries for EWT analysis can be defined. The non-stationary vibration signal can be decomposed into a finite number of IMFs with the improved EWT. When the IMFs are obtained, the instantaneous frequencies of each mode can be effectively identified by using Hilbert Transform. Based on the numerical simulations and experimental results, three conclusions can be obtained as 1) The improved EWT

approach with SET can be used to accurately decompose a non-stationary signal into several modes based on the predefined filtering boundaries from SET; 2) The proposed approach is effective and accurate for time-varying system identification to obtain the instantaneous frequencies of structures, even under the significant noise effect.

3. Chapter 4 proposes an enhanced vibration decomposition approach based on AMD and MSST. In the proposed approach, the MSST approach with a time varying cut-off frequency detection algorithm is used to automatically define the time-varying bisecting frequencies for the AMD analysis. Once the time varying cut-off frequencies are identified, AMD can be used to adaptively decompose the non-stationary signal into individual components. Based on the numerical simulations and experimental applications, some conclusions can be drawn as 1) The MSST based time-frequency representation with the proposed cut-off frequency detection algorithm can automatically define the time-varying cut-off frequencies of using AMD for non-stationary signal decomposition; 2) The proposed MSST-AMD approach can effectively and accurately decompose a non-stationary signal into several individual components, even the signal is polluted with significant noise; and 3) Based on the vibration decomposition results by using the developed approach, structural damage detection is conducted. The results indicate that the damage detection approach can successfully evaluate the damage severity of the structures subjected to the earthquake excitations.

4. In Chapter 5, a novel nonlinear damage detection approach is proposed based on the VMD. Based on the proposed procedure, the measured dynamic responses from nonlinear structures under earthquake excitations are adaptively decomposed into a finite number of mono-components by using VMD. Hilbert transform is then employed to identify the instantaneous modal parameters of the decomposed mono-modes, including instantaneous frequencies and mode shapes. Based on the identified modal parameters from the decomposed structural dynamic responses, two damage indices are defined to identify the location and severity of structural damage, respectively. Based on the identified results in numerical simulations and experimental applications, it can be concluded that the proposed approach can be successfully applied for nonlinear

structural damage quantification and localization. However, it should be noted that dynamic responses of all floors of the tested building frame need be recorded when using the proposed indices for damage detection of nonlinear structures. For the large-scale and complex structures, further studies on how to use a limited amount of structural responses for nonlinear structural damage detection therefore need be conducted.

5. Chapter 6 proposes a Bayesian based nonlinear model updating approach using the instantaneous amplitudes of the decomposed dynamic responses. Uncertainty quantification of the model updating results due to the measurement noise is conducted. The residual of the instantaneous amplitudes of the decomposed structural dynamic responses between the test structure and the analytical nonlinear model is used to construct the maximum likelihood function. The uncertainty in the updated nonlinear model parameters can be evaluated by using the Cram-Rao lower bound theorem with the exact Fisher Information matrix. Based on the updated results in numerical simulations and experimental applications, some conclusions can be drawn as 1) The proposed approach can effectively update the nonlinear model with a high accuracy, even with significantly noisy data; 2) In this study, measurement noise is considered as the uncertainty factor in nonlinear model updating. The propagation of the uncertainty effect in the identification process is investigated and quantified covariance results in the updated nonlinear parameters are given; 3) The computational efficiency is significantly improved since a less number of data points are used for nonlinear model updating based on the proposed approach; 4) The proposed approach aims to calibrate the main components of the measured dynamic responses, indicating that it is robust when the measurement noise level is high; 5) Modelling errors may have a significant effect on the structural identification and model updating of nonlinear structures. The quantification of the uncertainty effect sourced from the modeling errors will be further studied.

7.2 Recommendations for future works

In this research, the vibration based system identification, damage detection and nonlinear model updating of civil engineering structures subjected to normal and extreme operational conditions are presented. Various aspects of this research may be worth further investigation for possible improvements in future studies. These include but are not limited to the following:

1. The developed SAR-EWT approach has been successfully applied to identify structural modal parameters, including natural frequencies, damping ratios and mode shapes under ambient vibrations. However, the approach cannot be automatically performed. Therefore, the SAR-EWT approach can be further developed for adaptive automated modal parameter identification of civil engineering structures under ambient vibrations.
2. SET is used to enhance EWT approach for analysis of non-stationary signals. To realize an energy-concentrated time-frequency representation, the SET operation is performed based on the coefficients of the Short-time Fourier Transform of the vibration signal. To explore a higher-resolution time-frequency representation, the SET operation would be further applied by using wavelet transform and S-transform based time-frequency coefficients.
3. Nonlinear structural damage detection is investigated based on the identified instantaneous modal parameters of the decomposed dynamic responses of structures subjected to extreme operational conditions. However, it should be noticed that dynamic responses of all floors of the tested building frame need be recorded when using the proposed indices for damage detection of nonlinear structures. For the large-scale and complex structures, further studies on how to use a limited number of structural responses for nonlinear structural damage detection could be conducted.
4. To consider the effects of measurement noise in nonlinear structural model updating, a Bayesian based nonlinear model updating strategy is developed by using the identified instantaneous characteristics of the decomposed dynamic responses of nonlinear structures under extreme operational conditions. However, uncertainty quantification of

the updated results under the effect of model errors is still not considered. Therefore, the uncertainties of the calibrated nonlinear parameters under the effect of model errors would be further investigated.

APPENDIX I: Cut-off frequency detection algorithm in time-frequency domain

$\boldsymbol{Input}$:

m: $The\ \ number\ \ of\ \ the\ \ indivudal\ \ components\ \ included\ \ in\ \ a\ \ signal$;

S: $The\ \ number\ \ of\ \ the\ \ separated\ \ segmnets\ \ of\ \ time-frequency\ \ coefficients$;

$T_s^{(l)}[t,\varphi]$: *The time-frequency coefficients of the* l^{th} *MSST operation;*

ξ: $The\ \ frequency\ \ support\ \ of\ \ the\ \ window\ \ function$;

$\boldsymbol{for}\ \ k=1\ \ to\ \ m$

$\boldsymbol{for}\ \ \gamma=1\ \ to\ \ S$

$\boldsymbol{Find}\ \ \left(t_i^*,\varphi_j^*\right)=\arg max_{t,\varphi}\left|T_s^{(l)}[t_i,\varphi_j]\right|;\ \ t_i\in\left[(\gamma-1)\frac{N}{S},(\gamma)\frac{N}{S}\ \right]$;

$\boldsymbol{in\ \ which}\ \ N\ \ denotes\ \ the\ \ numbe\ \ of\ \ data\ \ points; t_i=[0,t_1,t_2,\cdots,t_{N-1}]$;

$\Rightarrow IF_{k,\gamma}(t_i^*)=\varphi_j^*$;

$\Rightarrow IF_{k,\gamma}(t_i^*-1)=\arg max_{\varphi}\left|T_s\left[t_i^*-1,\varphi_j\right]\right|$;

$\boldsymbol{for}\ \ t_i=t_i^*+1\ \ to\ \ N-1$

$\boldsymbol{Find}\ \ IF_{k,\gamma}(t_i)=\arg max\left\{\left|T_s^{(l)}[t_i,\varphi_j]\right|^2-\beta\left(\varphi_j-2IF_{k,\gamma}(t_i-1)+IF_{k,\gamma}(t_i-2)\right)^2\right\}$;

$\boldsymbol{in\ \ which}\ \ \varphi_j\in\left[IF_{k,\gamma}(t_i-1)-\xi,IF_{k,\gamma}(t_i-1)+\xi\right]$;

$\boldsymbol{end\ \ for}$

$\boldsymbol{for}\ \ t_i=t_i^*-1\ \ to\ \ 0$

$\boldsymbol{Find}\ \ IF_{k,\gamma}(t_i)=\arg max\left\{\left|T_s^{(l)}[t_i,\varphi_j]\right|^2-\beta\left(\varphi_j-2IF_{k,\gamma}(t_i+1)+IF_{k,\gamma}(t_i+2)\right)^2\right\}$;

$\boldsymbol{in\ \ which}\ \ \ \varphi_j\in\left[IF_{k,\gamma}(t_i+1)-\xi,IF_{k,\gamma}(t_i+1)+\xi\right]$;

$\boldsymbol{end\ \ for}$

$\boldsymbol{end\ \ for}$

$\Rightarrow IF_{k,\gamma}(t_i)=argmax\sum_{t=0}^{N-1}\left|T_s\left[t,IF_{k,\gamma}(t_i)\right]\right|$;

$\boldsymbol{then}$

$\boldsymbol{\psi}=[IF_1(\boldsymbol{t}),IF_2(\boldsymbol{t}),\cdots,IF_k(\boldsymbol{t})];\quad \boldsymbol{t}\in[t_1,t_2,\cdots,t_N]^T$;

$$\boldsymbol{C}_{filter}=\left[\frac{IF_1(\boldsymbol{t})+IF_2(\boldsymbol{t})}{2},\frac{IF_2(\boldsymbol{t})+IF_3(\boldsymbol{t})}{2},\cdots,\frac{IF_{m-1}(\boldsymbol{t})+IF_m(\boldsymbol{t})}{2}\right];$$

$\boldsymbol{end\ \ for}$

$\boldsymbol{Output}$: $\boldsymbol{C}_{filter}$

APPENDIX II COPYRIGHT CLEARANCE

The proof of the rights, granted by publishers for the publication that forms the chapters of this thesis, to reproduce the contribution in the thesis are attached below.

Xin, Y., Hao, H. & Li, J. (2019). Operational modal identification of structures based on improved empirical wavelet transform. *Structural Control & Health Monitoring*, *e2323*. https://doi.org/10.1002/stc.2232.

Thank you for your order!

Dear Mr. YU XIN,

Thank you for placing your order through Copyright Clearance Center's RightsLink® service.

Order Summary

Licensee:	CURTIN UNIVERSITY
Order Date:	Oct 5, 2020
Order Number:	4922510080902
Publication:	Structural Control and Health Monitoring
Title:	Operational modal identification of structures based on improved empirical wavelet transform
Type of Use:	Dissertation/Thesis
Order Ref:	4881221283623
Order Total:	0.00 USD

Xin, Y., Hao, H. & Li, J. (2019). Time-varying system identification by enhanced Empirical Wavelet Transform based on Synchroextracting Transform. *Engineering Structures*, *109313*. https://doi.org/10.1016/j.engstruct.2019.109313.

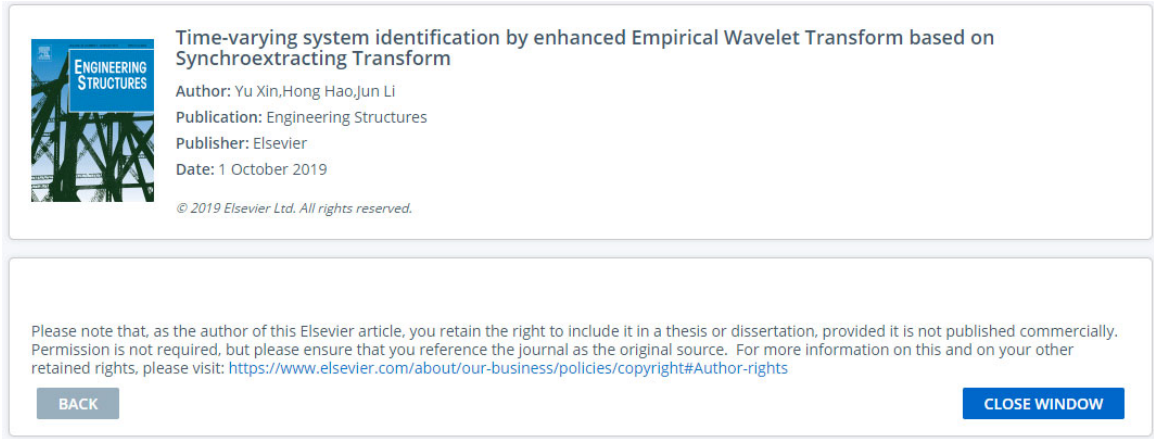

Xin, Y., Hao, H., Li, J., Wang Z., Wan H. & Ren W. (2019). Bayesian based nonlinear model updating using instantaneous characteristics of structural dynamic responses. *Engineering Structures*, 183:459-474. https://doi.org/10.1016/j.engstruct.2019.01.043.

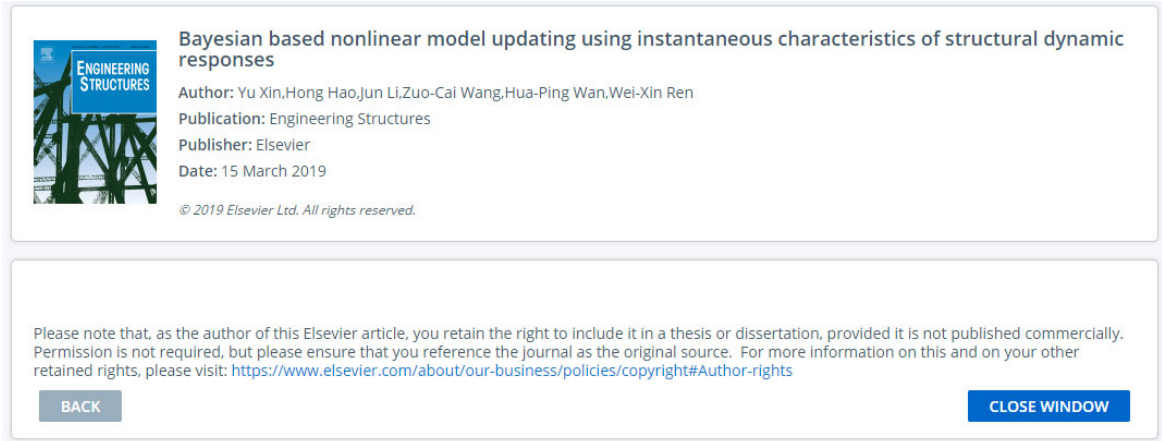

BIBLIOGRAPHY DISCLAIMER

Every reasonable effort has been made to acknowledge the owners of copyright material. I would be pleased to hear from any copyright owner who has been omitted or incorrectly acknowledged.